Narrowing Freeway Lanes and Shoulders to Create Additional Travel Lanes

PUBLICATION NO. FHWA-HRT-21-005

JUNE 2021

U.S. Department of Transportation
Federal Highway Administration

Research, Development, and Technology
Turner-Fairbank Highway Research Center
6300 Georgetown Pike
McLean, VA 22101-2296

FOREWORD

Traffic bottlenecks continue to be one of the top sources of congestion on our Nation's roadways. In their 2016 report, *Traffic Bottlenecks: Identification and Solutions*, Hale et al. (2016) identified lane width reduction as a possible low-cost treatment to increase roadway capacity. Lane width reduction is an effective strategy because it creates space to add an additional travel lane without incurring significant right-of-way or construction costs. This report describes the development of calibrated macroscopic and microscopic tools to enable State or local departments of transportation (DOTs) to evaluate the impacts of deploying this solution in their jurisdiction. Two case studies were conducted to illustrate the benefits of implementing the lane-narrowing treatment on real-world networks. Dynamic lane-narrowing technologies were also evaluated. This report will be of interest to State and local DOTs interested in a low-cost treatment to increase roadway capacity without increasing the footprint of their facility.

Brian P. Cronin, P.E.
Director, Office of Safety and Operations
Research and Development

TECHNICAL REPORT DOCUMENTATION PAGE

1. Report No. FHWA-HRT-21-005	2. Government Accession No.	3. Recipient's Catalog No.
4. Title and Subtitle Narrowing Freeway Lanes and Shoulders to Create Additional Travel Lanes		5. Report Date June 2021
		6. Performing Organization Code HRDO-20
7. Author(s) David Hale (ORCID: 0000-0001-5486-9367), Alexandra Kondyli (ORCID: 0000-0002-3462-0000), Juan Argote (ORCID: 0000-0003-0294-9247), Xiaoxiao Zhang (ORCID: 0000-0003-1545-8041), Bastian Schroeder (ORCID: 0000-0001-8916-421X), Levi Button (ORCID: 0000-0002-9697-1543), Jennifer Atkinson (ORCID: 0000-0002-5523-4205), Daniel Stock (ORCID: 0000-0002-6597-950X), Adil Cheema (ORCID: 0000-0003-3103-7757), Soheil Sajjadi (ORCID: 0000-0001-7635-4399), Murat Aycin (ORCID: 0000-0002-5798-3381), Mark Brackstone (ORCID: 0000-0003-2087-9385), Geline Canayon (ORCID: 0000-0001-7742-9399), Jordi Casas (ORCID: 0000-0002-7110-8751), Annique Lenorzer (ORCID: 0000-0003-3313-8623), Anxi Jia (ORCID: 0000-0001-5086-9693), Chetan Joshi (ORCID: 0000-0002-6242-5181), and Rachel James (ORCID: 0000-0001-9138-510X)		8. Performing Organization Report No.
		10. Work Unit No.
9. Performing Organization Name and Address Leidos, Inc. 11251 Roger Bacon Drive Reston, VA 20190 University of Kansas 1450 Jayhawk Boulevard Lawrence, KS 66045 Aimsun Inc. 20 W 22nd Street, Suite 612 New York, NY 10010 University of Virginia 1827 University Avenue Charlottesville, VA 22903 Kittelson & Associates, Inc. 851 SW 6th Avenue, Suite 600 Portland, OR 97204 PTV Group 9755 SW Barnes Road, Suite 290 Portland, OR 97225		11. Contract or Grant No. DTFH61-16-D-00030
12. Sponsoring Agency Name and Address U.S. Department of Transportation Federal Highway Administration 1200 New Jersey Ave SE Washington, DC 20590		13. Type of Report and Period Covered Final Report; September 2017–September 2019
		14. Sponsoring Agency Code HRDO-20
15. Supplementary Notes The Government Task Manager was Joe Bared (HRDO-20).		
16. Abstract The Federal Highway Administration is investigating narrowing freeway lanes and shoulders as a cost-effective mobility strategy. The objectives of this project were to develop improved macroscopic analysis tools, calibrate car-following models that capture narrowed lane driving behavior, conduct real-world case studies, develop narrowed lanes deployment recommendations, and investigate dynamic lane-narrowing technologies. The case studies showed that the lane-narrowing treatment improves mobility significantly without compromising safety.		
17. Key Words Lane narrowing, microscopic model calibration, dynamic narrow lane technologies, lane-narrowing treatments, lane design, high-occupancy vehicle lane	18. Distribution Statement No restrictions. This document is available to the public through the National Technical Information Service, Springfield, VA 22161. http://www.ntis.gov	

19. Security Classif. (of this report) Unclassified	20. Security Classif. (of this page) Unclassified	21. No. of Pages 150	22. Price N/A

Form DOT F 1700.7 (8-72) Reproduction of completed page authorized.

SI* (MODERN METRIC) CONVERSION FACTORS

APPROXIMATE CONVERSIONS TO SI UNITS

Symbol	When You Know	Multiply By	To Find	Symbol
		LENGTH		
in	inches	25.4	millimeters	mm
ft	feet	0.305	meters	m
yd	yards	0.914	meters	m
mi	miles	1.61	kilometers	km
		AREA		
in^2	square inches	645.2	square millimeters	mm^2
ft^2	square feet	0.093	square meters	m^2
yd^2	square yard	0.836	square meters	m^2
ac	acres	0.405	hectares	ha
mi^2	square miles	2.59	square kilometers	km^2
		VOLUME		
fl oz	fluid ounces	29.57	milliliters	mL
gal	gallons	3.785	liters	L
ft^3	cubic feet	0.028	cubic meters	m^3
yd^3	cubic yards	0.765	cubic meters	m^3
	NOTE: volumes greater than 1,000 L shall be shown in m^3			
		MASS		
oz	ounces	28.35	grams	g
lb	pounds	0.454	kilograms	kg
T	short tons (2,000 lb)	0.907	megagrams (or "metric ton")	Mg (or "t")
		TEMPERATURE (exact degrees)		
°F	Fahrenheit	5 (F-32)/9 or (F-32)/1.8	Celsius	°C
		ILLUMINATION		
fc	foot-candles	10.76	lux	lx
fl	foot-Lamberts	3.426	$candela/m^2$	cd/m^2
		FORCE and PRESSURE or STRESS		
lbf	poundforce	4.45	newtons	N
lbf/in^2	poundforce per square inch	6.89	kilopascals	kPa

APPROXIMATE CONVERSIONS FROM SI UNITS

Symbol	When You Know	Multiply By	To Find	Symbol
		LENGTH		
mm	millimeters	0.039	inches	in
m	meters	3.28	feet	ft
m	meters	1.09	yards	yd
km	kilometers	0.621	miles	mi
		AREA		
mm^2	square millimeters	0.0016	square inches	in^2
m^2	square meters	10.764	square feet	ft^2
m^2	square meters	1.195	square yards	yd^2
ha	hectares	2.47	acres	ac
km^2	square kilometers	0.386	square miles	mi^2
		VOLUME		
mL	milliliters	0.034	fluid ounces	fl oz
L	liters	0.264	gallons	gal
m^3	cubic meters	35.314	cubic feet	ft^3
m^3	cubic meters	1.307	cubic yards	yd^3
		MASS		
g	grams	0.035	ounces	oz
kg	kilograms	2.202	pounds	lb
Mg (or "t")	megagrams (or "metric ton")	1.103	short tons (2,000 lb)	T
		TEMPERATURE (exact degrees)		
°C	Celsius	1.8C+32	Fahrenheit	°F
		ILLUMINATION		
lx	lux	0.0929	foot-candles	fc
cd/m^2	candela/m2	0.2919	foot-Lamberts	fl
		FORCE and PRESSURE or STRESS		
N	newtons	2.225	poundforce	lbf
kPa	kilopascals	0.145	poundforce per square inch	lbf/in^2

*SI is the symbol for International System of Units. Appropriate rounding should be made to comply with Section 4 of ASTM E380. (Revised March 2003)

TABLE OF CONTENTS

EXECUTIVE SUMMARY 1
BACKGROUND AND MOTIVATION 1
RESEARCH PROJECT 1
PROJECT FINDINGS 2
CONCLUSIONS AND RAMIFICATIONS 2

CHAPTER 1. INTRODUCTION 5

CHAPTER 2. SYNTHESIS OF RESEARCH AND FINDINGS 9
OPERATIONAL EFFECTS 9
SAFETY EFFECTS 10
SIMILAR TREATMENTS 12
ANALYTICAL METHODS 13
CAR-FOLLOWING MODELS 13
CAR-FOLLOWING MODEL CALIBRATION 15
DYNAMIC LANE-NARROWING TECHNOLOGIES 15
SUMMARY 16

CHAPTER 3. DATA COLLECTION 17
MACROSCOPIC DATA COLLECTION 17
Data-Collection Approach 17
Site Overview 18
MICROSCOPIC DATA COLLECTION 20

CHAPTER 4. MODEL DEVELOPMENT 23
MACROSCOPIC MODEL DEVELOPMENT 23
HCM Basic Freeway Segments Overview 24
HCM Capacity Estimation 25
Field Data Results 25
FFS Regression Model Development 33
Example Applications of Macroscopic Model Development 34
Combined Effect of Narrow Lanes on Speeds and Capacities 39
Conclusions and Recommendations from Macroscopic Model Development 46
MICROSCOPIC MODEL DEVELOPMENT 47
Gipps Car-Following Model Development 47
Wiedemann 74 Car-Following Model Development 61
SAFETY MODEL DEVELOPMENT 82

CHAPTER 5. CASE STUDIES 93
SAFETY ANALYSIS 94
MACROSCOPIC MOBILITY ANALYSIS 99
Calculation of Benefits 100
Results 100
Worst-Case Scenario 100

MICROSCOPIC MOBILITY ANALYSIS 101
Gipps Model Case Studies 101
Wiedemann Model Case Studies 105
Analysis 117
CAPACITY IMPACTS OF LANE NARROWING 118
Macroscopic Field Data Analysis 119
Macroscopic Model Analysis 120
Gipps Model Analysis 120
Wiedemann Model Analysis 124
Secondary Macroscopic Model Analysis 126
Summary 126
CHAPTER 6. CONCLUSIONS 129
MODELING RESULTS: GENERAL 130
MODELING RESULTS: MACROSCOPIC 130
MODELING RESULTS: MICROSCOPIC 132
APPENDIX. GIPPS MODEL IMPLEMENTATION 133
REFERENCES 135

LIST OF FIGURES

Figure 1. Illustration. Addition of a lane via reduction of lane and shoulder widths. 5
Figure 2. Screenshot. Dynamic lane narrowing through changeable pavement markings. 7
Figure 3. Illustration. Microscopic data-collection process. 20
Figure 4. Graph. FFS versus lane width relationship. 28
Figure 5. Graph. Capacity versus lane width relationship. 29
Figure 6. Graph. FFS regression model sensitivity. 34
Figure 7. Graph. Speed–flow curve comparison for lane narrowing to 11-ft lanes. 37
Figure 8. Graph. Speed–flow curve comparison for lane narrowing to 10-ft lanes. 40
Figure 9. Charts. Charts depicting speed–flow observations and fitted curves. 46
Figure 10. Graphs. Headway histograms binned by speed ranges for all 12-ft lane width sites and each individual site with 12-ft lane widths. 51
Figure 11. Charts. Unfiltered speed–gap scatterplot and regression results for all 12-ft lane width sites and each individual site with 12-ft lane widths. 53
Figure 12. Charts. Filtered speed–gap scatterplot. 57
Figure 13. Charts. Hypothesis test regression results for the two sites with statistically significant effects on I-635 in Dallas, TX, and I-95 in Fort Lauderdale, FL. 60
Figure 14. Chart. Speed–density plot for 12-ft lane width observations. 65
Figure 15. Chart. Speed–flow plot for 12-ft lane width observations. 68
Figure 16. Chart. Calibration bounds plot for 12-ft lane width observations. 69
Figure 17. Chart. Speed–density plot for 11-ft lane width observations. 72
Figure 18. Chart. Speed–flow plot for 11-ft lane width observations. 74
Figure 19. Chart. Calibration bounds plot and 11-ft lane width observations. 75
Figure 20. Chart. Speed–density plot for 10-ft lane width observations. 77
Figure 21. Chart. Speed–flow plot for 10-ft lane width observations. 79
Figure 22. Chart. Calibration bounds plot for 10-ft lane width observations. 80
Figure 23. Graph. FI crashes versus hourly volume (four-lane to six-lane conversion). 88
Figure 24. Graph. FI crashes versus hourly volume (six-lane to eight-lane conversion). 89
Figure 25. Graph. FI crashes versus hourly volume (8-lane to 10-lane conversion). 89
Figure 26. Graph. PDO crashes versus hourly volume (four-lane to six-lane conversion). 90
Figure 27. Graph. PDO crashes versus hourly volume (six-lane to eight-lane conversion). 90
Figure 28. Graph. PDO crashes versus hourly volume (8-lane to 10-lane conversion). 91
Figure 29. Map. I-270 southbound case study conditions. 93
Figure 30. Map. I-580 eastbound case study conditions. 94
Figure 31. Map. I-270 case study site. 102
Figure 32. Map. I-580 case study site. 104
Figure 33. Map. Travel time and delay segment one, distance: 1.55 mi. 108
Figure 34. Map. Travel time and delay segment two, distance: 1.46 mi. 108
Figure 35. Map. Travel time and delay segment three, distance: 3.2 mi. 109
Figure 36. Map. Queue counter location. 110
Figure 37. Graph. I-270 link density by link (southbound links are 1–159, northbound links are 200–345). 111
Figure 38. Graph. I-270 flow rate by link (southbound links are 1–159, northbound links are 200–345). 112

Figure 39. Graph. I-270 speed by link (southbound links are 1–159, northbound links are 200–345). 113
Figure 40. Graph. I-270 relative delay by link (southbound links are 1–159, northbound links are 200–345). 113
Figure 41. Graph. I-270 speed by link under increased demand. 116
Figure 42. Graph. Baseline throughput time series (Gipps model) for I-270. 122
Figure 43. Graph. Throughput time series for 11-ft lane scenario (Gipps model) with 5-mi/h speed limit decrease. 123
Figure 44. Graph. Throughput time series for 10-ft lane scenario (Gipps model) with 5-mi/h speed limit decrease. 124
Figure 45. Graph. Throughput time series (Wiedemann model). 125
Figure 46. Graph. Reaction time versus freeway capacity. 134

LIST OF TABLES

Table 1. Site summary for macroscopic data collection. 19
Table 2. Adjustment to FFS for average lane width for basic freeway and multilane highway segments (reprinted from the Sixth Edition of the HCM, exhibit 12-20). 24
Table 3. Adjustment to FFS for f_{RLC} for basic freeway segments (reprinted from the Sixth Edition of the HCM, exhibit 12-21). 25
Table 4. Summary of speeds and capacities under ideal conditions. 27
Table 5. Average capacities (pc/h/ln) by lane width and segment type. 29
Table 6. CAFs by lane width and segment type. 29
Table 7. Capacities (pc/h/ln) and CAFs by speed limit. 30
Table 8. Recommended CAFs by lane width. 30
Table 9. Average FFSs (mi/h) by lane width. 31
Table 10. SAFs and CAFs for events interfering with speed and capacity (incidents or bad weather). 32
Table 11. FFS regression model results. 33
Table 12. FFS and capacity estimation for Dallas US 75 at 15th Street (southbound). 42
Table 13. FFS and capacity estimation for Hawaii H-1 at SL-71 (westbound). 42
Table 14. FFS and capacity estimation for Dallas US 75 at Galatyn South (northbound). 42
Table 15. Dallas US 75 at Renner (southbound). 43
Table 16. FFS and capacity estimation for San Antonio I-10 at LCU-0010E-574.114 (eastbound). 43
Table 17. Data-collection sites summary. 49
Table 18. Model calibration results using weighted linear squares regression (12-ft lanes). 55
Table 19. Model calibration results using weighted linear squares regression (11-ft lanes). 55
Table 20. Model calibration results using weighted linear squares regression (10-ft lanes). 55
Table 21. Combined data for 12-ft lane width observations. 67
Table 22. Combined data for 11-ft lane width observations. 73
Table 23. Combined data for 10-ft lane width observations. 78
Table 24. Site-specific Wiedemann results. 81
Table 25. Summary of geometric scenarios for the lane-narrowing safety model. 82
Table 26. Estimated FI crash reductions on I-270. 95
Table 27. Estimated FI crash reductions versus no-build on I-270. 95
Table 28. Estimated crash benefit versus no-build on I-270. 95
Table 29. Estimated PDO crash reductions on I-270. 96
Table 30. Estimated PDO crash reductions versus no-build on I-270. 96
Table 31. Estimated PDO crash benefit versus no-build on I-270. 96
Table 32. Estimated FI crash reductions on I-580. 97
Table 33. Estimated FI crash reductions versus no-build on I-580. 97
Table 34. Estimated FI crash benefit on I-580. 97
Table 35. Estimated PDO crash reductions on I-580. 97
Table 36. Estimated PDO crash reductions versus no-build on I-580. 98
Table 37. Estimated PDO crash benefit on I-580. 98
Table 38. Crash impacts holding traffic volumes constant per lane. 99
Table 39. Gipps model case study scenarios. 102
Table 40. Network statistics for the I-270 simulated case study scenarios. 103

Table 41. Network statistics for the I-580 simulated case study scenarios. 104
Table 42. Base model scenarios based on Maryland model. 106
Table 43. Lane-specific delay percentages at hotspot number one. 111
Table 44. Lane-specific delay change percentages at hotspot number one. 111
Table 45. Lane-specific speeds (mi/h) at hotspot number two. 114
Table 46. Lane-specific speed changes (mi/h) at hotspot number two. 115
Table 47. Lane-specific relative delay percentages at hotspot number two. 116
Table 48. Lane-specific relative delay percentage changes at hotspot number two. 116
Table 49. Throughput (veh/h) for key case study scenarios. 117
Table 50. Macroscopic model sensitivity analysis adjusting number of lanes from four to five. 120
Table 51. Macroscopic model sensitivity analysis adjusting number of lanes from three to four. 121
Table 52. Prebreakdown capacity (Wiedemann model). 126
Table 53. Estimated capacity impact (four- to five-lane and 65- to 55-mi/h speed limit conversion). 127

LIST OF ABBREVIATIONS

ADT	average daily traffic
BCA	benefit–cost analysis
CAF	capacity adjustment factor
Caltrans	California Department of Transportation
CAV	connected and automated vehicle
CDOT	Colorado Department of Transportation
CMF	crash modification factor
DOT	department of transportation
FAA	Federal Aviation Administration
FFS	free-flow speed
FHWA	Federal Highway Administration
FI	fatal-and-injury
GPS	global positioning system
HCM	*Highway Capacity Manual Sixth Edition: A Guide for Multimodal Mobility Analysis*
HOV	high-occupancy vehicle
HSM	*Highway Safety Manual*
HSR	hard shoulder running
LCU	local control unit
NCHRP	National Cooperative Highway Research Program
NPV	net present value
O&M	operations and maintenance
pc/h	passenger cars per hour
pc/h/ln	passenger cars per hour per lane
PDO	property-damage-only
PeMS	Caltrans Performance Measurement System
PTSU	part-time shoulder use
RITIS	Regional Integrated Transportation Information System
RMSE	root-mean-square error
ROI	return on investment
SAF	speed adjustment factor
SHRP2	second Strategic Highway Research Program
SPF	safety performance function
UAV	unmanned aerial vehicle
USDOT	United States Department of Transportation
v/c	volume-to-capacity
veh/h	vehicles per hour
veh/h/ln	vehicles per hour per lane
veh/mi	vehicles per mile

EXECUTIVE SUMMARY

BACKGROUND AND MOTIVATION

The Federal Highway Administration (FHWA) is pursuing several solutions intended to mitigate congestion on our Nation's roadways by improving mobility and safety. An example of a cost-effective strategy FHWA is currently investigating is the narrowing of freeway lanes and shoulders widths. In this strategy, agencies narrow freeway lane widths (e.g., from 12 to 10.5 ft wide) in the vicinity of a freeway bottleneck. Narrowing lanes and shoulders creates the necessary lateral space to add another narrow freeway lane, provided that the agency also converts a portion of the initial shoulder width to support a general purpose travel lane. Some States have already implemented the lane-narrowing strategy to reduce congestion at recurring bottleneck locations. As such, there is a growing need to predict the impacts of such conversions on a roadway's mobility and safety performance.

Speeds are typically lower when lanes are narrow because it is more difficult for drivers to maintain their position within a lane. However, the hope is that the addition of a new lane will consistently increase overall capacity without producing unsafe driving conditions. According to the basic principles of traffic flow, flow—or throughput—is the product of density and speed. Thus, lower speeds will likely result in lower per-lane throughput. However, the team hypothesized that, despite this per-lane reduction in throughput, the overall corridor might see an increase in throughput attributable to the additional lane(s). Despite the positive outcomes of some treatments across the nation, lane narrowing may not be feasible in some areas due to extenuating circumstances (e.g., large numbers of heavy vehicles, sharp horizontal curvatures). Moreover, agencies must consider the possibility of activating nearby "hidden" bottlenecks, as this could negate any benefits from the treatment.

RESEARCH PROJECT

Some prior studies evaluated the operational and safety impacts of lane narrowing, but these studies appear to be outdated and oversimplified. The five objectives of this project were as follows:

- Develop improved macroscopic analysis methods (i.e., *Highway Capacity Manual Sixth Edition: A Guide for Multimodal Mobility Analysis [*HCM*]*) to predict the impacts of narrowed freeway lanes (Transportation Research Board 2016).
- Calibrate microsimulation models to accurately reflect changes in driving behavior attributable to narrowed freeway lanes.
- Conduct real-world case studies using macroscopic and microscopic tools to assess mobility and safety impacts of narrowed freeway lanes.
- Develop multiobjective (i.e., operations and safety) recommendations surrounding the deployment of narrowed freeway lanes.
- Conduct a preliminary investigation of dynamic lane-narrowing technologies.

The first phase of the project involved a review of relevant existing literature and findings. The available material implied that lane narrowing on freeways generally produces positive mobility

benefits without undue safety effects. To confirm the findings in the literature, the team planned to develop an HCM model from sensor data, derive a safety model using *Highway Safety Manual* (HSM) methods, and calibrate microsimulation models from high-resolution vehicle data collected aerially (AASHTO 2014). Initially, the team planned to calibrate both the car-following and lane-changing models within the microsimulation model. However, the aerially collected trajectories did not capture sufficient lane-changing behavior to support the calibration of lane-changing models. Thus, the team dropped calibrating lane-changing models from the research plan and focused resources on developing calibrated car-following models.

PROJECT FINDINGS

The HCM model development was straightforward, though not without a few challenges. For example, some speed reductions could not be solely attributable to lane width (i.e., may have been caused by queue spillback). Additionally, sensor data were not available for all desired combinations of lane width and speed limit. The safety model development produced a set of convenient nomographs but was derived entirely from the HSM and not based on any new data collection. The car-following model calibration involved the use of filtered data for the Gipps model and unfiltered data for the Wiedemann 74 model. This is because the simplified form of the Gipps model used for this project is valid only during steady-state car-following; thus, the team discarded vehicle trajectory data points associated with nonsteady state conditions (i.e., large accelerations, decelerations, or headways). By contrast, the Wiedemann 74 model calibration applied all data points (i.e., unfiltered) for model calibration, applying a well-documented methodology published by Rakha and Gao (2010). For the Gipps car-following model, average reaction times are shorter on narrow lane segments, indicating that drivers are more attentive while traversing a narrowed lane segment. For the Wiedemann 74 car-following model, average headways are larger on narrow lane segments, possibly suggesting more conservative driving behaviors. The team did not consider these results contradictory. It stands to reason that drivers, reasonably behaving more cautiously and being more attentive as lanes narrow, could exhibit both lower reaction times and longer headways under these conditions.

The project's case studies, which exercised the newly developed HCM-compliant model and newly calibrated car-following models, supplied more evidence that the lane-narrowing treatment improves mobility without compromising safety. Predicted mobility benefits from the macroscopic HCM model, Gipps model, and Wiedemann 74 model were all consistent. Predicted safety impacts were minimal according to the HSM-based nomographs.

CONCLUSIONS AND RAMIFICATIONS

The lane-narrowing strategy reduces vehicle speeds at freeway bottlenecks. The research team observed that lane narrowing produces a de facto speed harmonization strategy (i.e., even without the additional freeway lane, the lane-narrowing treatment appears to improve mobility). Furthermore, increasing the headways between vehicles at freeway bottlenecks appears to provide more opportunities for lane changing at merge locations. Given the cumulative benefits of speed harmonization, smoother merge maneuvers, and added lane capacity, the lane-narrowing strategy appears to be even more positively impactful on mobility than was initially believed.

Scenario analyses revealed that most mobility benefits, such as improved travel speeds, diminish if the mobility benefits induce sufficient demand (i.e., demand increases to match new capacity). However, even in this worst-case scenario, throughput on the facility is net positive. Based on the research conducted as part of this project, the team recommends that agencies consider lane narrowing as a potential cost-effective congestion-mitigation strategy.

CHAPTER 1. INTRODUCTION

Unnecessary traffic delays and vehicle emissions produce adverse impacts on quality of life. The 2017 *Urban Mobility Report* summarizes how the Nation's economy drives traffic problems (Schrank, Eisele, and Lomax 2017). *Traffic Congestion and Reliability: Linking Solutions to Problems* established that bottlenecks are a significant cause of traffic congestion and that recurring bottlenecks are the single largest source of traffic congestion (Cambridge Systematics, Inc. and Texas Transportation Institute 2004). Thus, mitigating or eliminating bottlenecks is a top priority for reducing traffic congestion in the United States.

Hale et al. (2016) focused on low-cost, deployment-ready congestion mitigation and examined solutions involving dynamic lane use, contraflow or reversible lane use, hard shoulder lane use, lane width reduction, and modest extensions of auxiliary lanes. These solutions produced significant operational benefits, with only minor modifications to existing infrastructure. Hale et al. (2016) also provided design guidance on signing, signalization, and striping for these strategies. Finally, Hale et al. (2016) included benefit-cost analyses (BCAs) for the featured strategies.

One of the strategies in Hale et al. (2016)—lane width reduction—was particularly interesting to the Federal Highway Administration (FHWA), which motivated this follow-up research. This report focuses on developing a more rigorous, modernized evaluation of the lane width reduction strategy. On congested freeway segments, a reduction of lane widths across all lanes provides a valuable amount of new space for adding a brand-new lane. For example, suppose a congested freeway has four 12-ft lanes in one direction, plus a 10-ft shoulder. If the governing agency converted this cross section to a configuration having five 10.5-ft lanes and a 5.5-ft shoulder (figure 1), the availability of the additional lane could provide significant congestion relief without requiring expensive construction to widening the roadway. This approach to bottleneck mitigation, henceforth referred to as the lane-narrowing strategy, has provided real-world congestion relief in California, Florida, Hawaii, Texas, and Washington. In this report, any cross-sectional width smaller than the HCM-recommended 12-ft lane width (e.g., 10-, 10.5-, and 11-ft lane widths) are considered lane-narrowing treatments. Typically, some amount of shoulder width reduction is needed to avoid additional construction.

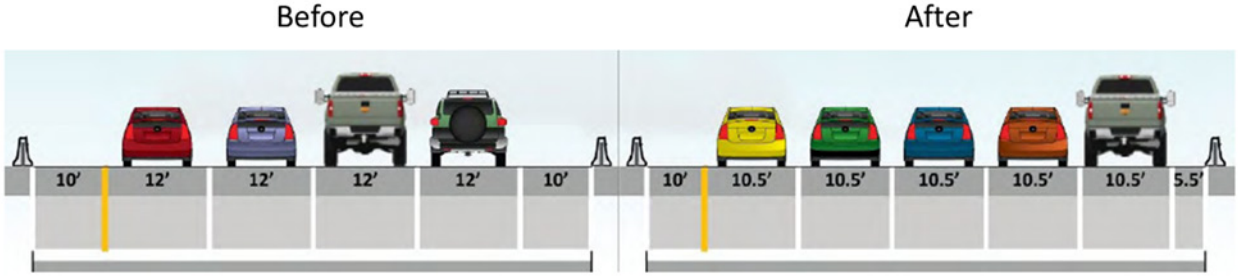

Source: FHWA.

Figure 1. Illustration. Addition of a lane via reduction of lane and shoulder widths.

A limited number of studies have evaluated the operational and safety impacts of lane narrowing, but these studies appear to be outdated and oversimplified. The goal of this project was to

develop improved macroscopic and microscopic analysis methods for assessing the impact of lane narrowing on freeways. The research team developed the improved macroscopic methods using the existing HCM models to predict facility free-flow speed (FFS) and capacity. The developed microscopic methods involved the calibration of car-following models in commercial microsimulation software packages. The project scope further required real-world case studies for these new models, the development of multiobjective (i.e., operations and safety) recommendations, and a preliminary investigation of dynamic lane-narrowing technologies.

In the literature, there is consensus that narrower lane widths lead to reduced average travel speeds. Using the basic properties of traffic flow, one can conclude that this is likely to lead to diminished per-lane capacities. However, the narrowed lane width enables the addition of a new travel lane. The capacity added by the additional narrow lane, albeit smaller than what would be added by an additional standard sized lane, may potentially be larger than the capacity reduction caused by reduced speeds across all the lanes. If true, this would mean that the facility gains overall capacity. Simulation studies described in Hale et al. (2016) estimated that, while the addition of a new 12-ft lane could reduce freeway delays by 43 percent, the addition of a new 10-ft lane would reduce freeway delays by 21 percent. In these simulation experiments, the researchers simulated the narrow lane effects through an assumed speed reduction stated in the HCM. Using 12-ft lanes as a baseline, reduced speeds of 2 and 7 mi/h applied for 11- and 10-ft lanes, respectively.

Although the above simulation results and analytical HCM-based results are intuitive, they may not be robust. One weakness of Hale et al. (2016) is that it assumed identical car-following and lane-changing behaviors on all freeways, regardless of lane width. Although different lane widths will likely produce different car-following and lane-changing behaviors among drivers, this assumption was necessary because no high-resolution data were available to calibrate models at different lane widths. Moreover, according to Roess and Prassas (2014), the HCM lane width adjustment factors for basic freeway segments—used in Hale et al. (2016) to determine the speed reduction in reduced lane width areas—are outdated, judgmental, and based on low-speed multilane highway observations. Thus, although the lane width reduction strategy showed benefits in Hale et al. (2016), more rigorous analysis is needed before recommending the deployment of this strategy. The emergence of lane narrowing as a top congestion relief strategy motivated the need for this project and report. These products will address a modernized set of analytical and simulation models designed to predict the effects of lane narrowing on traffic flow efficiency.

Although the new analytical and simulation models represent the core project objective, this project cannot ignore accompanying issues. The first is safety. At the outset of this project, the impact of narrower lanes on traffic safety was an open question. The safety impact could potentially be affected by numerous factors (e.g., congestion levels, weather, the percentage of heavy vehicles). A limited number of prior research efforts examined the impacts of narrower lanes on safety; however, the impacts seemed challenging to predict due to complex, interacting factors.

This project conducted a thorough investigation into the safety impacts of narrowed freeway lanes and shoulders as the foundation for providing multiobjective recommendations for when and where to implement narrow lanes. The team also investigated dynamic lane-narrowing

technologies. Such technologies would allow agencies to operate this treatment only during peak periods of congestion; the dynamic nature of the treatment would enable a return to standard lane widths during off-peak periods, as illustrated in figure 2. This treatment would differ from the current practice of permanently striping lanes to a narrower width, which could potentially create less safe driving conditions during off-peak periods when traveling speeds are higher.

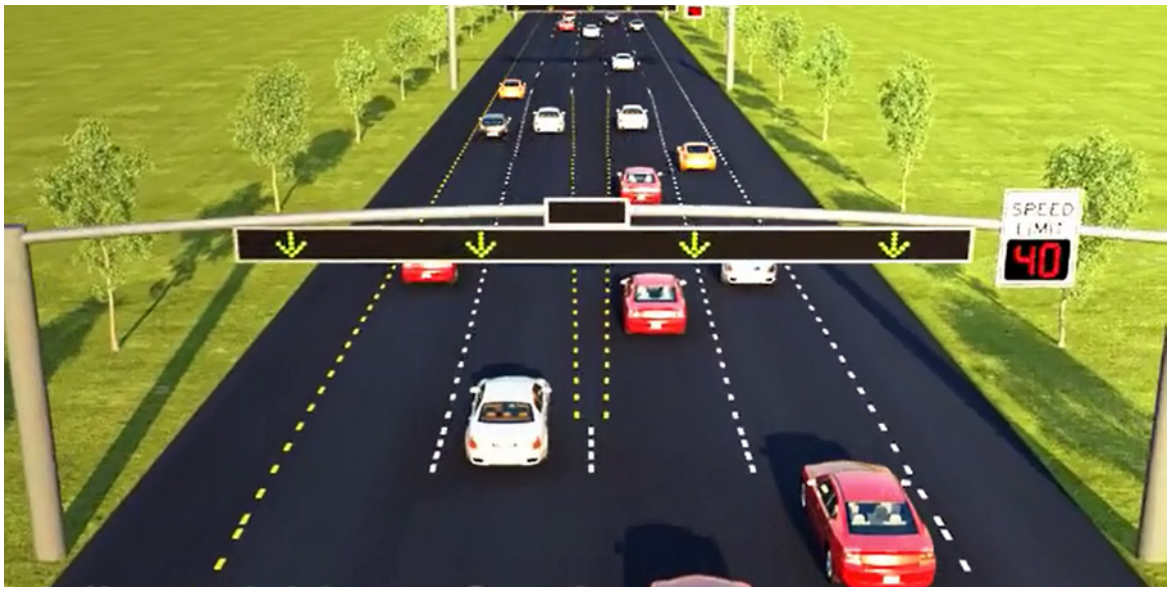

Figure 2. Screenshot. Dynamic lane narrowing through changeable pavement markings.

CHAPTER 2. SYNTHESIS OF RESEARCH AND FINDINGS

At the outset of this project, the team conducted a review and synthesis of relevant research and findings, also known as a state-of-the-practice review. This report uses the term "findings" to convey that some of the most valuable information in this area is only available through practitioners and real-world implementations, as opposed to traditional literature sources. As such, the team performed outreach to various information sources and individuals, in addition to traditional reviews of literature.

OPERATIONAL EFFECTS

According to most research and findings, lane narrowing that facilitates the addition of a new lane is beneficial in terms of improving traffic flow efficiency. Neudorff et al. (2016) and Hale et al. (2016) reported this improved efficiency in terms of increased throughput, increased capacity, reduced delay, and reduced travel times. Not surprisingly, average FFSs sometimes decrease (e.g., from 65 to 55 mi/h), which may not be considered an improvement by everyone (Waard et al. 1995; Dixon et al. (2015)). Waard et al. (1995) wrote that narrow roads make drivers work harder to maintain driving within their lane, which eventually leads them to decrease their speeds. However, reduced travel speeds caused by narrower lanes could enable other benefits, such as reduced emissions, reduced accident severity, and easier lane changing. Moreover, when the lane addition eliminates a severe bottleneck, peak-period average speeds may increase from stop-and-go levels (e.g., 10 mi/h) to more functional levels (e.g., 40 mi/h). These benefits could also reduce emissions, which are typically minimized at speeds in the 30–40 mi/h range.

FHWA funded the development of a primer on narrow lane impacts (Neudorff et al. 2016). The primer reports that the addition of a new lane due to narrowed individual lanes produced significant traffic flow improvements at most real-world implementations (i.e., Houston, TX; Los Angeles, CA; Miami, FL; and Seattle, WA). At one of the Houston, TX, narrow lane sites, operations did not improve. Neudorff et al. (2016) suggested that this was because a hidden bottleneck was activated (i.e., the location of the bottleneck was merely shifted). The primer further noted that, according to the HCM, reducing lane width from 12 to 10.5 ft and shoulder width to 4 ft would reduce FFS by 10 mi/h. This speed reduction would have the effect of reducing lane-specific capacity by 4.2 percent, from 2,350 to 2,250 vehicles per hour per lane (veh/h/ln). However, as mentioned in chapter 1, the HCM lane width and lateral clearance models are not trusted by experts, and this project attempts to modernize those models.

Fitzpatrick, Dixon, and Avelar (2016) and Dixon et al. (2015) also conducted recent studies on narrow lane impacts. These studies primarily focused on freeway facilities with 11-ft lane widths in Dallas, TX; Houston, TX; and San Antonio, TX. The findings related to shoulder width were mixed. Fitzpatrick, Dixon, and Avelar (2016) found that shoulder widths have a significant impact on narrow lane speeds, but not on 12-ft lane speeds. Dixon et al. (2015) found that left shoulder width has a significant impact on speed, but right shoulder width does not. However, the findings related to traveling speed were consistent with documented effects in the HCM. Specifically, Dixon et al. (2015) found that the FFS reductions caused by 11-ft lanes were approximately 2 mi/h, similar to the HCM.

Other researchers have reported related findings. Rosey et al. (2009) concluded that lane width impacts are probably affected by shoulder configuration. Ben-Bassat and Shinar (2011) claimed that shoulder width is less critical than the distance to the nearest roadside object (e.g., a guardrail). Stamatiadis et al. (2009) speculated that wider shoulders provide a security buffer, which can reduce speed reductions within narrow lane corridors.

Therefore, based on the other studies referenced, the authors concluded the following:

- Reducing lane widths from 12 to 11 or 10 ft would reduce drivers' FFSs.
- This FFS reduction would be magnified by smaller shoulder clearances, especially if there is a nearby roadside object.
- The exact amount of FFS reduction is unknown, but the amount may increase exponentially as lane widths drop below 11 ft.
- Nominally, a 2 mi/h FFS drop for 11-ft lanes can be assumed if the shoulder clearance is at least 10 ft.
- According to most research and findings, lane narrowing that facilitates the addition of a new lane is significantly beneficial in terms of improving traffic flow efficiency.

SAFETY EFFECTS

As stated in chapter 1, the safety impact of narrow lanes is potentially affected by numerous factors (e.g., congestion levels, weather, the percentage of heavy vehicles). A limited number of prior research efforts examined the impacts of narrower lanes on safety; however, due to complex interacting factors, the impact appears challenging to predict. This project conducted a thorough investigation into safety impacts as part of the goal of providing multiobjective recommendations for when and where to implement narrow lanes.

The richest source of material appears to be the HSM, whose lane width methodology was derived from National Cooperative Highway Research Program (NCHRP) Report 17-45 (Bonneson et al. 2012). According to Bonneson et al. (2012), blanket statements about narrow lane safety impacts cannot be made. Although it is possible that many factors (e.g., weather, heavy vehicles, shoulder clearance) could intervene, it appears that transitioning from near-capacity to under-capacity conditions could reduce crashes in some cases. Similarly, transitioning from severely oversaturated to at-capacity conditions could slightly increase crashes, although this could simply reflect drivers' ability to start moving again. Overall, it appears that safety would not rule out the lane-narrowing approach to bottleneck mitigation in many cases. FHWA (2014) summarized some exceptions to this, including low speed limit compliance, excess roadway curvature, and high numbers of heavy vehicles.

Neudorff et al. (2016) reported some favorable safety impacts. Specifically, based on HSM-style crash prediction analysis, narrow lanes and shoulders would improve safety and reduce crashes on I-94 in Milwaukee, WI. Moreover, the observed crash rate in Seattle, WA, was significantly reduced after lanes and shoulders were narrowed. However, Neudorff et al. (2016) noted that narrow lanes and shoulders may require design exceptions (e.g., inadequate sight distance), and incident clearance times are much longer when shoulders are not exclusively available to emergency vehicles. Potts, Harwood, and Richard (2007) reported that narrow lane widths (down to 9 ft) had no negative safety impacts, but their study was conducted on signalized

arterials instead of freeways. In a 1987 California study, Urbanik and Bonilla (1987) found that inside shoulder removals either produced no significant change in overall accident rates or achieved a significant reduction in overall accident rates.

Other studies were more pessimistic. Dixon et al. (2015) stated that narrow lanes and shoulders produce more crashes than standard-width lanes. Bauer et al. (2004) concluded that lane narrowing to add a new lane might have a negative safety impact, either increasing crashes by 10 percent or migrating accidents to one or more hidden bottleneck locations (as a result of eliminating the subject bottleneck location).

This project developed an easy-to-use safety prediction model for the lane-narrowing strategy for bottleneck mitigation. This safety prediction model is primarily based on methods outlined in HSM (chapter 18) and NCHRP Report 17-45. In cases of very small shoulder clearance, this safety prediction model might predict relatively high crash rates under a narrowed lane configuration. The safety prediction model developers noted that HSM chapter 18 does not mention the effects of heavy vehicles, FFSs, or posted speed limits, even though these factors would likely influence crash predictions. When this question was posed to the NCHRP Report 17-45 principal investigator, James Bonneson, he provided the following explanation:[1]

> Correct, HSM chapter 18 does not include input variables that describe heavy vehicle effects, free-flow speed, and posted speed. These limitations are true for all of the HSM Part C methodological chapters. It reflects the fact that safety prediction methods are empirically based regression models using data representing one or more years (contrast this to most operations model that often have theoretic constructs that are calibrated using field measurements for time periods measured in minutes or hours). As a result, the formulation of safety prediction models is based on the information available in agency crash reports, automatic traffic recorder data, and road infrastructure inventory databases. These agency-based characteristics of safety data limit the sophistication of safety prediction models to the data that agencies are willing to collect. For chapter 18, the speed variables you are interested in were not available in the databases provided by the participating States (i.e., Maine, Washington, California). The data for Washington and California included annualized truck percentage estimates, but the associated database documentation indicated that these percentages were rough estimates. Maine did not include truck percentage. As a result, we were not able to confidently look at speed or heavy vehicles effects for chapter 18. Data for the three aforementioned States were used in the project because they were the only three States that make their data available to researchers (through the FHWA Highway Safety Information System) and that have data for interchange ramps. In short, the models in chapter 18 went as far as the available data allowed. This outcome is also true of the other HSM Part C models.

As such, under boundary conditions like high heavy vehicle percentages, sharp horizontal curvature, or high posted speed limits, an agency might be appropriately skeptical of the safety impacts of lane narrowing based on professional engineering judgment. However, given the full

[1]Personal interview conducted with J. Bonneson on June 8, 2017.

set of research and findings, it still appears that safety considerations would not rule out the lane-narrowing bottleneck mitigation strategy in many, or most, cases.

SIMILAR TREATMENTS

Some insight into the potential effectiveness of lane narrowing may be found through similar treatments and conditions like hard shoulder running (HSR) and work zones, which typically have temporarily implemented suboptimal lane widths. In HSR, drivers are faced with reduced shoulder clearances and traveling heavily on pavement that was perhaps not originally designed for full-time travel. Some of this pavement may have been "refurbished" to support increased use. HSR is also similar to lane narrowing in the sense that, although HSR has brought demonstrable capacity increases to certain corridors, these capacity increases have not matched the level of increase that would have been achieved by simply widening the freeway. Regarding work zones, these sections of freeway often contain similar challenges for drivers. Lane widths and shoulder clearances often become limited, and speeds and capacities are degraded in comparison to conventional mainline segments.

Margiotta et al. (2014) found that shoulder lane capacities range from 1,250 veh/h/ln for a low-quality hard shoulder to 1,700 veh/h/ln for a high-quality hard shoulder. According to Thomas (2003), the Netherlands HSR implementation produced significant congestion and accident density reductions. Technologies they applied include embedded in-road sensors and variable message signs to control access. Shahin, Engelmann, and Friedrich (2003) found that, at HSR sites, temporal restrictions and signed speed limits are often disregarded. This may be a helpful warning for narrow lane segments where speed limits could be lowered and where temporal restrictions may someday be applied (i.e., in conjunction with dynamic lane narrowing). However, according to Chase and Avineri (2008), driver education may be helpful for HSR and similar treatments. Lane narrowing is a similar treatment, and it stands to reason that driver education could potentially help to improve traffic efficiency and/or safety.

Another term for HSR is part-time shoulder use (PTSU). In a webinar conducted by representatives of the Colorado Department of Transportation (CDOT), the presenters reported that CDOT appreciates the operational improvements made possible by PTSU but discourages PTSU during off-peak periods (Rice and Lee 2016). This finding is consistent with this project's motivation to pursue dynamic lane-narrowing technologies, which could revert to conventional lane widths during off-peak periods.

Regarding work zones, researchers' findings were similar to those from standard freeway facilities having narrow lanes. For example, driving simulator results from Petzoldt et al. (2016) showed that narrow passing lanes did not influence participants' willingness to pass slower vehicles in work zones, but did produce lower mean speeds. Chitturi and Benekohal (2005) determined that a lack of lateral clearance tends to reduce average speeds by 6 mi/h in work zones. Chitturi and Benekohal (2005) also found that narrow lanes have a greater impact on heavy vehicle FFS than on passenger car FFS.

In summary, observations of HSR and work zones in various areas imply that the lane-narrowing strategy has positive potential despite the modest reductions in lane-specific capacity. However, some important lessons should be taken into account, including the following:

- Driver education could help to improve traffic efficiency and/or safety when lane-narrowing treatments are implemented.
- Signed speed limits may be disregarded without education or other coercive measures.
- FFS reductions are probably magnified when percentage of heavy vehicles is high and lateral clearances are reduced.

ANALYTICAL METHODS

The HCM is believed to be the primary resource for analytical analysis and prediction of freeway capacities, speeds, densities, and other measures. However, Roess and Prassas (2014) claimed that HCM lane width adjustment factors for basic freeway segments were outdated, judgmental, and based on low-speed multilane highway observations. The emergence of lane narrowing as a top congestion relief strategy motivated this project's effort to redevelop these adjustment factors. In the HCM, lane width and shoulder width (lateral clearance) affect the FFS of basic freeway segments (Transportation Research Board 2016). Chapter 12 of the HCM presents equations of FFS for these segments. According to Roess and Prassas (2014), these adjustment factors are judgmental and based on multilane highway segments data with lower FFSs. The 1996 Edition of the HCM first presented these adjustment factors, which means that data are more than 20 yr old. The HCM also states that narrow lanes or low lateral clearances may affect basic freeway segment capacities. To produce more accurate predictions, the HCM recommends the use of capacity adjustment factors (CAFs) to calibrate for local conditions. However, the document provides no further guidance. Thus, the HCM analytical model development effort in this project needs to focus on incorporating lane width and lateral clearance effects in existing methods, as the literature does not adequately address this.

Melo et al. (2012) evaluated the effect of lane and shoulder width variation using a driving simulator. A logistic regression model was proposed to establish a relationship between FFS, lane width, shoulder width, and other variables. The analysis results indicated that both lane width and shoulder width affect FFS. Moreover, the interaction between the effects of these two parameters is not cumulative, in contrast to what the HCM suggests. Note that the data used in this paper are for two-lane highways, not freeways. Additionally, the authors relied on data collected in Europe (Portugal), where different geometric and environmental characteristics and driver behaviors apply. Other HCM studies in the literature found minor differences in the HCM predicted speed effects and field-measured effects.

In summary, the HCM adjustment factors for narrow lanes and shoulders are generally not considered reliable. As such, the emergence of lane narrowing as a congestion relief strategy is motivating the redevelopment of this method.

CAR-FOLLOWING MODELS

Car-following models are a type of stimulus-response model that the transportation modeling community has studied since the 1950s (Brackstone and McDonald 1999). These models use drivers' perceptions (e.g., time gap, relative velocity, following distance, lead vehicle speed) as input and output drivers' longitudinal behavioral decisions (e.g., acceleration, updated position, updated velocity) (Raney 1994; Brackstone and McDonald 1999; Rothery 2001; Toledo 2007; Sauifuzzaman and Zhang 2014; and Hammit 2018).

As summarized by Rothery (2001), the following are the four primary reasons for studying car-following behavior:

- Studying car-following models provides a means to better understand actual driver behavior.
- Understanding individual vehicle movements is critical for understanding macroscopic traffic flow.
- Capturing projected throughput to better understand the impacted of car-following behaviors on this performance metric.
- Understanding human driving behavior helps inform improved models of automated vehicle behavior.

Transportation researchers have developed numerous car-following models over the last 70 yr. Numerous studies have documented the importance of capturing inter- and intradriver heterogeneity in car-following behavior (James 2019). This project is a contribution to the literature because it studies how drivers alter their behavior because of the driving environment (i.e., varying lane width), which contributes to the transportation modeling community's understand of intra-driver heterogeneity.

During 2016 and 2017, FHWA hosted a series of roundtables as part of a National Capability Assessment in Traffic Analysis Fundamentals. An unpublished summary of the results of the roundtables revealed that there are five primarily used microscopic simulation tools in the traffic analysis tools community[2]. This insight, in combination with the team's levels of expertise with various traffic analysis tools, motivated the decision to calibrate the Wiedemann 74 and Gipps car-following models as part of this project. Additionally, the selected car-following models are significantly different from one another—a psychophysical and a safety-distance model; these model differences enable a comprehensive exploration of the impact of lane width on car-following behavior.

The Wiedemann 74 model is a psychophysical model, which seeks to capture natural oscillations in car-following models attributable to human perception limits (Wiedemann 1974). On the relative speed–relative spacing plane, the Wiedemann 74 model has four distinct regimes of car-following behavior: free driving, approaching, following, and emergency braking. Each of these regimes is defined by different governing equations and parameters. The Wiedemann 74 model produces the driver's acceleration behavior as output.

By contrast, the Gipps model is a safety-distance or collision-avoidance model that produces a prediction of driver behavior such that the following vehicle can safety react to the leading vehicle should that vehicle decide to come to an abrupt stop (Gipps 1981). Unlike the Wiedemann 74 model, which is based on driver perception, the Gipps model uses all physically measurable parameters.

[2] *Outcomes Memorandum for 2017 Virtual Roundtables* (unpublished).

CAR-FOLLOWING MODEL CALIBRATION

Car-following models used in microsimulation may be calibrated to match real-world vehicle trajectories. One way to obtain vehicle trajectories is from aerial imagery. In their paper on aerial imagery from low-flying unmanned aerial vehicles (UAVs), Babinec and Apeltauer (2016) concluded that the best camera position to optimize both accuracy and coverage is 400 ft. directly above the scene center. United States legal restrictions against flying UAVs directly over traffic posed a challenge for the team because the team believed human-operated helicopter data collection at more than one site would be cost-prohibitive. Kesting and Treiber (2008) compared different methods for acquiring trajectory data, such as low-altitude helicopters, vehicles instrumented with a global positioning system (GPS), radar, and lidar detection. For this project, the team believed data collection via instrumented vehicles at more than one site would be cost-prohibitive. Moreover, no simple process exists for obtaining numeric vehicle trajectory data from such vehicles. This effectively ruled out the work-zone-specific car-following model development strategies pursued by Brockfeld, Kühne, and Wagner (2005); Lochrane (2014); and Berthaume (2015). The expense of helicopter-collected data ruled out the data-collection method used by Wang et al. (2010).

The team originally considered the use of archived vehicle trajectory data. These sources included the 0.1 s resolution Next Generation Simulation data, and the second Strategic Highway Research Program (SHRP2) Naturalistic Driving Study data. However, these sources did not contain any archived data associated with existing narrow lane treatment sites in the United States. This lowered the priority of available archived data-related research (e.g., from Barceló, Casas, and Funes [2006]; Chen et al. [2010]; Zheng, Suzuki, and Fujita [2012]; and Treiber and Kesting [2013]) in the context of data collection, although their lessons learned could still be considered in the context of car-following model development.

Some studies evaluated the accuracy of existing car-following models (Casas and Lenorzer 2009; Chandler, Herman, and Montroll 1958; Fritzsche 1994; Gazis, Herman, and Rothery 1961; Gipps 1981; Newell 2002; Ossen, Hoogendoorn, and Gorte 2006; Tampère 2004; and Treiber, Hennecke, and Helbing 2000). The team was skeptical as to whether these sources could inform their car-following model development process. Other literature related to trajectory-based car-following model calibration was more promising (Li, Chen, and Zhang 2016; Ossen and Hoogendoorn 2005; Ossen and Hoogendoorn 2008; Punzo and Simonelli 2005; Ranjitkar, Nakatsuji, and Asano 2004; and Hammit 2018). When the narrow lanes simulation developers were asked about whether their approach to car-following model calibration would be influenced by any literature source, or documented within any literature source, they noted that many of the techniques they use are those commonly in use and reported in those references. Therefore, the technique used on this project depends on who undertakes the work, as everyone seems to have their own favored or trusted method.

DYNAMIC LANE-NARROWING TECHNOLOGIES

The original project work statement called for a preliminary investigation of dynamic lane-narrowing technologies, which could revert to standard lane widths during off-peak periods. While developing the research work plan, the team identified a company that had recently patented a system and method for dynamic lane-narrowing technologies. Other identified

possibilities for dynamic lane narrowing mostly revolved around pedestrian crosswalks or research papers that were not practice-ready.

In October 2016, a representative of the company with the patented system gave a 90-min presentation on dynamic lane-narrowing technologies to a project team member. Their system consisted of lanes being turned back to their original 12-ft widths when the peak period was over, in-pavement lighting to handle various lighting and weather conditions, algorithms to activate and deactivate lane markings at various locations, and a dynamic message signing plan for handling transition and midcorridor areas. The company said the system would cost $10–$14M per mile in startup costs, which they believe would automatically be regained (via reduced delays) within 2.5 yr. The company then followed up with a similar presentation to FHWA in December 2016.

SUMMARY

This research and findings synthesis intended to identify information and concepts that could inform this project's research approach. It was no surprise that, according to most research and findings, lane narrowing that facilitates the addition of a new lane is significantly beneficial in terms of improving traffic flow efficiency. Although FFS could decrease (e.g., from 65 to 55 mi/h) due to lane keeping difficulty, peak-period speeds could increase from stop-and-go levels (e.g., 10 mi/h) to more functional levels (e.g., 40 mi/h) when lane addition eliminates a serious bottleneck. Most mobility-based impacts and results found in the literature would have little effect on the research approach. One possible exception was a Chinese study in which narrow lanes produced statistically insignificant impacts or benefits under relatively low posted speed limits (e.g., 50 mi/h) (Zheng, Sun, and Yang 2015). This was an interesting finding because at least one prominent American narrow lane corridor (H-1 in Honolulu, HI) also has low posted speed limits. Therefore, it would be interesting to see whether posted speed limits would have a significant impact on this project's collected data and developed models.

The available set of research and findings implies that safety considerations do not rule out the lane-narrowing strategy for bottleneck mitigation in many cases. However, it is noted that the lane-narrowing option may be reasonably avoided on the basis of safety concerns under boundary conditions (e.g., unusually high heavy vehicle percentages, unusually high posted speed limits, unusually sharp horizontal curvature, close proximity to roadside objects with insufficient lateral clearance).

The HCM is the primary resource for analytical analysis and prediction of freeway capacities, speeds, densities, and other measures. However, Roess and Prassas (2014) observed that HCM lane width adjustment factors for basic freeway segments are outdated, judgmental, and based on low-speed multilane highway observations. The emergence of lane narrowing as a top congestion relief strategy motivated this project's effort to redevelop these adjustment factors.

The team anticipates that narrow lanes and shoulders have a greater impact on car-following behavior than lane-changing behavior. Specifically, the team hypothesizes that, with narrow lanes and shoulders, drivers will adapt their behavior and keep longer headways. Despite a wealth of proposed trajectory-based car-following model calibration approaches, there is little apparent consensus on a common approach.

CHAPTER 3. DATA COLLECTION

After developing the detailed research work plan in late 2016, the team collected data during the first half of 2017. This chapter describes the selected data-collection sites, methodology, and parameters.

MACROSCOPIC DATA COLLECTION

Data-Collection Approach

The team employed a 10-step macroscopic data-collection analysis approach to identify bottlenecks within narrow lane sections, download sensor data, apply data filtering, and ultimately analyze FFS and capacity estimates. The steps were as follows:

1. Use Google® Traffic™ to identify and explore congestion patterns for freeway segments with narrow lanes. The "typical traffic" feature in Google allowed the team to evaluate historical average performance. Correlating narrow lane treatment sites and typical traffic patterns allowed the team to identify the most desirable sensors for further evaluation.

2. Identify target sensor(s). Based on the observed congestion patterns, the team identified one or more sensors for each location to use for analysis. Sensors were selected to contain some recurring congestion and ideally were located in segments likely to be the bottleneck. In addition to the target sensor, the team evaluated upstream and downstream sensors.

3. Download/extract sensor data. In this step, the team either downloaded data for the identified sensors or extracted specific data from larger sensor databases made available by agencies.

4. Aggregate data to 15-min intervals. The HCM analysis unit is 15 min. For sensor sources provided in shorter aggregation intervals (e.g., 20 s, 1 min, 5 min), data were aggregated to the 15-min level before analysis.

5. Identify and filter weather events. Using archived weather data, the team identified days with poor weather and filtered those out for separate analysis. Data were automatically extracted from the website using a macro script developed by the team.

6. Identify and filter incident events. Using data from agency-provided crash and incident logs, the team identified days with incidents and filtered those out for separate analysis.

7. Process data. The team used a custom-developed analysis macro spreadsheet to calculate FFS, prebreakdown capacity, and queue discharge flow rate using the HCM analysis procedure. The team analyzed on a lane-by-lane basis. The analysis was performed separately for clear weather days, inclement weather days, and incident days for the narrow lane segments.

8. Estimate capacity and CAF. Using the procedure in the HCM, the team estimated the segment capacity as the average prebreakdown flow rate. This capacity was estimated for narrow lane treatment sites (with and without weather and incidents), as well as for a nearby comparison site (control site) with 12-ft lanes to obtain a CAF. The researchers calculated the resulting CAF as the ratio of the treatment site capacity divided by the control site capacity.

9. Estimate adjustments to FFS. Researchers identified the average FFS at all sites (treatment and control) as the speed under very low traffic conditions (average flow of fewer than 800 veh/h/ln). The team developed a regression model capturing the impact of several variables on FFS.

10. Develop a summary report for each site. For each site, the team developed a summary report to document the analysis and provide sample size and analysis results.

Site Overview

The team included nine data-collection sites distributed across five U.S. cities in the macroscopic model development portion of this project. Each physical site contained one or more sensors used for data collection. The sites were selected based on agency outreach in earlier portions of the project and were screened further through direct coordination with operating agencies. All sites featured freeway sections with less-than-12-ft lanes, as well as some expectation of recurring congestion to allow for estimation of capacities. Table 1 summarizes the characteristics of all data-collection sites.

The team decided to drop the Florida and Washington sites because sensor data showed significant data gaps. In the end, the team applied data collected at locations in Dallas, TX; San Antonio, TX; and Honolulu, HI.

From these sites, the team had sufficient data to analyze 21 narrow lane segments. In addition, the team collected six segments with 12-ft lanes to use as control sites. Control sites were all in the vicinity of narrow lane segments. Given sensor availability at study corridors, as well as the occurrence of breakdown events, various types of segments (basic, merge, and diverge) were eventually analyzed.

One of the challenges the team faced during the data-collection effort was sensor availability and position at active bottleneck locations with narrow lane segments. Not all active bottlenecks have sensors at the appropriate position (downstream of the merge or upstream of the diverge segment). Therefore, there were possibly additional active bottlenecks at narrow lane segments that the team could not analyze due to sensor unavailability. Field data collection could have helped in these cases.

In addition, the data preparation steps required considerable resources from the team. Downloading or obtaining large quantities of traffic data, conducting quality checks, screening out days with bad weather and incidents, and aggregating data to 15-min intervals took a significant amount of time and effort.

Table 1. Site summary for macroscopic data collection.

Site Number	State	City	Roadway	Segment	Type	Lane Information	Width (ft)	Shoulder Width
TX-75-1	Texas	Dallas	US 75	I-635 to Spring Creek	Several	Four 11-ft lanes, HOV lane	11	No left (HOV), 6–10-ft right
TX-75-2	Texas	Dallas	US 75	Spring Creek Parkway	Several	Three 11-ft lanes, HOV lane	11	No left (HOV), 10-ft right
TX-10-1	Texas	San Antonio	I-10	Northbound/southbound Hildebrand Avenue to W Summit Avenue	Several (1 mi)	Five 11-ft lanes, one HOV lane	11	10-ft left, 10-ft right
TX-410-1	Texas	San Antonio	I-410	Eastbound/westbound I-10 interchange to Perrin Beitel Road	Several (9 mi)	Five 11-ft lanes	11	5-ft left, 10-ft right
HI-H1-1	Hawaii	Honolulu	H-1	Northbound Punahou Street to Middle Street	Several (4.5 mi)	Four 10-ft lanes	10	6-ft left, 6-ft right
HI-H1-2	Hawaii	Honolulu	H-1	Southbound Middle Street to Punahou Street	Several (4.5 mi)	Four 10-ft lanes	10	6-ft left, 6-ft right
FL-95	Florida	Miami	I-95	I-95 in Fort Lauderdale (I-595 to Miami-Dade line)	Several	Four 11-ft lanes, two 11-ft HOT lanes	11	Varies
WA-AWV-1	Washington	Seattle	Alaskan Way Viaduct	Northbound S Main Street to Seneca Street	Basic/ diverge	Four 10-ft lanes	10	No left No right
WA-AWV-2	Washington	Seattle	Alaskan Way Viaduct	Northbound S Massachusetts Street to West Seattle Bridge	Basic (1 mi)	Two 11-ft lanes plus one BOS lane	11	No left, 4-ft right

BOS = bus-only shoulder; HOT = high-occupancy toll.

MICROSCOPIC DATA COLLECTION

In addition to the macroscopic/analytical data-collection effort, the team needed to obtain microscopic vehicle trajectory data for data collection to support the simulation model development effort. The team considered three microscopic data-collection options:

- Aerial videos.
- Instrumented vehicles.
- Archived data (e.g., SHRP2 naturalistic driving data).

The primary concern with the aerial video option was the cost of obtaining aerial video data via helicopter. The primary concerns with the instrumented vehicle option were the widely dispersed geographic locations of treatment sites (i.e., Florida, Hawaii, Texas, and Washington) and the training required to operate such vehicles. The primary concern with the archived data option was the price of the naturalistic data, plus the fact that such data potentially covered only one treatment site (i.e., the Seattle, WA, area).

At one point, the team considered UAV video collection as a cost savings mechanism (relative to manned helicopters), plus a video post-processing company that could automatically convert such videos into numeric vehicle trajectories. The overall methodology is illustrated in figure 3.

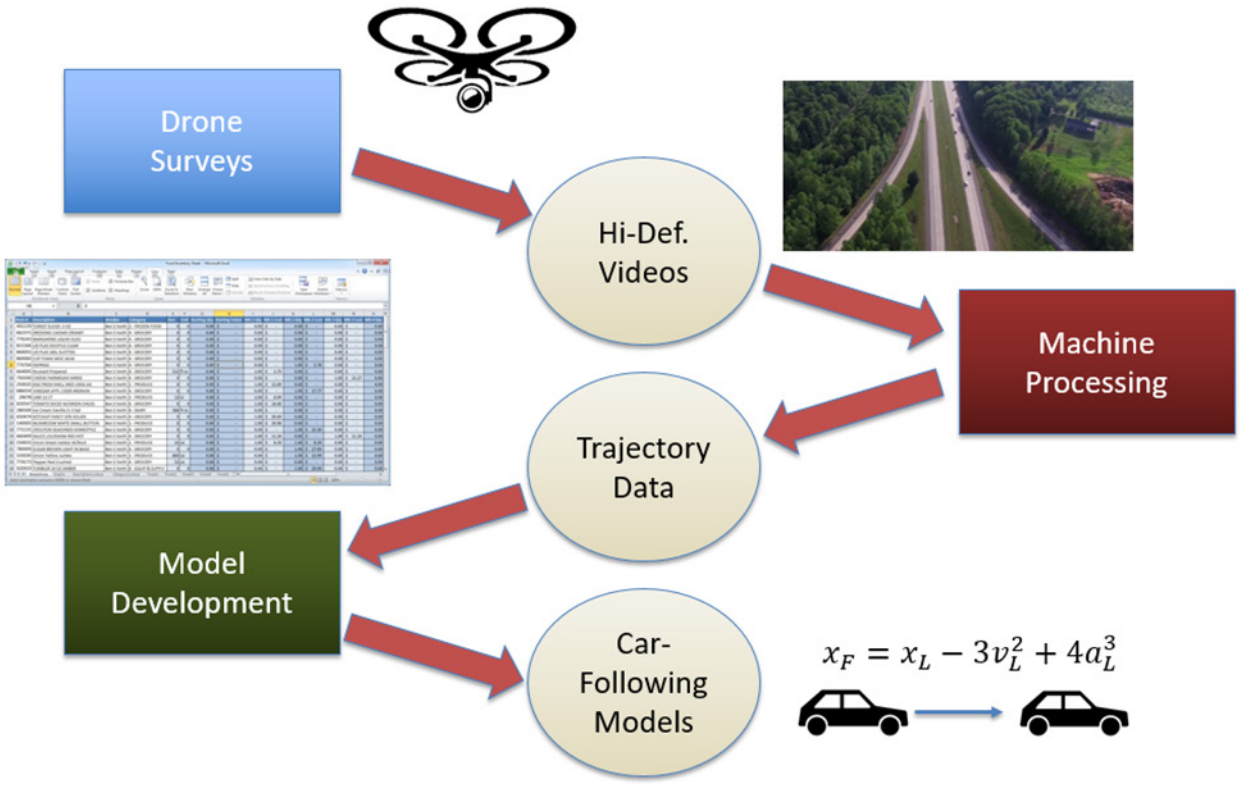

Source: FHWA.
Hi-Def. = high definition.

Figure 3. Illustration. Microscopic data-collection process.

The team created detailed maps of locations for launching UAVs. These maps captured upstream transition areas, downstream transition areas, midcorridor areas, and nearby control sites with standard lane widths. However, it was also necessary to capture near-capacity or at-capacity conditions such that vehicle trajectories were affected by lane width. Thus, the team used Google Traffic to estimate time periods likely to capture desired conditions.

UAV video collection specifications were somewhat detailed. In the United States, UAVs are not allowed to fly directly above the roadway, so a slight angle was needed. Team leaders discussed various options for adhering to Federal Aviation Administration (FAA) requirements while still meeting engineering needs. At one point, the team was trying to conceive a technical approach that would balance the following considerations:

- UAV capabilities.
- FAA requirements.
- Video postprocessing abilities.
- Project needs.

This planning process ultimately produced the following UAV specifications:

- Minimum video resolution of 4k (4,096 × 2,160 pixels) to facilitate video post-processing.
- Extended battery life.
- Minimum object resolution of 16 × 16 pixels for successful tracking.
- Minimum frames per second of 10. The video was 23 frames per second.
- Viewing angle of 25 degrees above top/down.
- Linear processing area was maximized at 1,115 ft (i.e., approximately 0.25 mi) using a single UAV.
- No sun glare allowed.
- Medium cloud cover to provide soft, omnidirectional ambient lighting.
- Stable UAV position via gimbal to provide steady video.

The planning process further produced the following site specifications:

- I-635 westbound, Dallas, TX (6:30–9:00 a.m.).
- I-635 eastbound, Dallas, TX (4:30–6:30 p.m.).
- I-635 control, Dallas, TX (6:30–9:00 a.m.; 4:30–6:30 p.m.).
- US 75 southbound, Dallas, TX (7:00–9:00 a.m.; 4:30–6:30 p.m.).
- US 75 northbound, Dallas, TX (4:00–7:00 p.m.).
- H-1 eastbound, Honolulu, HI (7:00–8:30 a.m.; 4:00–5:30 p.m.).
- H-1 westbound, Honolulu, HI (4:30–5:30 p.m.).
- H-1 control, Honolulu, HI (7:00–8:30 a.m.; 4:00–7:00 p.m.).
- H-1 eastbound 2, Honolulu, HI (7:00–8:00 a.m.; 4:00–7:00 p.m.).
- I-99 northbound, Seattle, WA (3:30 p.m., 4:30 p.m., 5:30 p.m.).
- I-95 northbound, Fort Lauderdale, FL (7:30–9:00 a.m.; 4:00–7:00 p.m.).
- I-95 control, Fort Lauderdale, FL (7:30–9:00 a.m.; 4:00–7:00 p.m.).
- I-410 westbound, San Antonio, TX (7:30–8:30 a.m.; 5:30–6:30 p.m.).

- I-410 control, San Antonio, TX (7:30–8:30 a.m.; 5:30–6:30 p.m.).
- I-10 eastbound, San Antonio, TX (5:00–6:00 p.m.).
- I-10 control, San Antonio, TX (5:00–6:00 p.m.).

The team inquired about the positional accuracy of video post-processing software. The data-collection company noted that accuracy is variable on a case-by-case basis. However, it is reasonable to assume that fault in the position of the vehicle is within 3.3 ft, usually only about 20 inches. This error is not accidental, so measuring the speed/time of the passage is either not affected by this error or is only affected to a very limited extent. The estimated error in speed measurement was a maximum of 3 percent. In many cases, the percentage error is even lower. To generate lane-specific headway data through video post-processing software, the analyst drew virtual gates along the observed roadway. This software limitation prevented the collection of full trajectories. As a result, the team adopted a calibration method used by the simulation developers that uses as input loop detector data.

As stated earlier in this section, the objective was to capture near-capacity or at-capacity conditions such that vehicle trajectories were affected by lane width. However, a modest amount of under-capacity and over-capacity video footage was also needed to capture all regimes of the fundamental speed–flow diagram. UAV and helicopter videos were typically 5 or 10 min in length because the aerial vehicle would record video for approximately 15 min. However, the maximum size of each video was 10 min, so the video recording software would automatically splice the 15-min video into a 10- or 5-min video.

The team reviewed over 100 videos from sites listed previously in this chapter. If a video exhibited under-capacity or over-capacity conditions throughout most of its timeframe, the video was omitted. Only videos that primarily exhibited near-capacity or at-capacity conditions were added to the master list of videos whose trajectory data would be mined. After all videos were reviewed, the final master list contained 78 videos—a total of 9.25 h of footage. Roughly 40 percent of this footage was from control sites having 12-ft lanes. The remaining 60 percent was from treatment sites with 11- or 10-ft lane widths. Lane width information was obtained from Google Maps™ and/or State DOTs. City-specific footage from the master list was distributed as follows:

- Dallas, TX, I-635 and US 75 (14 percent).
- San Antonio, TX, I-10 and I-410 (7 percent).
- Honolulu, HI, H-1 (47 percent).
- Seattle, WA, Alaskan Way Viaduct (8 percent).
- Fort Lauderdale, FL, I-95 (24 percent).

Note that 75 percent of the Honolulu, HI, video footage was for 10-ft lane widths. No other cities had 10-ft lane widths. No 12-ft control site footage was captured for Honolulu, HI, or Seattle, WA.

The data-collection team collected the entire set of video footage between July 2017 and November 2017. Subsequently, the video analysis company post-processed that footage between September 2017 and January 2018 to produce vehicle trajectory data.

CHAPTER 4. MODEL DEVELOPMENT

The model development effort began shortly after the end of the data-collection phase. However, due to FAA application requirements for UAV surveys, macroscopic and safety models were nearly complete by the time microscopic data collection began in August 2017.

This chapter first discusses the development of a macroscopic model capable of better estimating the impact of narrowed lane widths on lane capacity; the developers based the new method on the Sixth Edition of the HCM (Transportation Research Board 2016). Next, this chapter discusses the development of a microscopic modeling tool to assess the impact of altered driver behavior through narrowed freeway lane segments. This was accomplished through calibration of Gipps and Wiedemann 74 car-following models, which are the featured car-following models in Aimsun and Vissim commercial software, respectively. Finally, this chapter closes with a discussion of the development of models that assess the impact of reduced lane widths on the safety performance of a facility (i.e., expected number of fatal and injury [FI] and property-damage-only [PDO] crashes); this is based on methods established in the HSM.

MACROSCOPIC MODEL DEVELOPMENT

This subsection discusses macroscopic model development. The first two sections summarize modeling tools currently available to assess the impact of reduced freeway lane widths on lane capacity (i.e., HCM). The third subsection discusses sensor data collected in the field; this subsection provides evidence that field capacity and FFS are statistically significantly different between various lane widths, supporting the development of new CAFs, and more importantly, that the HCM methods inadequately capture these differences. The following subsection discusses the development of an improved regression model to predict impact of narrowed lane widths on facility FFS, which ultimately impacts expected capacity. Next, example calculations are provided for hypothetical scenarios where a four-lane basic freeway segment is narrowed to five 11-ft lanes and five 10-ft lanes; this example helps further illustrate differences between the existing HCM method and the newly developed FFS regression model. The next subsection validates the newly developed FFS regression model and CAFs by comparing various capacity estimation methods (i.e., HCM, new FFS regression model, and new FFS regression model and CAFs) against field sensor data. Finally, conclusions and recommendations are provided.

The team analyzed a total of 21 narrow lane segments in this project. In addition, six segments with 12-ft lanes were used as control sites. Control sites were all in the vicinity of narrow lane segments. Given sensor availability at study corridors, as well as the occurrence of breakdown events, various types of segments (e.g., basic, merge, and diverge) were eventually analyzed.

This research uses the HCM definitions of segments to distinguish between basic, merging, diverging, and weaving segments for model development. According to the HCM, ramp–freeway junctions that accommodate merging maneuvers are classified as on-ramps. Junctions that accommodate diverging maneuvers are classified as off-ramps.

For on-ramps located on the right-hand side of the freeway (the majority of cases), the ramp influence area includes the acceleration lane(s) and lanes one and two of the freeway mainline (rightmost and second rightmost) for 1,500 ft downstream of the merge point. For off-ramps

located on the right-hand side of the freeway (also the majority of cases), the ramp influence area includes the deceleration lane(s) and lanes one and two of the freeway for a distance of 1,500 ft upstream of the diverge point.

According to the HCM, a ramp weave is formed by a one-lane on-ramp closely followed by a one-lane off-ramp and connected by a continuous auxiliary lane. Vehicles traveling from the on-ramp to the freeway or the freeway to the off-ramp must cross paths, and these are therefore called weaving movements. The influence area of a weaving segment includes its length from gore to gore, plus 500 ft upstream and downstream.

A basic freeway segment is defined in the HCM as a segment that is outside the influence area of any merging, diverging, or weaving segments.

HCM Basic Freeway Segments Overview

The HCM methodology development focuses on estimation of FFSs and segment capacities for segments with narrow lanes (relative to standard lanes). Specifically, the HCM estimates FFS based on equation 1:

$$FFS_{adj} = BFFS - f_{LW} - f_{RLC} - 3.22TRD^{0.84} \quad (1)$$

Where:

FFS_{adj} = basic segment FFS adjusted for lane width, right lateral clearance, and total ramp density (mph).
$BFFS$ = base FFS measured for the segment (mph).
f_{LW} = adjustment to FFS for average lane width for basic freeway and multilane highway segments (mph).
f_{RLC} = adjustment to FFS for the facility right-side lateral clearance (mph).
TRD = total ramp density within a 6-mi radius.

The adjustment to reflect f_{LW} is shown in table 2. The adjustment to FFS for f_{RLC} is provided in table 3.

Table 2. Adjustment to FFS for average lane width for basic freeway and multilane highway segments (reprinted from the Sixth Edition of the HCM, exhibit 12-20).

Average Lane Width (ft)	Reduction in FFS, f_{LW} (mi/h)
≥12	0.0
≥11–12	1.9
≥10–11	6.6

Table 3. Adjustment to FFS for f_{RLC} for basic freeway segments (reprinted from the Sixth Edition of the HCM, exhibit 12-21).

Right-Side Lateral Clearance (ft)	Two Lanes (mi/h)	Three Lanes (mi/h)	Four Lanes (mi/h)	≥Five Lanes (mi/h)
≥6	0.0	0.0	0.0	0.0
5	0.6	0.4	0.2	0.1
4	1.2	0.8	0.4	0.2
3	1.8	1.2	0.6	0.3
2	2.4	1.6	0.8	0.4
1	3.0	2.0	1.0	0.5
0	3.6	2.4	1.2	0.6

Capacity of basic freeway segments is then calculated in equation 2:

$$c = 2{,}200 + 10(FFS_{adj} - 50) \quad (2)$$

Note that equation 1 and equation 2 are for basic freeway segments. For merge or diverge segments, the HCM methodologies do not provide capacity estimates; however, the HCM assumes that these capacities are equal to the capacities of their upstream or downstream basic freeway segments, respectively.

HCM Capacity Estimation

According to the HCM (p. 26-15): "…capacity is commonly understood to be a maximum flow rate that is associated with the occurrence of some type of breakdown, which results in lower speeds and higher densities following the breakdown event." The HCM defines flow breakdown to occur when speeds drop abruptly at least 25 percent below the FFS for a sustained period of at least 15 min, resulting in queueing upstream of the bottleneck. Furthermore, capacity is defined as the prebreakdown flow rate, which is the 15-min average flow rate immediately prior to the breakdown event.

To account for driver behavior variability, the HCM suggests obtaining prebreakdown flow rates for several months up to an entire year and estimating the distribution of these flow rates. In this project, the sample size was small for several of the study sites (2–3 mo), and as such, it was not possible to establish the prebreakdown flow rates distribution. For the purposes of this report, the average prebreakdown flow rate was assumed to be the facility's capacity.

Field Data Results

Table 4, which summarizes the results of the analysis, shows estimated FFS and capacity values based on the HCM procedures (equation 1 and equation 2), as well as the field-measured FFSs and capacities (prebreakdown flow rates). Truck percentages were not available from the sensor data, but approximate percentages were obtained from microscopic data collection. More specifically, trucks and buses accounted for approximately 1.2 percent of the traffic stream in

Honolulu, HI; 2.3 percent in Dallas, TX; and 2.4 percent in San Antonio, TX. These measurements took place during peak periods.

Six segments along US 75 in Dallas, TX, were found to experience congestion due to downstream spillback, and as such, breakdown-related capacities were not estimated for those sites. In addition, field data showed that, on several occasions, traffic on the shoulder lane (oftentimes the lane that was added after the narrowing) was flowing at very low speeds and carried low traffic volumes. This was particularly true at several sites in Honolulu, HI. This imbalance in the operating conditions was taken into account when identifying breakdown events and resulting capacities. More specifically, to avoid situations were only the right-most lanes broke down, breakdowns were defined to occur when speeds across all lanes, and not just the average speed, dropped sharply.

Table 4. Summary of speeds and capacities under ideal conditions.

Location	Detector	Segment Type	Lane Width (ft)	Speed Limit (mi/h)	Measured FFS (mi/h)	Capacity (veh/h/ln)	Capacity (pc/h/ln)	HCM FFS (mi/h)	HCM Capacity (pc/h/ln)
Honolulu, HI	SL-58 eastbound	Merge	12	50	51.2	1,748	1,769	70.3	2,403
Honolulu, HI	SL-58 westbound	Diverge	12	50	53.4	1,712	1,733	70.3	2,403
Honolulu, HI	724A eastbound	Diverge	12	50	53.7	1,708	1,728	70.3	2,403
Honolulu, HI	724A westbound	Basic	12	50	52.1	1,769	1,790	70.3	2,403
Honolulu, HI	Radar03 eastbound	Diverge	11	50	55.8	1,741	1,762	68.4	2,384
Honolulu, HI	SL-71 eastbound	Merge	10	50	53.5	1,403	1,420	63.7	2,337
Honolulu, HI	SL-71 westbound	Diverge	10	50	53.5	1,528	1,547	63.7	2,337
Honolulu, HI	SL-15 eastbound	Basic	11	50	55.3	1,505	1,523	63.7	2,337
Honolulu, HI	SL-15 westbound	Basic	11	50	55.4	1,640	1,660	63.7	2,337
San Antonio, TX	LCU-0010E-574.114	Merge	11	65	61.0	1,557	1,594	67.3	2,373
San Antonio, TX	LCU-0010E-574.563	Diverge	11	65	54.0	1,809	1,852	67.3	2,373
San Antonio, TX	LCU-0410W-022.945	Merge	11	65	61.6	1,826	1,870	67.3	2,373
San Antonio, TX	I-10 control	Merge	12	65	64.7	2,351	2,408	67.3	2,373
San Antonio, TX	I-410 control	Merge	12	65	65.1	1,811	1,855	69.4	2,394
Dallas, TX	12 southbound	Merge	11	60	60.3	—	—	66.9	2,377
Dallas, TX	5 southbound	Basic	11	65	64.4	—	—	66.9	2,369
Dallas, TX	10 southbound	Merge	11	65	65.9	—	—	66.9	2,369
Dallas, TX	6 southbound	Diverge	11	65	65.8	—	—	66.9	2,369
Dallas, TX	4 southbound	Basic	11	65	66.4	1,826	1,868	67.3	2,373
Dallas, TX	1 southbound	Basic	11	65	65.7	1,592	1,629	66.5	2,365
Dallas, TX	8 southbound	Merge	11	65	66.1	—	—	66.9	2,369
Dallas, TX	7 southbound	Basic	11	65	65.5	—	—	66.9	2,369
Dallas, TX	9 southbound	Merge	11	70	69.5	1,657	1,696	66.9	2,369
Dallas, TX	2 northbound	Basic	11	70	71.3	1,722	1,761	66.9	2,369
Dallas, TX	3 northbound	Basic	11	70	67.7	1,545	1,581	67.3	2,373
Dallas, TX	11 northbound	Basic	11	70	70.5	1,385	1,417	68.6	2,386

—Breakdown-related capacities were not estimated for these sites.
pc/h/ln = passenger cars per hour per lane; LCU = local control unit.

According to table 4, segment types, speed limits, and FFSs demonstrated significant variability among study sites. Lane widths of 10 ft were available only along the H-1 corridor in Honolulu, HI, but due to sensor availability and placement, only two segments (one merge and one diverge) were eventually analyzed. Notably, the 10-ft merge segment (SL-71 eastbound) displays very low capacity values. This merge junction is located just upstream of another merge junction; however, sensor data are not available there to evaluate whether the downstream junction experiences breakdowns or not. This location was considered an outlier and removed from the analysis given the low capacity values at the site and close proximity to a downstream merge, which could potentially be another bottleneck. Based on analysis, it appears that the HCM method overestimates both speeds and capacities for different lane widths. This relationship is shown more clearly in figure 4 and figure 5.

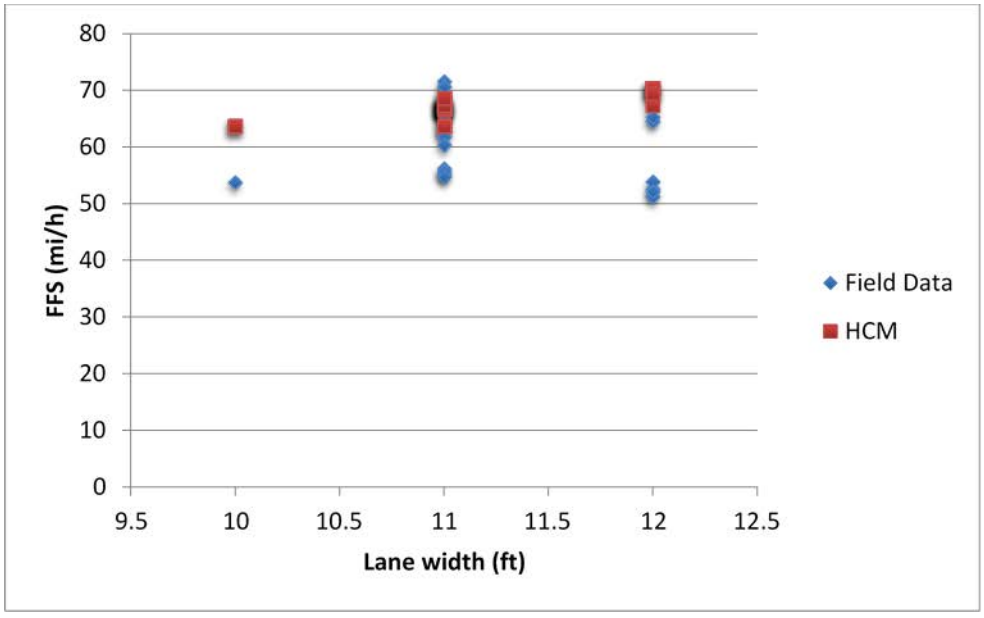

Figure 4. Graph. FFS versus lane width relationship.

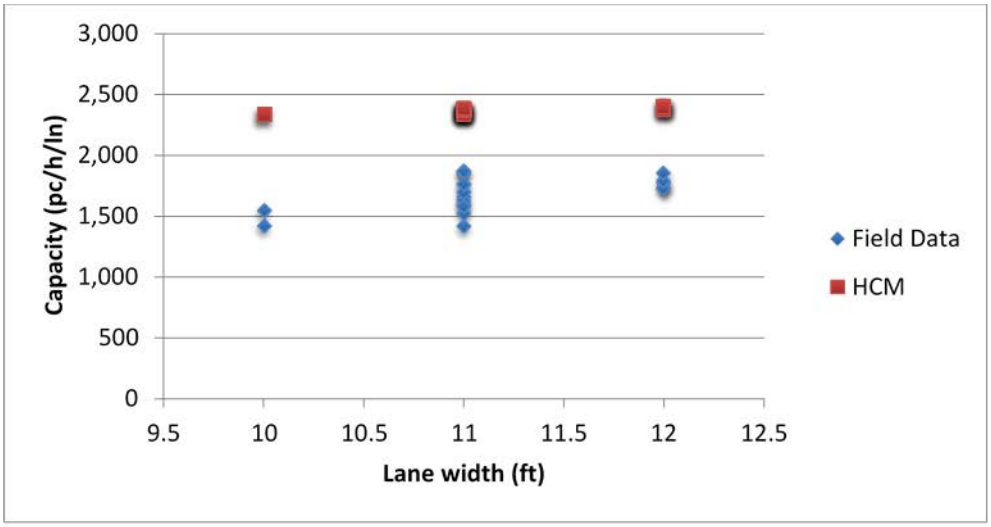

Figure 5. Graph. Capacity versus lane width relationship.

Field-measured capacity values were averaged across the different types of study segments. The results are shown in table 5. Based on these values, CAFs for 10- and 11-ft lanes were calculated using the 12-ft lane capacity values as the reference point. The CAFs are displayed in table 6 and show that narrow lane segments have reduced capacities compared to 12-ft lane segments. Only one 10-ft-wide segment was eventually used, and capacities at that site were significantly lower than capacities at remaining sites with wider lanes. Analysis of variance and Tukey's (1977) statistical test were performed to investigate whether capacities differ among various segment types and lane widths. Results revealed that capacities differ significantly among segments with different lane widths.

Table 5. Average capacities (pc/h/ln) by lane width and segment type.

Segment Type	12-ft Lanes	11-ft Lanes	10-ft Lanes
Merge	1,836	1,708	—
Diverge	1,730	1,795	1,547
Basic	1,790	1,639	—
All segments	1,781	1,695	1,547

—Not analyzed.
pc/h/ln = passenger cars per hour per lane.

Table 6. CAFs by lane width and segment type.

Segment Type	11-ft Lanes CAF	10-ft Lanes CAF
Merge	0.93	—
Diverge	1.04	0.89
Basic	0.92	—

—Not analyzed.

As shown in table 6, CAFs by segment type do not show any particular trend, which can be attributed both to the fact that capacity varies significantly, even for the same site, and also to the

wide range of operating conditions among study sites. Table 7 presents variations of average capacity by speed limit, segment type, and lane width. Wherever possible, CAFs were also calculated.

Table 7. Capacities (pc/h/ln) and CAFs by speed limit.

Speed Limit (mi/h)	Segment Type	12-ft Lanes	11-ft Lanes	10-ft Lanes	Inference	CAF
50	Basic	1,769	1,601	—	Significantly different	0.91
50	Merge	1,748	—	—	—	—
50	Diverge	1,710	1,741	1,528	12–11-ft not significantly different	0.89
65	Basic	—	1,686	—	—	—
65	Merge	1,858	1,674	—	Significantly different	0.90
65	Diverge	—	1,809	—	—	—
70	Basic	—	1,551	—	—	—
70	Merge	—	1,657	—	—	—
70	Diverge	—	—	—	—	—

—No data.

Given the lack of capacity measurements for a range of operating conditions at different segments, capacities and corresponding adjustment factors were further aggregated. Therefore, final capacities and CAFs, irrespective of segment types or operating conditions, are shown in table 8.

Table 8. Recommended CAFs by lane width.

Lane Width (ft)	12-ft Lanes	11-ft Lanes	10-ft Lanes
12	—	0.95	0.87
11	—	—	0.91
10	—	—	—

—No data and/or insufficient data.

FFSs measured using sensor data were found to be very close to the speed limit, which ranged from 50 to 70 mi/h. As such, calculating an average SAF using all data would not be a good approach. Table 9 presents average FFS by speed limit for the three lane widths under investigation. For 10-ft-wide lanes, FFS measurements were only available for segments with speed limits of 50 mi/h. FFS measurements for 12-ft-wide lanes were only available for segments with speed limits of 50 and 65 mi/h. FFSs for segments with speed limits of 50 and 65 mi/h were significantly different among lane width groups. All speeds shown in table 9 are statistically different.

Table 9. Average FFSs (mi/h) by lane width.

Speed Limit (mi/h)	12-ft Lanes	11-ft Lanes	10-ft Lanes
50	52.4	55.7	53.6
60	—	60.3	—
65	64.8	64.0	—
70	—	69.8	—

—No data and/or insufficient data.

As outlined in table 9, and contrary to the team's expectation, FFS does not decrease with decreasing lane width at very low speeds (i.e., around 50 to 55 mi/h). However, there is a slight decrease from 64.8 to 64.0 mi/h at freeways with a speed limit of 65 mi/h when lane width is reduced to 11 ft, which is statistically significant. This decrease denotes an SAF of 0.99. It is not possible to fully examine this relationship given the unavailability of data at different lane widths or speed limits. Lastly, in many cases, FFSs or capacities under an event (bad weather or incident) decreased compared to values under ideal conditions. Table 10 summarizes SAFs and CAFs for cases where the difference was statistically significant.

Table 10. SAFs and CAFs for events interfering with speed and capacity (incidents or bad weather).

Detector	Segment Type	Lane Width (ft)	FFS (mi/h) Measurement	FFS (mi/h) SAF	FFS (mi/h) Statistical Information	Capacity (veh/h/ln) Measurement	Capacity (veh/h/ln) CAF	Capacity (veh/h/ln) Statistical Information
SL-58 eastbound	Merge	12	51.0	1.00	Not significant	1,584	0.91	Significant
SL-58 westbound	Diverge	12	54.2	1.01	Not significant	1,364	0.80	Significant
724A eastbound	Diverge	12	54.2	1.01	Significant	1,550	0.91	Significant
724A westbound	Basic	12	51.6	0.99	Significant	1,537	0.87	Significant
Radar03 eastbound	Diverge	11	55.5	1.00	Not significant	1,484	0.85	Significant
SL-71 eastbound	Merge	10	53.1	0.99	Significant	1,224	0.87	Significant
SL-71 westbound	Diverge	10	53.2	0.99	Not significant	1,459	0.95	Not significant
SL-15 eastbound	Basic	11	55.3	1.00	Not significant	1,405	0.93	Significant
SL-15 westbound	Basic	11	55.0	0.99	Significant	1,468	0.89	Significant
LCU-0010E-574.114	Merge	11	60.6	0.98	Significant	1,454	0.93	Significant
LCU-0010E-574.563	Diverge	11	53.3	0.98	Significant	1,703	0.94	Not significant
LCU-0410W-022.945	Merge	11	58.3	0.95	Significant	1,703	0.93	Significant
I-10 control	Merge	12	62.5	0.97	Significant	—	—	—
I-410 control	Merge	12	62.5	0.96	Significant	—	—	—
12 southbound	Merge	11	60.4	1.00	Not significant	—	—	—
5 southbound	Basic	11	62.3	0.97	Significant	—	—	—
10 southbound	Merge	11	66.6	1.01	Significant	—	—	—
6 southbound	Diverge	11	66.7	1.01	Significant	—	—	—
4 southbound	Basic	11	66.5	1.00	Not significant	—	—	—
1 southbound	Basic	11	65.2	0.99	Not significant	—	—	—
8 southbound	Merge	11	66.7	1.01	Significant	—	—	—
7 southbound	Basic	11	64.7	0.99	Not significant	—	—	—
9 southbound	Merge	11	66.0	0.95	Significant	1,342	0.81	Significant
2 northbound	Basic	11	69.3	0.97	Significant	—	—	—
3 northbound	Basic	11	66.4	0.98	Significant	—	—	—
11 northbound	Basic	11	70.2	1.00	Not significant	—	—	—

—No data.
LCU = local control unit.

As shown in table 10, FFSs and capacities under an event are generally lower compared to ideal conditions. On average, FFS under an event is approximately 3 percent less than under ideal conditions, indicating an adjustment factor of 0.97. Similarly, capacity due to an event was 12 percent less than under ideal conditions, indicating an adjustment factor of 0.88. These adjustment factors were estimated for all lane widths.

FFS Regression Model Development

From field-collected data, the team developed a regression model to predict narrow lane segment FFS as a function of several independent variables. The independent variables included the following:

- Number of lanes (*N*).
- Lane width (*LW*).
- Right-side shoulder width (*SW*).
- Posted speed limit equal to 50 mi/h (SL_1).
- Posted speed limit greater than 50 mi/h (SL_2).
- Merge segment (*M*).
- Diverge segment (*D*).
- Total ramp density (ramps/mi).
- Presence of HOV lane (binary).

Table 11 shows results of the FFS prediction model, which predicts FFS as a function of lane width, number of lanes, shoulder width, posted speed limit, and segment type. All variables shown in table 11 are significant at $p < 0.05$, and the model has an overall R-squared value of 0.8257. The presence of HOV lanes and the total ramp density (number of ramps within 6 mi upstream and downstream of the segment's midpoint) were not found to be statistically significant. The model also differentiates between speed limits above and below 50 mi/h, which were found to have opposite effect on FFS (figure 6).

Table 11. FFS regression model results.

Term	Coefficient	Standard Error of the Coefficient	*T*-Value	*p*-Value
Constant	6.040	1.580	3.82	0
LW	−0.440	0.080	−5.54	0
N	1.127	0.087	12.97	0
SW	0.076	0.011	6.66	0
SL_1	0.987	0.021	46.61	0
SL_2	0.660	0.032	20.75	0
$LW \times SL_2$	0.022	0.003	8.18	0
D	−1.809	0.093	−19.5	0
M	−1.257	0.081	−15.6	0

The newly developed FFS regression equation (hereby referred to as the new model) is shown in equation 3:

$$FFS = 6.04 + 1.13N + 0.08SW + 0.99SL_1 + 0.66SL_2 - 0.44LW + 1.81D - 1.26M + 0.02(LW \times SL_2) \quad (3)$$

Segment type variables have a value of either 1.0 or 0.0. There is no additional speed reduction for basic segments (term "basic" = 1). At diverge and merge segments, FFS is reduced by 1.809 and 1.2571 mi/h, respectively. Figure 6 shows the regression model sensitivity with respect to lane width at various speed limits ranging from 50 to 75 mi/h. Figure 6 also displays FFS values based on the current HCM model. The following assumptions were considered when creating figure 6: number of lanes = 3, shoulder width = 4 ft, number of ramps within 6 mi = 10, basic freeway segment. As shown in figure 6, the FFSs predicted by the HCM do not capture the variability observed in collected data. Figure 6 also shows the adverse impact of lane width at very low speeds.

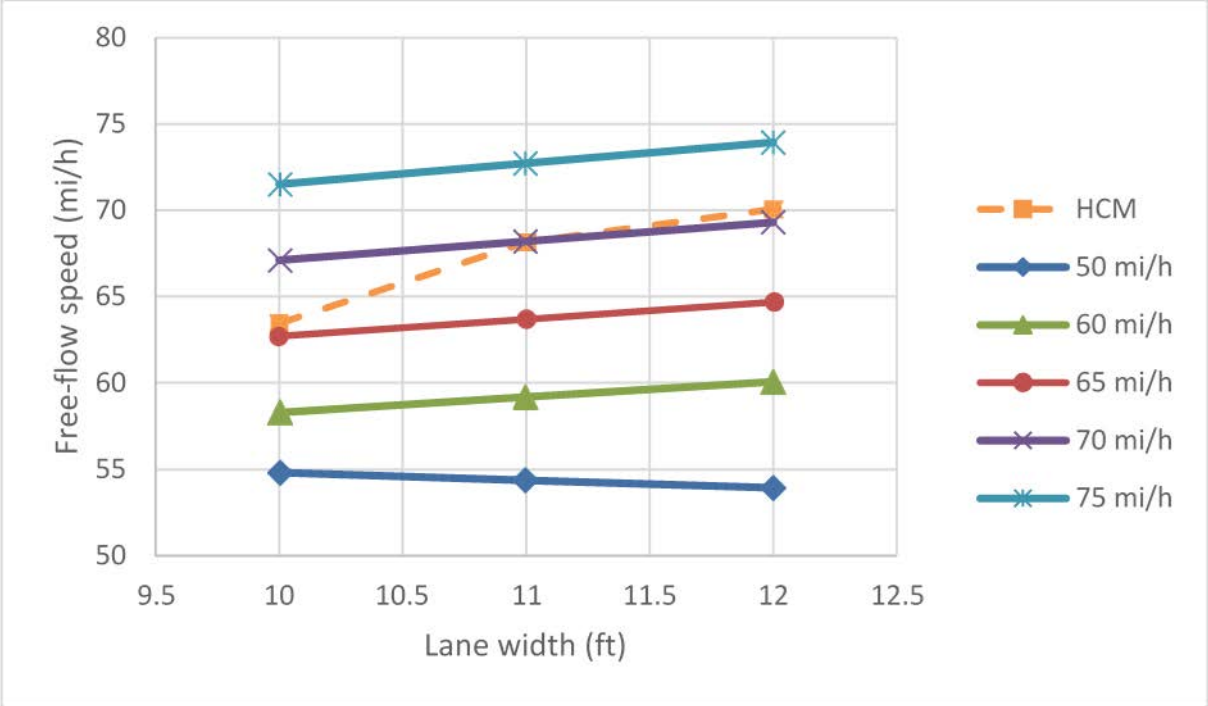

Figure 6. Graph. FFS regression model sensitivity.

Example Applications of Macroscopic Model Development

Example 1: Basic Freeway Segment Narrowing to 11-ft Lanes

In this example, it is assumed that a basic freeway segment with a 70-mi/h speed limit and four 12-ft lanes is restriped to five 11-ft lanes. It is also assumed that the speed limit will be reduced to 65 mi/h. In addition, the segment has a 5-ft-wide shoulder and 10 ramps within a 6-mi radius. In this example, speeds and capacities are calculated before and after the change using both HCM and the new FFS model approach (equation 3).

First, the analyst calculates the before-restriping adjusted FFS and capacity as a baseline value using both the existing (HCM) and new FFS regression equation (equation 3) methods.

HCM method:

According to the HCM, the adjusted FFS for the base conditions (calculated in equation 4) is based on equation 1, table 1, and table 2 as:

$$FFS_{adj} = BFFS - f_{LW} - f_{RLC} - 3.22 \times TRD^{0.84} = 75.4 - 0.2 - 3.22\left(\frac{10}{6}\right)^{0.84} = 70.25 \text{ mi/h} \quad (4)$$

Equation 5 estimates the corresponding capacity for the base conditions (based on equation 2) as:

$$c = 2{,}200 + 10\left(FFS_{adj} - 50\right) = 2{,}200 + 10(70.25 - 50) = 2{,}400 \text{ pc/h/ln} \quad (5)$$

The breakpoint of the speed–flow curve is calculated in equation 6:

$$BP = \left[1{,}000 + 40\left(75 - FFS_{adj}\right)\right] \times CAF^2 = [1{,}000 + 40(75 - 70.25)] \times 1^2 = 1{,}190 \text{ pc/h/ln} \quad (6)$$

New FFS and CAF models:

According to the models and adjustment factors developed in this project, the FFS estimated using the new FFS regression model for the base conditions is calculated in equation 7:

$$FFS_{adj} = 6.04 + 1.13 \times 4 + 0.08 \times 5 + 0.66 \times 70 - 0.44 \times 12 + 0.02(12 \times 70) = 70.36 \text{ mi/h} \quad (7)$$

Next, the estimated FFS calculated using the new FFS regression model was used to calculate the unadjusted capacity of the base conditions in equation 8:

$$c = 2{,}200 + 10(70.36 - 50) = 2{,}404 \text{ pc/h/ln} \quad (8)$$

The breakpoint of the speed–flow curve is calculated in equation 9:

$$BP = \left[1000 + 40\left(75 - FFS_{adj}\right)\right] \times CAF^2 = [1000 + 40(75 - 70.36)] \times 1^2 = 1{,}186 \text{ pc/h/ln} \quad (9)$$

For the before-restriping conditions, the two models (i.e., the HCM method and the new FFS regression model) predict very similar capacities and FFSs.

Next, the analyst calculates the treatment conditions (i.e., after restriping) adjusted FFS and capacity using both the existing (HCM) and new FFS regression model (equation 3) methods.

HCM method:

The HCM method for calculating FFS is provided in equation 10:

$$FFS_{adj} = BFFS - f_{LW} - f_{RLC} - 3.22 \times TRD^{0.84} = 75.4 - 0.2 - 1.9 - 3.22\left(\frac{10}{6}\right)^{0.84} = 68.35 \text{ mi/h} \quad (10)$$

Equation 11 estimates the corresponding capacity:

$$c = 2{,}200 + 10\left(FFS_{adj} - 50\right) = 2{,}200 + 10(68.35 - 50) = 2{,}384 \text{ pc/h/ln} \quad (11)$$

The breakpoint of the speed–flow curve is calculated in equation 12:

$$BP = \left[1000 + 40\left(75 - FFS_{adj}\right)\right] \times CAF^2 = [1000 + 40(75 - 68.35)] \times 1^2 = 1{,}266 \text{ pc/h/ln} \quad (12)$$

New FFS regression and CAF models:

According to the models and adjustment factors developed in this project (equation 3 and table 8), equation 13 estimates the FFS for the basic segment with five 11-ft lanes and a speed limit of 65 mi/h:

$$FFS_{adj} = 6.04 + 1.13 \times 5 + 0.08 \times 5 + 0.66 \times 65 - 0.44 \times 11 + 0.02(11 \times 65) = 65.9 \text{ mi/h} \quad (13)$$

Next, equation 14 calculate the unadjusted capacity using the adjusted FFS calculated with the new FFS regression equation:

$$c = 2{,}200 + 10\left(FFS_{adj} - 50\right) = 2{,}200 + 10(65.9 - 50) = 2{,}359 \text{ pc/h/ln} \quad (14)$$

The breakpoint of the speed–flow curve is calculated in equation 15:

$$BP = \left[1000 + 40\left(75 - FFS_{adj}\right)\right] \times CAF^2 = [1000 + 40(75 - 65.9)] \times 1^2 = 1{,}365 \text{ pc/h/ln} \quad (15)$$

Then, the CAF of 0.95 based on table 8 applies, and the adjusted capacity is calculated in equation 16:

$$c_{adj} = c \times CAF = 2{,}395 \times 0.95 = 2{,}241 \text{ pc/h/ln} \quad (16)$$

The corresponding breakpoint is calculated in equation 17:

$$BP = [1000 + 40(75 - FFS_{adj})] \times CAF^2 = [1000 + 40(75 - 65.9)] \times 0.95^2 = 1{,}232 \text{ pc/h/ln} \quad (17)$$

Figure 7 shows four speed–flow curves. The line with square markers represents the initial speed–flow curve before restriping using the HCM method. The line with triangle markers represents the speed–flow curve after restriping according to the HCM method. The line with "X" markers shows the speed–flow curve after restriping according to the new FFS model, assuming no adjustment for capacities. The line with diamond markers adds the CAF to the previous curve and shows adjustments to both FFS and capacity due to lane narrowing.

As shown in example 1, total capacity before restriping is 4 × 2,404 = 9,616 passenger cars per hour (pc/h), and after restriping (and assuming the new FFS regression equation) total capacity across all five lanes becomes 5 × 2,241 = 11,204 pc/h. Therefore, lane narrowing resulted in a capacity increase of 1,588 pc/h or 17 percent.

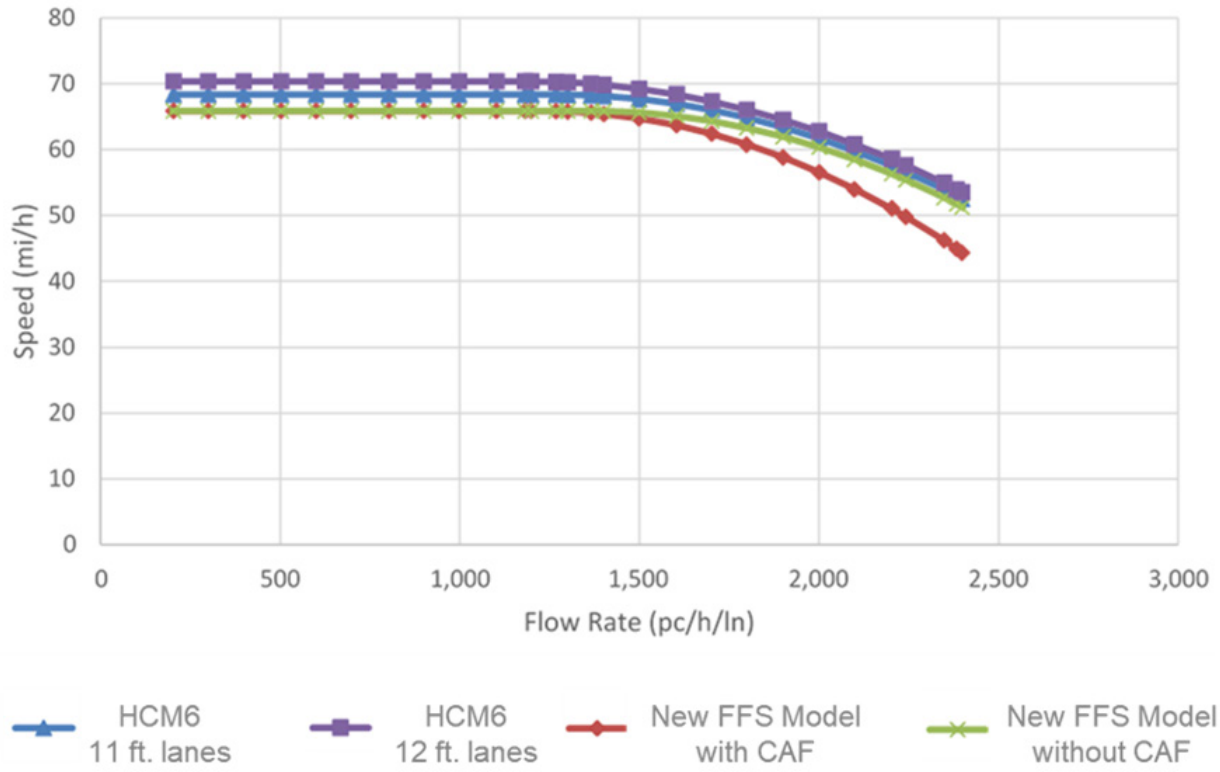

Figure 7. Graph. Speed–flow curve comparison for lane narrowing to 11-ft lanes.

Example 2: Basic Freeway Segment Narrowing to 10-ft Lanes

In this example, it is assumed that a basic freeway segment with a 70-mi/h speed limit and four 12-ft lanes is restriped to five 10-ft lanes. It is also assumed that the speed limit will be reduced to 65 mi/h. In addition, the segment has a 5-ft-wide shoulder and 10 ramps within a 6-mi radius.

In this example, the speeds and capacities are calculated before and after the change, using both the new model and the HCM approach.

First, the analyst calculates the before-restriping adjusted FFS and capacity as a baseline value using both the existing (HCM) and new FFS regression (equation 3) methods.

The base conditions in example 1 are identical to example 2. Thus, the capacities and FFSs are the same as those calculated in example 1.

Next, the analyst calculates the treatment conditions (i.e., after restriping) adjusted FFS and capacity using both the existing (HCM) and new FFS regression model (equation 3) methods.

HCM method:

Equation 18 calculates the HCM estimated FFS for the treatment conditions:

$$FFS_{adj} = BFFS - f_{LW} - f_{RLC} - 3.22 \times TRD^{0.84} = 75.4 - 0.2 - 6.6 - 3.22\left(\frac{10}{6}\right)^{0.84} = 63.65 \text{ mi/h} \quad (18)$$

Equation 19 estimates the corresponding capacity as:

$$c = 2{,}200 + 10\left(FFS_{adj} - 50\right) = 2{,}200 + 10(63.65 - 50) = 2{,}337 \text{ pc/h/ln} \quad (19)$$

The breakpoint of the speed–flow curve is calculated in equation 20:

$$BP = \left[1000 + 40\left(75 - FFS_{adj}\right)\right] \times CAF^2 = [1000 + 40(75 - 63.65)] \times 1^2 = 1{,}454 \text{ pc/h/ln} \quad (20)$$

New FFS and CAF models.

Equation 21 calculates the adjusted FFS for the basic segment with five 10-ft lanes and a speed limit of 65 mi/h using the new FFS regression equation:

$$FFS_{adj} = 6.04 + 1.13 \times 5 + 0.08 \times 5 + 0.66 \times 65 - 0.44 \times 10 + 0.02(10 \times 65) = 64.9 \text{ mi/h} \quad (21)$$

Next, the adjusted FFS using the new method is used to calculate the unadjusted capacity in equation 22:

$$c = 2{,}200 + 10\left(FFS_{adj} - 50\right) = 2{,}200 + 10(64.9 - 50) = 2{,}349 \text{ pc/h/ln} \quad (22)$$

The breakpoint of the speed–flow curve is calculated in equation 23:

$$BP = \left[1000 + 40\left(75 - FFS_{adj}\right)\right] \times CAF^2 = [1000 + 40(75 - 64.9)] \times 1^2 = 1{,}405 \text{ pc/h/ln} \quad (23)$$

Then, the CAF of 0.87 based on table 8 applies, and the adjusted capacity is calculated in equation 24:

$$c_{adj} = c \times CAF = 2{,}349 \times 0.87 = 2{,}043 \text{ pc/h/ln} \quad (24)$$

The corresponding breakpoint is calculated in equation 25:

$$BP = \left[1000 + 40\left(75 - FFS_{adj}\right)\right] \times CAF^2 = [1000 + 40(75 - 64.9)] \times 0.87^2 = 1{,}063 \text{ pc/h/ln} \quad (25)$$

Figure 8 shows the resulting speed–flow curves for example 2. As shown in example 2, total capacity before restriping is 4 × 2,404 = 9,616 pc/h, and after restriping (and applying the new FFS regression equation) total capacity across all five lanes becomes 5 × 2,043 = 10,217 pc/h. Therefore, lane narrowing resulted in a capacity increase of 601 pc/h or 6 percent.

Combined Effect of Narrow Lanes on Speeds and Capacities

To evaluate whether derived CAFs duplicate the effect of the new FFS regression model, the proposed adjustments were applied to five data-collection sites used in this project. To test this hypothesis, three speed–flow curves were designed at each site:

- Based on the existing HCM FFS equation (equation 1).
- Based on the proposed FFS equation (equation 3).
- Based on the proposed FFS equation (equation 3) and CAF from table 8.

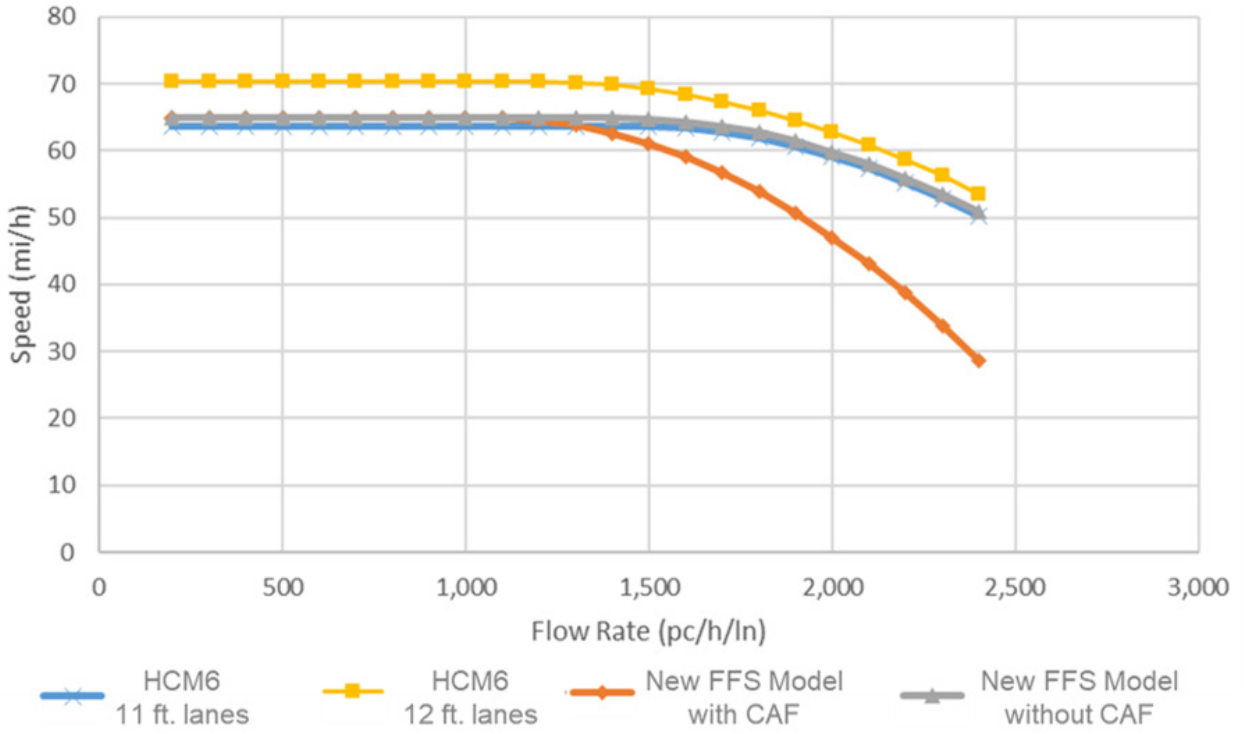

Figure 8. Graph. Speed–flow curve comparison for lane narrowing to 10-ft lanes.

The five selected sites are as follows:

1. Dallas US 75 at 15th Street (southbound): Basic freeway segment, 65 mi/h speed limit, 11-ft lane width, 4 lanes, 10-ft shoulder width, 15 ramps within 6 mi upstream/downstream of segment's midpoint.

2. Honolulu H-1 at SL-71 (westbound): Diverge freeway segment, 50 mi/h speed limit, 10-ft lane width, 4 lanes, 6-ft shoulder width, 15 ramps within 6 mi upstream/downstream of segment's midpoint.

3. Dallas US 75 at Galatyn South (northbound): Basic freeway segment, 70 mi/h speed limit, 11-ft lane width, 4 lanes, 9-ft shoulder width, 14 ramps within 6 mi upstream/downstream of segment's midpoint.

4. Dallas US 75 at Renner (southbound): Merge freeway segment, 70 mi/h speed limit, 11-ft lane width, 4 lanes, 6-ft shoulder width, 14 ramps within 6 mi upstream/downstream of segment's midpoint.

5. San Antonio I-10 at local control unit (LCU)-0010E-574.114 (eastbound): Merge freeway segment, 65 mi/h speed limit, 11-ft lane width, 5 lanes, 7-ft shoulder width, 13 ramps within 6 mi upstream/downstream of segment's midpoint.

Table 12 through table 16 include capacity estimates for assumed control sites at these locations. Control sites have one less lane, 12-ft lanes, and a speed limit of 5 mi/h higher than treatment sites. The column Segment-Wide Capacity Increase (New Model) of table 12 through table 16 presents the segment-wide capacity increase, assuming the proposed FFS model and CAF.

Table 12. FFS and capacity estimation for Dallas US 75 at 15th Street (southbound).

Performance Measure	New FFS Model, No CAF	HCM Model	New FFS Model, No CAF	New FFS Model with CAF	Segment-Wide Capacity Increase (New Model)
Configuration	Three 12-ft lanes, 70 mi/h speed limit	Four 11-ft lanes, 65 mi/h speed limit	Four 11-ft lanes, 65 mi/h speed limit	Four 11-ft lanes, 65 mi/h speed limit	N/A
FFS (mi/h)	69.6	66.5	65.1	65.1	N/A
Capacity (pc/h/ln)	2,396.0	2,365.0	2,351.0	2,234.0	1,746 pc/h (24 percent)
Break point	1,215.0	1,338.0	1,395.0	1,259.0	N/A
CAF	1.0	1.0	1.0	0.95.0	N/A

N/A = not applicable; pc/h/ln = passenger cars per hour per lane.

Table 13. FFS and capacity estimation for Hawaii H-1 at SL-71 (westbound).

Performance Measure	New FFS Model, No CAF	HCM Model	New FFS Model, No CAF	New FFS Model with CAF	Segment-Wide Capacity Increase (New Model)
Configuration	Three 12-ft lanes, 55 mi/h speed limit	Four 10-ft lanes, 50 mi/h speed limit	Four 10-ft lanes, 50 mi/h speed limit	Four 10-ft lanes, 50 mi/h speed limit	N/A
FFS (mi/h)	54.2	61.8	54.1	54.10	N/A
Capacity (pc/h/ln)	2,242.0	2,318.0	2,241.0	1,950.00	1,074 pc/h (16 percent)
Break point	1,833.0	1,526.0	1,835.0	1,389.00	N/A
CAF	1.0	1.0	1.0	0.87	N/A

N/A = not applicable; pc/h/ln = passenger cars per hour per lane.

Table 14. FFS and capacity estimation for Dallas US 75 at Galatyn South (northbound).

Performance Measure	New FFS Model, No CAF	HCM Model	New FFS Model, No CAF	New FFS Model with CAF	Segment-Wide Capacity Increase (New Model)
Configuration	Three 12-ft lanes, 75 mi/h speed limit	Four 11-ft lanes, 70 mi/h speed limit	Four 11-ft lanes, 70 mi/h speed limit	Four 11-ft lanes, 70 mi/h speed limit	N/A
FFS (mi/h)	75.4	66.9	69.6	69.60	N/A
Capacity (pc/h/ln)	2,454.0	2,369.0	2,396.0	2,276.00	1,742 pc/h (24 percent)
Break point	985.0	1,322.0	1,218.0	1,099.00	N/A
CAF	1.0	1.0	1.0	0.95	N/A

N/A = not applicable; pc/h/ln = passenger cars per hour per lane.

Table 15. Dallas US 75 at Renner (southbound).

Performance Measure	New FFS Model, No CAF	HCM Model	New FFS Model, No CAF	New FFS Model with CAF	Segment-Wide Capacity Increase (New Model)
Configuration	Three 12-ft lanes, 75 mi/h speed limit	Four 11-ft lanes, 70 mi/h speed limit	Four 11-ft lanes, 70 mi/h speed limit	Four 11-ft lanes, 70 mi/h speed limit	N/A
FFS (mi/h)	72.7	66.9	68.1	68.10	N/A
Capacity (pc/h/ln)	2,427.0	2,369.0	2,381.0	2,262.00	1,767 pc/h (24 percent)
Break point	1,093.0	1,322.0	1,277.0	1,152.00	N/A
CAF	1.0	1.0	1.0	0.95	N/A

N/A = not applicable; pc/h/ln = passenger cars per hour per lane.

Table 16. FFS and capacity estimation for San Antonio I-10 at LCU-0010E-574.114 (eastbound).

Performance Measure	New FFS Model, No CAF	HCM Model	New FFS Model, No CAF	New FFS Model with CAF	Segment-Wide Capacity Increase (New Model)
Configuration	Four 12-ft lanes, 70 mi/h speed limit	Five 11-ft lanes, 65 mi/h speed limit	Five 11-ft lanes, 65 mi/h speed limit	Five 11-ft lanes, 65 mi/h speed limit	N/A
FFS (mi/h)	69.3	67.3	64.8	64.80	N/A
Capacity (pc/h/ln)	2,393.0	2,373.0	2,348.0	2,230.00	1,743 pc/h (24 percent)
Break point	1,230.0	1,307.0	1,409.0	1,272.00	N/A
CAF	1.0	1.0	1.0	0.95	N/A

N/A = not applicable; pc/h/ln = passenger cars per hour per lane.

Figure 9 shows the speed–flow curves along with speed–flow data points at all five sites.

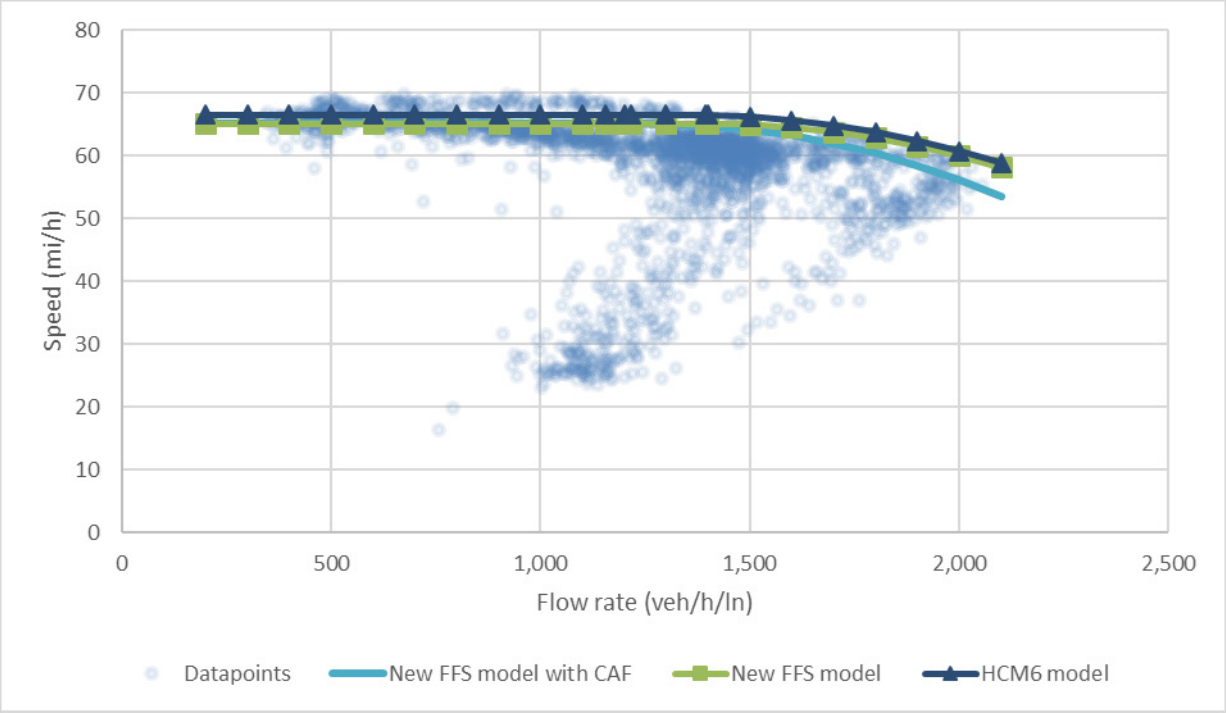

A. Dallas US 75 at 15th Street (southbound).

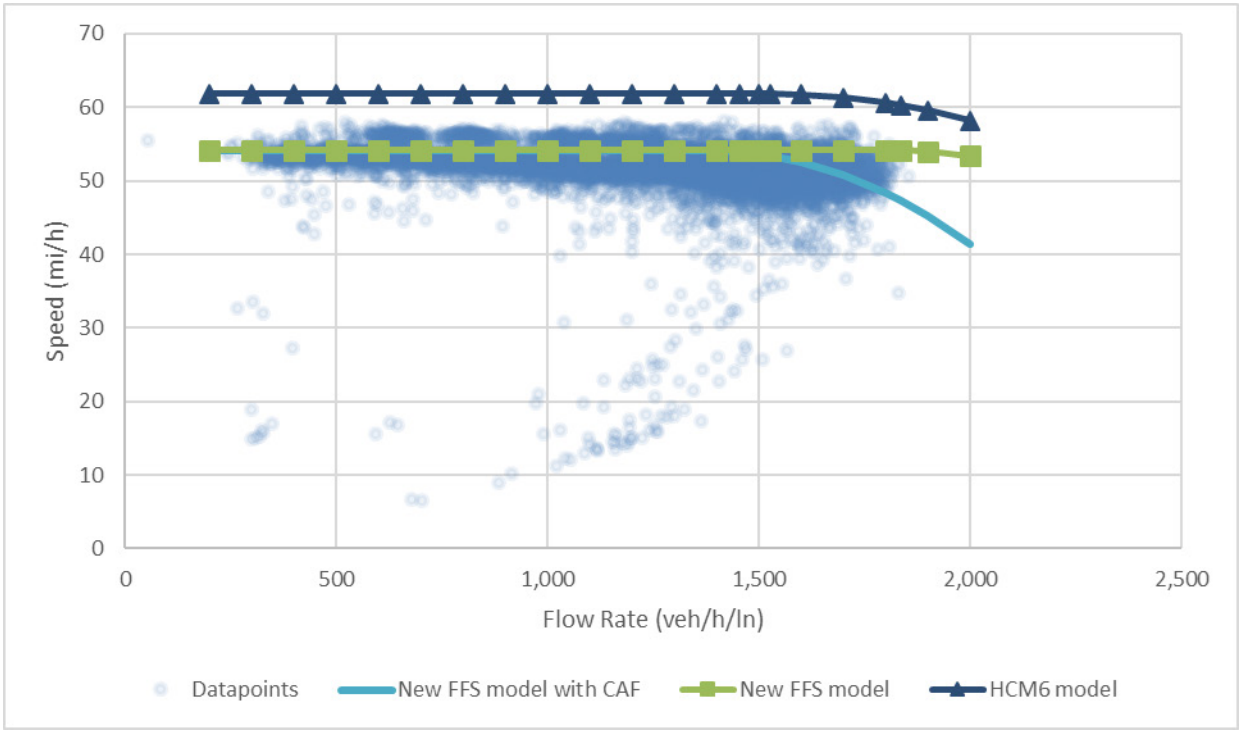

B. Honolulu H-1 at SL-71 (westbound).

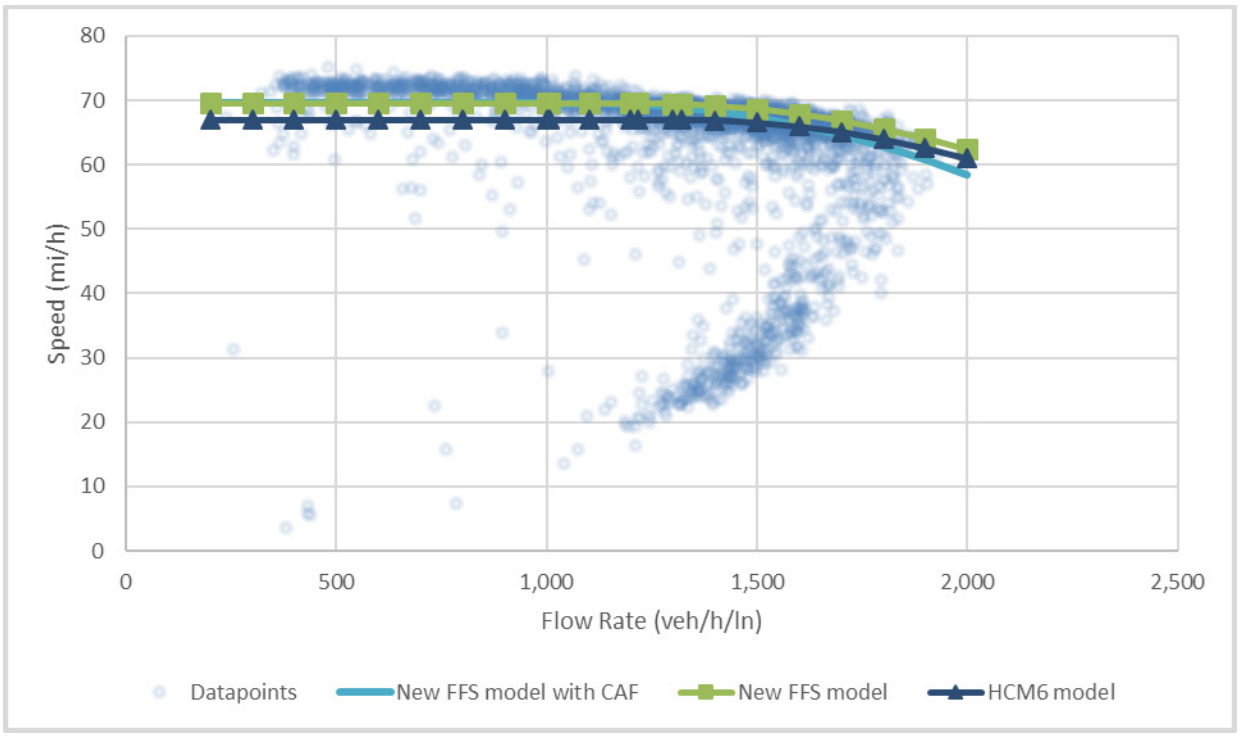

C. Dallas US 75 at Galatyn South (northbound).

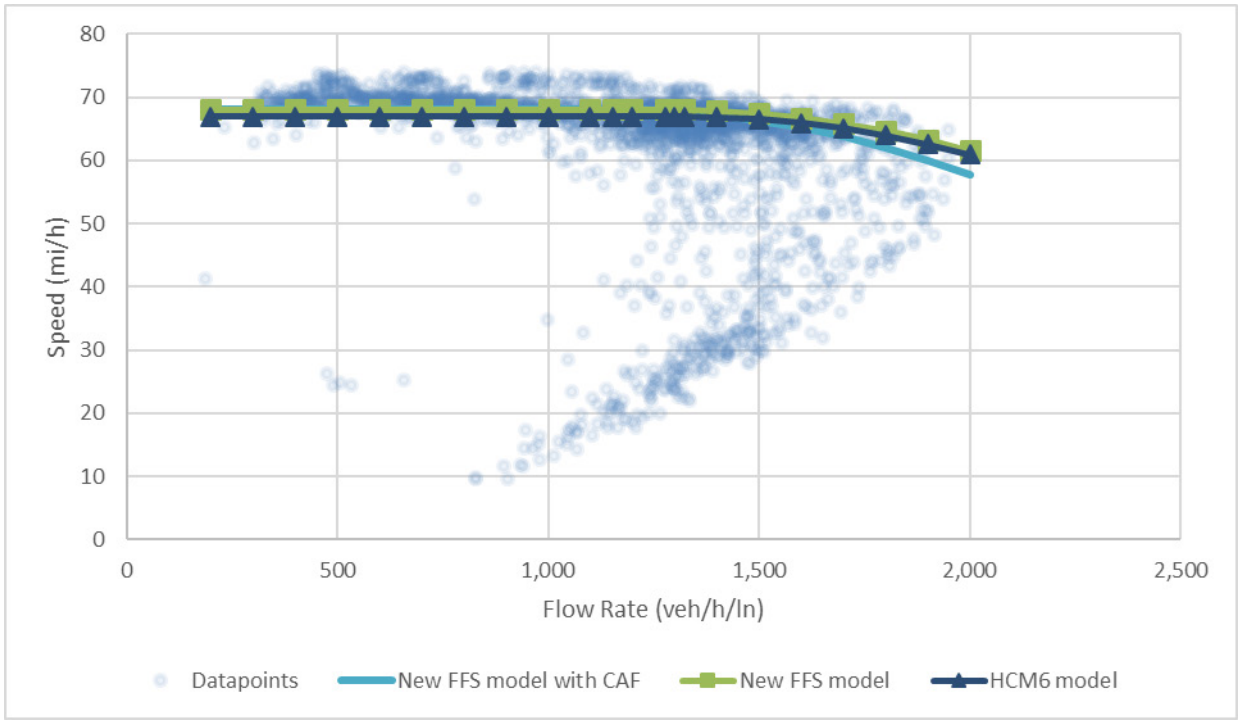

D. Dallas US 75 at Renner (southbound).

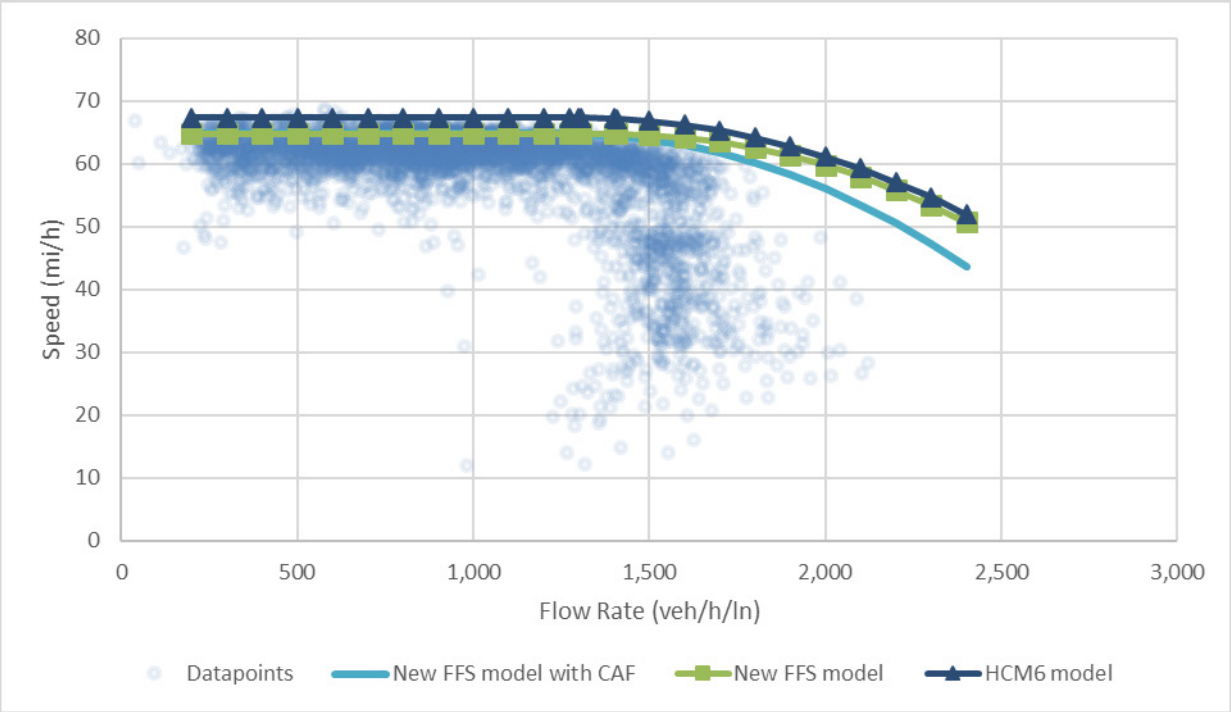

E. San Antonio I-10 at LCU-0010E-574.114 (eastbound).

Figure 9. Charts. Charts depicting speed–flow observations and fitted curves.

According to figure 8, the speed–flow curve, which is based on the new regression model, is closer to field data compared to the HCM curve. Also, further adjusting capacities using the proposed CAFs brings the curve closer to field data without over penalizing for the effect of narrow lanes.

Conclusions and Recommendations from Macroscopic Model Development

The team used macroscopic traffic flow data to quantify the effect of narrow lane segments by calculating adjustment factors for capacity and FFS as well as for an FFS regression model. Results show that capacities are significantly different among segments with different lane widths. Per-lane capacity is reduced by 5 percent on 11-ft lane widths compared to 12-ft lanes. The effect of narrow lanes is more adverse on 10-ft lane widths, where per-lane capacity is reduced by 13 percent compared to 12-ft lanes.

FFSs are also affected at narrow lane segments. The regression model presented in table 11 captures the impact of various factors, including lane and shoulder width, on FFS—and it produces a very good fit to the data. SAFs were also estimated for different segment types and speed limits. Further testing of the developed model showed that combining the new FFS estimation equation with the derived CAFs describes field data well.

The model, as well as field data, show an overall segment capacity increase when narrowing freeway lanes to create an additional lane. The magnitude of this capacity increase depends on speeds, lane widths, and number of lanes on the freeway.

Although the macroscopic data obtained for this project were exhaustive, the team recommends obtaining additional data at segments not covered herein, which would allow the completion of missing items within table 9.

MICROSCOPIC MODEL DEVELOPMENT

This section is divided into two subsections. The first subsection details the calibration of a reduced Gipps model, valid during steady-state car-following conditions, applying a weighted linear squares regression model to establish the relationship between vehicle headway and driver reaction time at various lane widths. The second subsection details the calibration of the Wiedemann 74 model using a method developed by the Virginia Tech Transportation Institute that establishes a relationship between macroscopic traffic flow properties (e.g., FFS, jam density) and the Wiedemann 74 calibration parameters (e.g., standstill distance) (Rakha and Gao 2010).

In this project, UAV footage was collected to retrieve detailed vehicle trajectory information and assess the impacts of lane-narrowing treatments on drivers' behavior. After automated post-processing of the video data, headway measurements were collected for all vehicles crossing a stationary virtual line spanning all lanes. Due to the stationary nature of the data at hand, the team decided to focus specifically on adapting the car-following model to try to capture the effects that narrowing freeway lanes have on vehicles in a microsimulation framework. Calibration of the lane-changing model required a different and more challenging type of data collection and processing, one that could dynamically follow the trajectory of vehicles to precisely capture lane changes as they occur.

Gipps Car-Following Model Development

The original Gipps models have been extended in Aimsun Next to better represent more sophisticated vehicle interactions (e.g., cooperation and aggressiveness) and to account for additional constraints that capture the effects that certain environmental elements pose on drivers (e.g., posted speed limit, road grade) (Aimsun, Inc. 2017). Due to the nature of the data collected, the team focused on adapting the car-following model to capture the effects of narrowed lanes on vehicles in a microsimulation framework.

The Gipps car-following model basically captures two behavioral components that determine vehicles' acceleration and deceleration patterns. The first component represents the intention of a vehicle to achieve a certain desired speed, while the second component reproduces limitations imposed by the preceding vehicle when trying to drive at the desired speed.

The first model component states that the maximum speed to which n can accelerate during $t + \tau$ is calculated using equation 26:

$$V_n^a(t+\tau_n) = V_n(t) + 2.5a_n\tau_n\left(1 - \frac{V_n(t)}{V_n^*}\right)\sqrt{0.025 + \frac{V_n(t)}{V_n^*}} \quad (26)$$

Where:

v^a_n = maximum velocity to which following vehicle n can accelerate during $t+\tau$.
$V_n(t)$ = velocity of following vehicle n at time t.
V_n^* = desired velocity of following vehicle n.
τ_n = reaction time.
a_n = maximum acceleration of following vehicle n.

On the other hand, the maximum speed that the same n can reach during the previous $t + \tau$ according to its own characteristics and the limitations imposed by the presence of a lead vehicle is calculated using equation 27:

$$V_n^b(t+\tau_n) = b_n\tau_n + \sqrt{(b_n\tau_n)^2 - b_n\left(2(x_l(t) - x_n(t) - s) - V_n(t)\tau_n - \frac{V_l(t)^2}{b_l}\right)} \quad (27)$$

Where:

V^b_n = maximum speed that the same n can reach during the previous $t + \tau$.
b_n = maximum desired deceleration rate of following vehicle n.
τ_n = reaction time.
$x_l(t)$ = position of lead vehicle at t.
$x_n(t)$ = position of following vehicle n at t.
s = vehicle size plus minimum following distance at a stop.
$V_n(t)$ = velocity of following vehicle n at time t.
$V_l(t)$ = velocity of following vehicle n at time t.
b_l = maximum estimated desired deceleration rate of leading vehicle.

This model also considers a minimum gap distance between leader and follower as a restriction. In the Aimsun Next simulation framework, this constraint is applied before updating the position and speed of any following vehicle n. This minimum gap is calculated using equation 28:

$$G(t) = (x_l(t) - x_n(t) - s) = \frac{v_l(t)^2}{2b_l} - \frac{v_n(t+\tau_n)^2}{2b_n} + \left(0.5V_n(t) + V_n(t+\tau_n)\right)\tau_n \quad (28)$$

Where G is the minimum gap.

Note that equation 28 can be simplified and approximated in instances where the two vehicles have similar speeds and negligible acceleration (i.e., steady-state car-following). This simplified minimum gap under steady state car-following conditions is shown in equation 29:

$$G(t) \approx 1.5\tau_n V_n(t) \tag{29}$$

In the section that follows, headway and speed data are collected at multiple control and treatment sites to try to match this functional form. The goal was to determine if there is a dependency between lane width (w) and road capacity. The latter is inversely proportional to the safety distance maintained between vehicles under dense traffic conditions. Variation in this safety distance can be modeled via a change in average reaction time $\tau(w)$ in the Gipps model. Using this assumption, the effect of lane width changes on similar driver populations was characterized.

Data Analysis and Model Calibration

Data to assess the effects of lane narrowing was obtained at seven different locations, shown in table 17. These locations yield dataset pairs that allow a direct comparison of the effects of lane narrowing in similar driver populations. This is relevant since one may argue that driver response to a lane-narrowing treatment in one location (e.g., Honolulu, HI) does not necessarily need to match that observed in another site far apart (e.g., Texas). Thus, having data gathered at multiple geographical locations is useful when trying to uncover any general trends.

Table 17. Data-collection sites summary.

City	Route	Widths (ft)
Dallas, TX	I-635	12, 11
Dallas, TX*	US 75	11
San Antonio, TX	I-410	12, 11
San Antonio, TX	I-10	12
Honolulu, HI*	H-1	11, 10
Seattle, WA	SR 99	11
Fort Lauderdale, FL	I-95	12, 11

*Data available for more than one direction (e.g., north, south) because of optimal data-collection conditions (i.e., no occlusion, desired traffic density).

The original datasets were obtained by processing video recordings captured by UAVs. Each of them contained information on the vehicle type, time of measurement, speed, tangential (or longitudinal) acceleration, lateral acceleration, and headway for individual vehicles traversing a stationary location. From these data, instantaneous gaps were inferred by multiplying the headway and speed values.

An initial data validation stage revealed that most of these datasets covered a wide array (range/span) of traffic conditions (i.e., measurements were collected for a multitude of speed values ranging from free flow conditions to near stopped congestion). Figure 10, which illustrates the speed coverage spectrum, shows a series of headway histograms using measurements collected at different speed bins (0, 20], (20, 40], (40, 60], (60, 80], (80, 100],

(100, + ∞) in mi/h for the 12-ft lane width sites. A particular binned histogram is only shown if it contains at least 5 percent of the total number of measurements in the dataset. As shown in figure 10, the Fort Lauderdale dataset is most complete, but in all cases, the speed range between 0 and 37 mi/h is well covered. Figure 10 also shows that headway distributions are consistent with the intuitive expectation to observe higher headway variability at higher speeds, since free flow conditions tend to present bigger spacing observations than those present in congested states. The first attempt to regress the simplified $G(t)$ equation (equation 29) on the available data was conducted performing an ordinary linear square regression on the speed gap measurements using the unfiltered datasets (figure 11) (Montgomery, Peck, and Vining 2012).

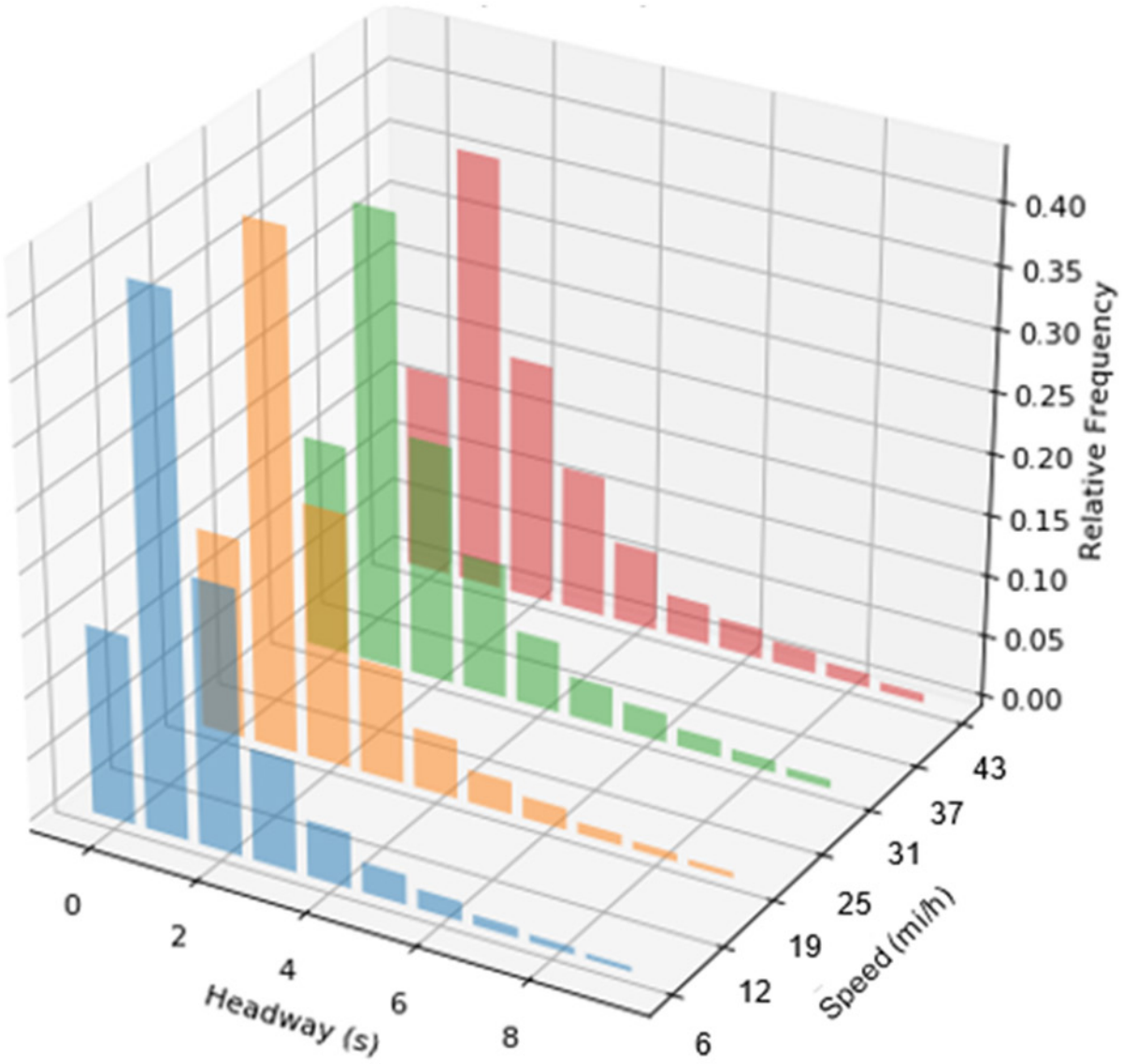

A. Control (width = 12 ft).

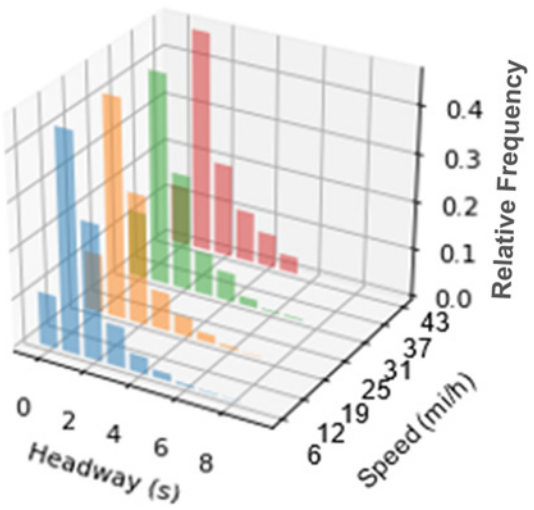

B. I-10 (width = 12 ft).

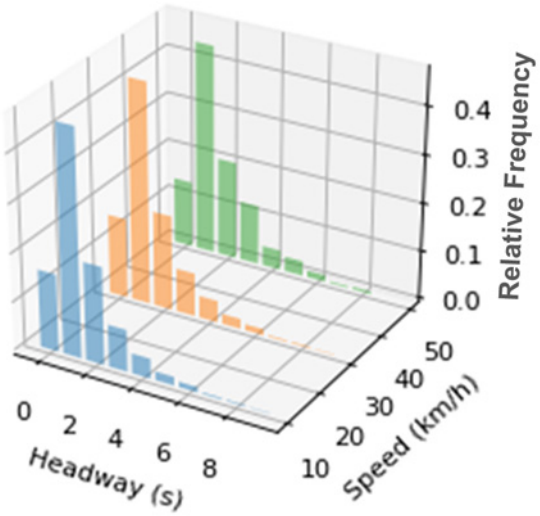

D. I-410 (width = 12 ft).

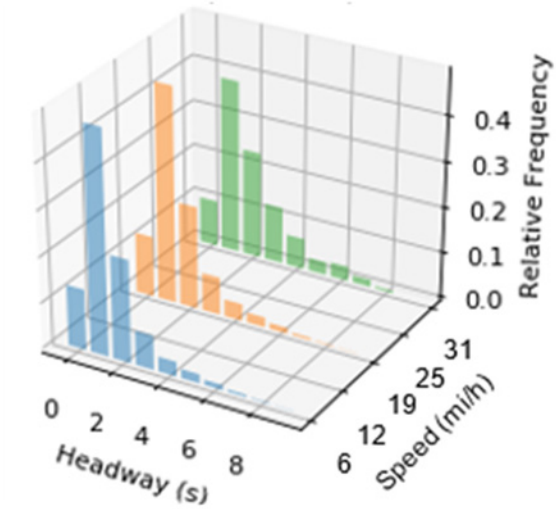

C. I-635 (width = 12 ft).

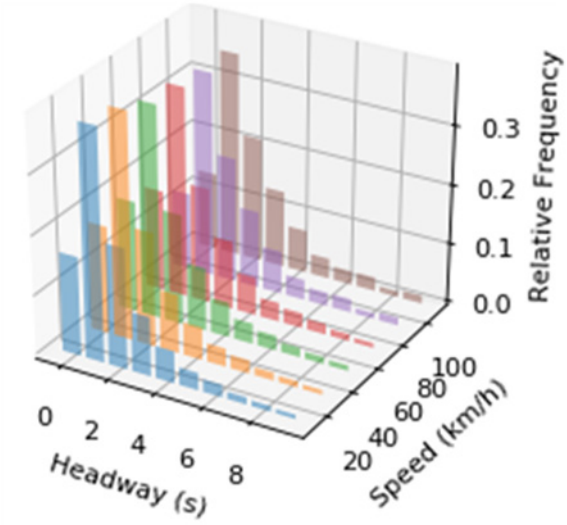

E. I-95 (width = 12 ft).

Figure 10. Graphs. Headway histograms binned by speed ranges for all 12-ft lane width sites and each individual site with 12-ft lane widths.

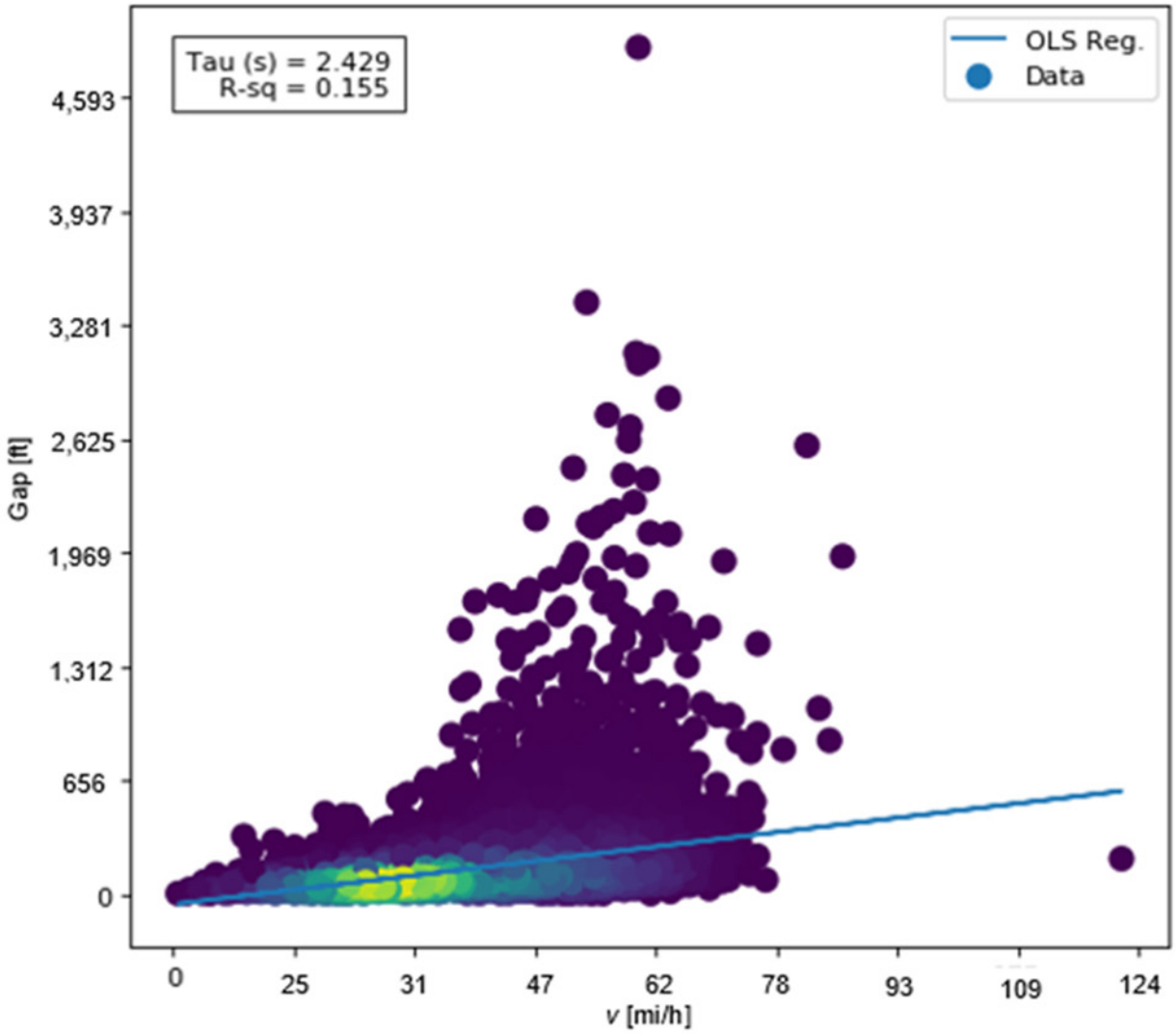

OLS Reg. = ordinary least squares regression.

A. Control (width = 12 ft).

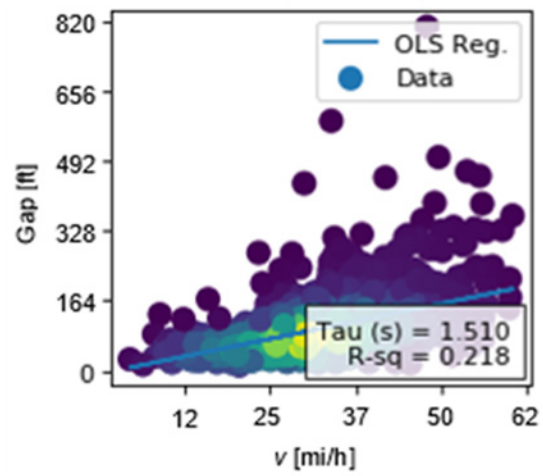

OLS Reg. = ordinary least squares regression.

B. I-10 (width = 12 ft).

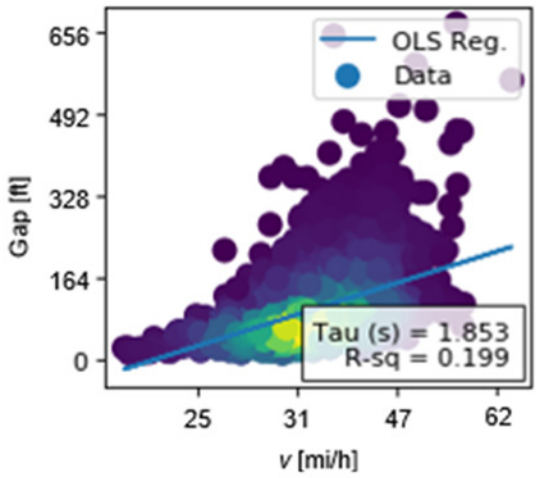

OLS Reg. = ordinary least squares regression.

D. I-410 (width = 12 ft).

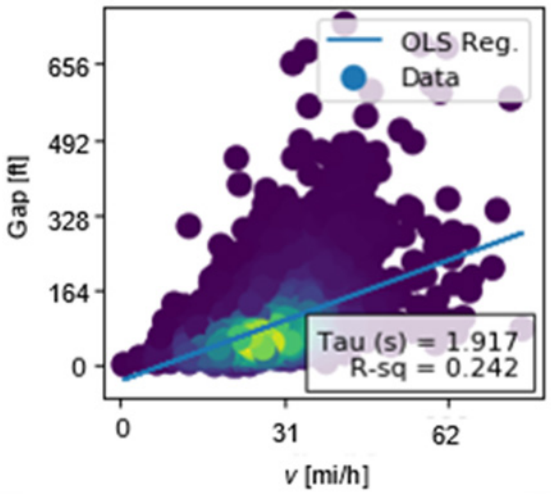

OLS Reg. = ordinary least squares regression.

C. I-635 (width = 12 ft).

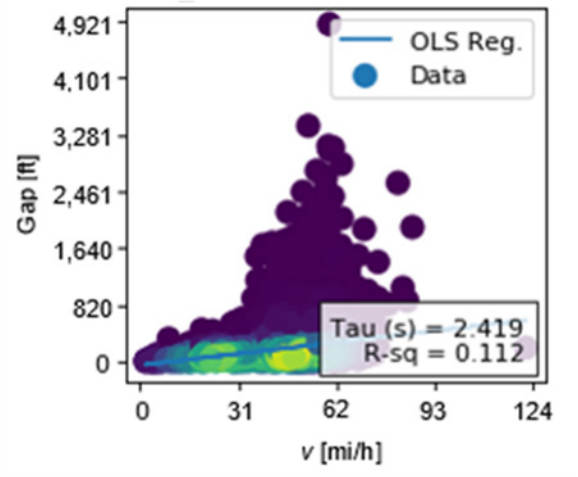

OLS Reg. = ordinary least squares regression.

E. I-95 (width = 12 ft).

Figure 11. Charts. Unfiltered speed–gap scatterplot and regression results for all 12-ft lane width sites and each individual site with 12-ft lane widths.

This preliminary analysis revealed various relevant findings. Under moderate traffic conditions, a significant fraction of vehicles' speed and position are not influenced by presence of any leader. Gaps ahead of those vehicles are therefore not constrained by their τ. A fit, assuming they would be constrained, produces values exceeding those commonly observed in literature (Gipps 1981; Kesting and Treiber 2008). In other words, the assumption that the follower vehicle's behavior is dictated by the deceleration component of the car-following model does not hold for them.

Bearing this in mind, the team performed actual calibration analysis after filtering the data with consideration of two conditions:

- Excluding all headway measurements beyond 2.5 s, as those were clearly not following the behavior dictated by the deceleration component of the car-following model.
- Excluding all tangential acceleration values outside of the −1.0–1.0 ft/s^2 range to guarantee close to negligible acceleration values.

It was clear that variability of the dependent variable, the gap, increased with the independent variable, speed. This was a sign of heteroscedasticity in the data, which should be accounted for by using an alternative regression technique: weighted linear squares. This approach results in more accurate and less variable estimates, also affecting potential hypothesis testing results. Figure 12 presents scatterplots of the filtered data, as well as regression lines and inferred reaction times values for all of the different sites, including aggregated datasets.

The results are also summarized in table 18 through table 20. Inferred reaction times values show a tendency for drivers to accept narrower gaps in cases where the treatment narrowed lanes from 12 to 11 ft, such as those on I-635 in Dallas, TX; I-410 in San Antonio, TX; and I-95 in Fort Lauderdale, FL. Even though the R-squared values differ across these site pairs, in all cases, reaction time appears to decrease at the treatment site by a percentage ranging from 3.0 percent in Fort Lauderdale, FL, to 13.8 percent in the case of I-635 in Dallas, TX, when comparing the models regressed using each site-specific dataset in isolation. The trend, however, appears to be reversed on H-1 in Honolulu, HI, where the treatment narrows lanes from 11 to 10 ft. In this case, the two directly comparable sites where measurements were collected reveal an increase of average reaction time of 1.1 and 19.5 percent, respectively.

Table 18. Model calibration results using weighted linear squares regression (12-ft lanes).

Site	Aggregate	I-635	I-410	I-95	I-10	US 75 North	US 75 South	SR 99	H-1 East	H-1 Add	H-1 West	H-1 8:15 a.m.
τ (s)	0.831	0.998	0.922	0.799	1.032	—	—	—	—	—	—	—
R-squared	0.447	0.429	0.34	0.46	0.528	—	—	—	—	—	—	—
Count	2,546	646	232	1570	98	—	—	—	—	—	—	—

—Insufficient data at this lane width.

Table 19. Model calibration results using weighted linear squares regression (11-ft lanes).

Site	Aggregate	I-635	I-410	I-95	I-10	US 75 North	US 75 South	SR 99	H-1 East	H-1 Add	H-1 West	H-1 8:15 a.m.
τ (s)	0.779	0.86	0.89	0.775	—	0.943	0.937	1.09	0.973	0.888	—	—
R-squared	0.519	0.254	0.408	0.358	—	0.072	0.374	0.551	0.554	0.688	—	—
Count	5,532	546	291	1755	—	619	428	422	887	584	—	—

—Insufficient data at this lane width.

Table 20. Model calibration results using weighted linear squares regression (10-ft lanes).

Site	Aggregate	I-635	I-410	I-95	I-10	US 75 North	US 75 South	SR 99	H-1 East	H-1 Add	H-1 West	H-1 8:15 a.m.
τ (s)	0.955	—	—	—	—	—	—	—	1.163	0.898	1.124	1.388
R-squared	0.717	—	—	—	—	—	—	—	0.643	0.733	0.615	0.167
Count	3,966	—	—	—	—	—	—	—	2192	603	685	486

—Insufficient data at this lane width.

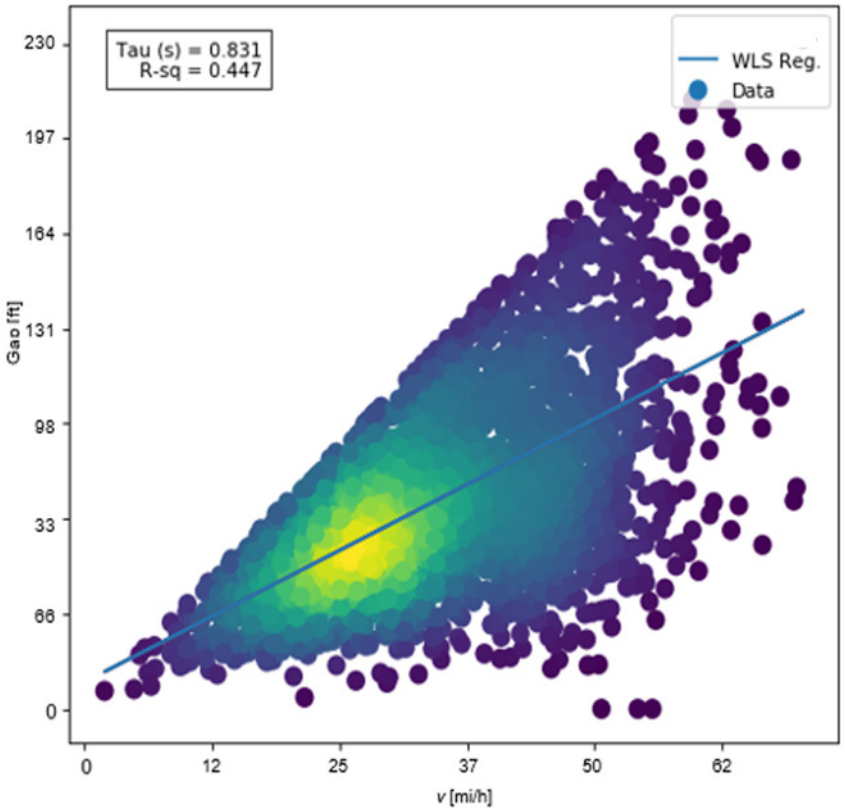

WLS Reg. = weighted least squares regression.

A. Control sites with 12-ft lanes.

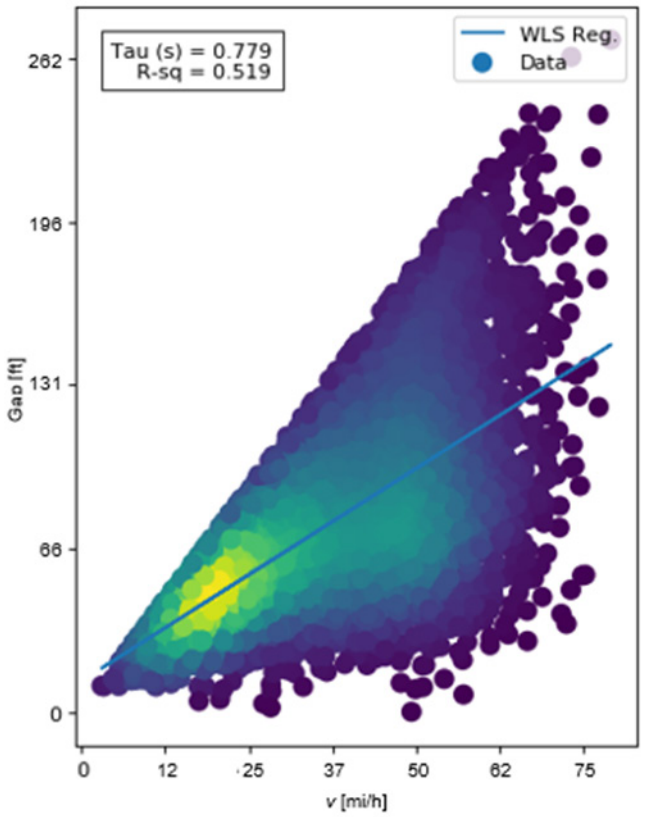

WLS Reg. = weighted least squares regression.

B. Treatment sites with 11-ft lanes.

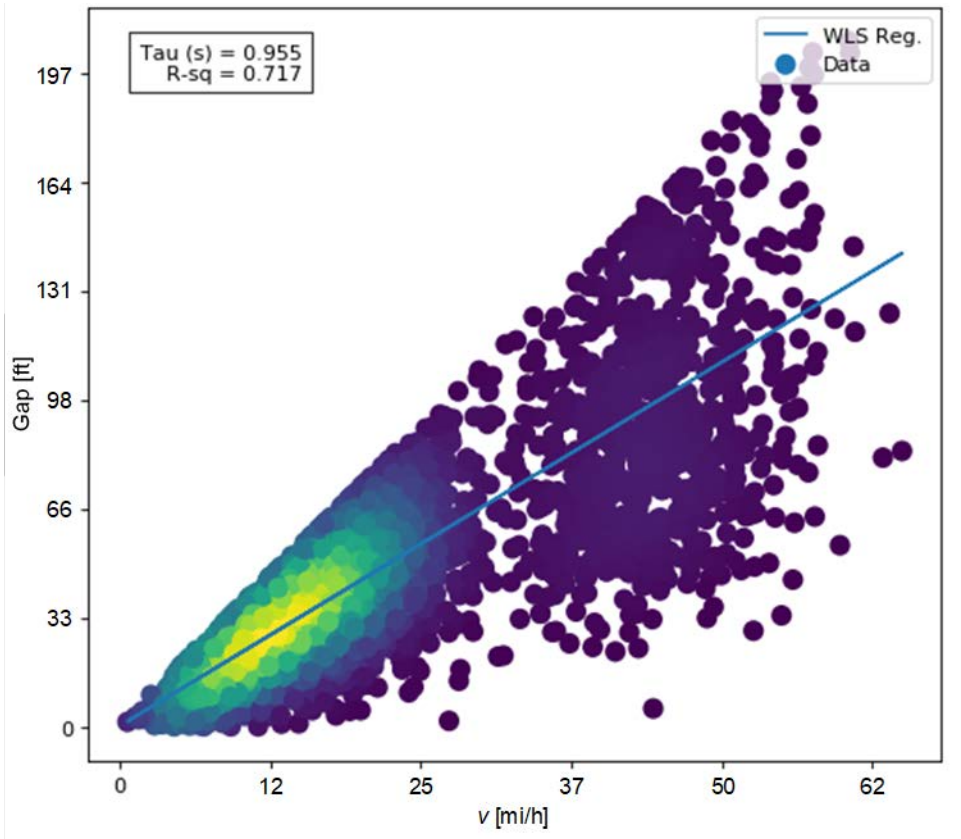

WLS Reg. = weighted least squares regression.

C. Treatment sites with 10-ft lanes.

Figure 12. Charts. Filtered speed–gap scatterplot.

The results shown in figure 12 and table 18 through table 20 beg the question: Are changes in inferred reaction times relevant or just a construct due to inherent variability in the data collected? To answer this and assess the statistical significance of observed trends, a hypothesis test on the regression slope change was conducted for each of the comparable pairs: I-635 in Dallas, TX; I-410 in San Antonio, TX; I-95 in Fort Lauderdale, FL; and the two H-1 datasets collected at similar locations in Honolulu, HI.

To do so, the paired datasets were combined, and a new categorical variable identifying measurements collected at the treatment site (the site with narrower lane widths) was added. The regression model was then augmented to consider not only speed measurements, but also a variable that interacts speed values and with the categorical "treatment" variable to identify the significance of the treatment effects. Thus, instead of running a regression for simplified $G(t)$ equation, the model calibrated to perform the hypothesis test is shown in equation 30:

$$G_n(t) \approx 1.5\tau V_n(t) + \beta T(w) V_n(t) \tag{30}$$

Where:

β = coefficient indicating the magnitude of the treatment impact on average T.
$T(w)$ = categorical variable depending on the site's lane width.

$T(w)$ has a value of 1 for measurements collected at the treatment sites (sites with 11-ft lanes (I-635 in Dallas, TX; I-410 in San Antonio, TX; and I-95 in Fort Lauderdale, FL) and 10-ft lanes on the H-1 freeway in Honolulu, HI) and 0 for control site measurements (sites with an extra foot in lane width). The results are aligned with those observed while performing a simpler regression on individual datasets. That is, reaction times in those cases where lanes where narrowed from 12 to 11 ft were accompanied by a reaction time decrease in the treatment locations. Figure 13 shows a scatterplot and regression lines for the two statistically significant cases. They indicate that T decreases by up to 8 percent at treatment sites having narrow lane widths. This result is intuitive because drivers should be more attentive under driving conditions that are more physically challenging. The appendix shows how an 8-percent decrease in reaction time would increase freeway capacity by approximately 100 veh/h/ln.

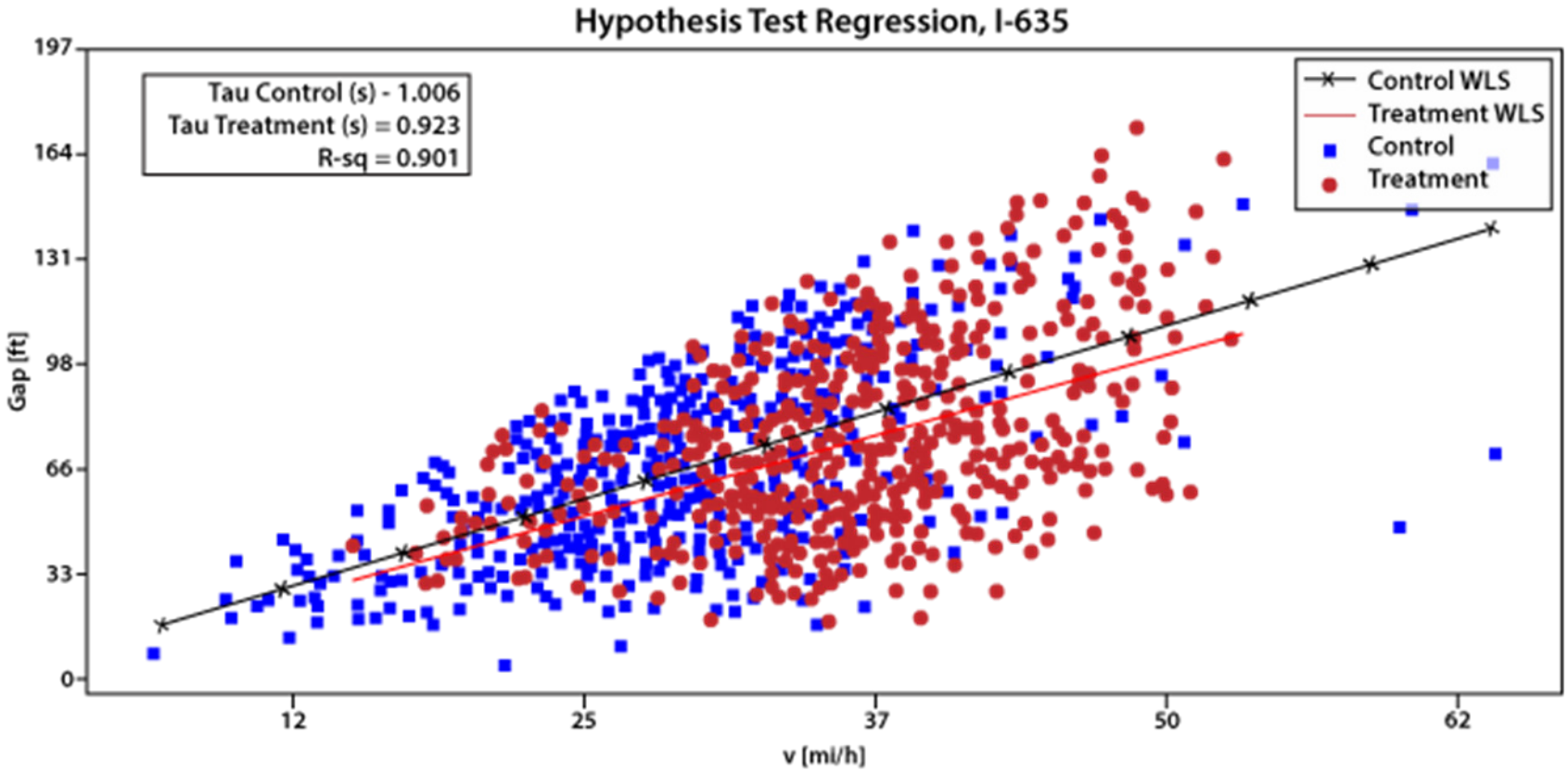

WLS = weighted least squares regression.

A. I-635 Dallas, TX.

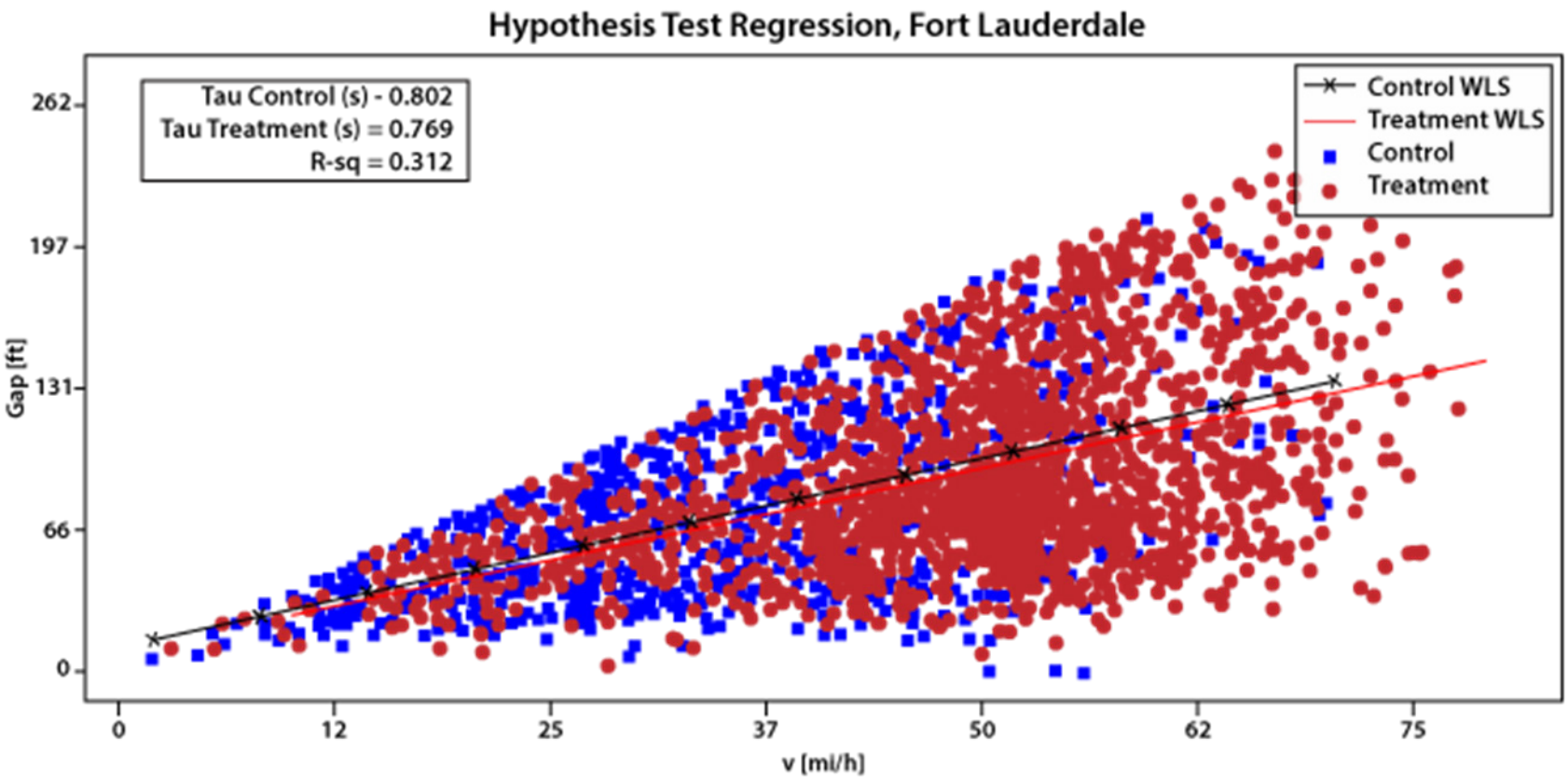

WLS = weighted least squares regression.

B. I-95 Fort Lauderdale, FL.

Figure 13. Charts. Hypothesis test regression results for the two sites with statistically significant effects on I-635 in Dallas, TX, and I-95 in Fort Lauderdale, FL.

Wiedemann 74 Car-Following Model Development

The narrow lanes car-following model was derived from the 12-, 11-, and 10-ft site data collected via UAV video analysis in Honolulu, HI; Seattle, WA; San Antonio, TX; Fort Lauderdale, FL; and Dallas, TX. The key assumptions of this model are threefold:

- Under standard lane conditions (12-plus ft wide), drivers on narrow lane freeway segments would possess similar following behaviors to those drivers observed at the Dallas, TX; San Antonio, TX; and Fort Lauderdale, FL, 12-ft test sites.
- Under 11-ft lane width conditions, drivers on narrow lane freeway segments would possess similar following behaviors to those drivers observed at the Dallas, TX; San Antonio, TX; Fort Lauderdale, FL; Honolulu, HI; and Seattle, WA, test sites.
- Under 10-ft lane width conditions, drivers on narrow lane freeway segments would possess similar following behaviors to those drivers observed at the Honolulu, HI, test sites.

Data from different sites, collected from various locations, timeframes, and number of lanes, were first aggregated into location- and time-of-day-specific files each containing 1-min bins yielding lane number, flow rates, average speed, and headway. Headway was captured via UAV by measuring the amount of time between vehicles.

For this project, a method from Virginia Tech Transportation Institute was used to calibrate the Wiedemann model (Rakha and Gao 2010). This method calculates calibrated car-following parameters required to simulate a sample set of data in Vissim from that sample's standstill distance, space–mean FFS, average saturation flow rate, and jam density. This method was chosen because lane-specific headways extracted by video post-processing are similar to macroscopic loop-detector-type raw data, which is a common form of field data collection. Since the Wiedemann model covers multiple congestion regimes, the full set of unfiltered data were used to calibrate the model instead of using filtered data, as with the Gipps model.

The Rakha and Gao (2010) method for calibrating car-following models using macroscopic loop detector data was derived specifically for metric units. Therefore, the data the team collected in English units were converted into metric units for this portion of the analysis. The location- and time-of-day-specific files were first compiled into a location summary file in which the following attributes were calculated for each 1-min bin:

- Flow rate, collected in vehicles per hour (veh/h), equivalent value in English and metric units.
- Speed, collected in mi/h, converted to km/h.
- Space headway, collected in feet, converted to meters.
- Density, collected in vehicles per mile (veh/mi), converted to veh/km.

For ease of access, the required unit conversions applied are summarized here. To convert to speed, collected in mi/h, to the necessary metric unit (km/h), original data were multiplied by 1.609. To convert space headway, collected in feet, to the necessary metric unit (meters), original data were divided by 3.281. Finally, to convert density, collected in veh/mi, to the necessary metric unit (veh/km), original data were divided by 1.609.

From this, location, summary binned data, and average, maximum, minimum, standard deviation, and percentiles (every 5th percentile) were extracted for each of the types of data. Finally, binned data from each site were combined into 12-ft (control site), 11-ft (treatment site), and 10-ft (treatment site) data. Again, average, maximum, minimum, standard deviation, and percentiles (every 5th percentile) were extracted for each of the types of data.

Each set of calibrated parameters was validated by applying them to a test network within Vissim and recording the speed, flow rate, density, and headways. After running the test network with the calibrated following behaviors, test network data were compared to control or treatment site data. The driver behavior model used for this data is the Wiedemann 74 car-following behavior model, which is more effective than the Wiedemann 99 model for emulating reduced speed traffic conditions likely to prevail under reduced lane widths. The Wiedemann 74 model calculates a trailing vehicle's minimum following distance (*Safety Distance*) from its current speed as shown in equation 31:

$$Safety\ Distance = AX + BX\sqrt{v} \tag{31}$$

Where:

AX = standstill distance.
BX = at-speed safety distance.
v = velocity.

BX is calculated using equation 32:

$$BX = BX_{additive} + BX_{multiplicative} \times z \tag{32}$$

Where:

$BX_{additive}$ = average at-speed safety distance.
$BX_{multiplicative}$ = at-speed safety distance variation.
z = random variable ϵ [0,1]; normally distributed with a mean of 0.5 and a standard deviation of 0.15.

The Rakha and Gao (2010) method used to calibrate Wiedemann 74 car-following parameters from control and treatment site data fits the field data between two bounds—more specifically, the relationship between speed and spacing between vehicles. Raw field data should generally fit between the lower bounding function with speed as the independent variable (*ABX*) and the upper bounding function with speed as the independent variable (*SDX*) (equation 33):

$$ABX \leq spacing \leq SDX \tag{33}$$

Where *spacing* is the vehicle spacing data from raw field data.

$$ABX = s_j + BX\sqrt{u} \tag{34}$$

Where:

s_j = standstill distance.

u = speed.

$$SDX = s_j + BX * EX\sqrt{u} \tag{35}$$

Where EX is calculated in equation 37.

The unitless parameters BX and EX are calculated from field data using the methodology developed by Rakha and Gao (2010) using equation 36 and equation 37:

$$BX = 1000\sqrt{3.6}\sqrt{u_f}\left[\frac{1}{\alpha q_c} - \frac{1}{k_j u_f}\right] \tag{36}$$

Where:

u_f = space–mean free flow speed (km/h).

α = parameter ranging between 1.5 and 2.5.

q_c = mean saturation flow (veh/h/ln).

k_j = jam density (veh/km/ln).

$\alpha \epsilon$ [1.5, 2.5].

$$EX = \frac{\frac{k_j u_f}{q_c} - 1}{\frac{k_j u_f}{\alpha q_c} - 1} \tag{37}$$

Once the bounds are fit to the field data, the Wiedemann 74 parameters (AX, $BX_{additive}$, and $BX_{multiplicative}$) are calculated using equation 38 through equation 40, respectively:

$$AX = s_j \tag{38}$$

$$BX_{additive} = BX \tag{39}$$

$$BX_{multiplicative} = BX(EX - 1) \tag{40}$$

Thus, this method requires the determination of standstill distance, space-mean FFS, mean saturation flow rate, and jam density from the headway data collection via UAV and mined through the video post-processing software.

12-ft (Control Site) Car-Following Model Development

As a reminder, the Rahka and Gao (2010) method applied in this section required that data be in metric units. Therefore, the analysis in this section must be completed with data (i.e., flow rate, space headway, speed, and density) in metric units. For ease of access, the required unit conversions applied are summarized here. To convert to speed, collected in mi/h, to the necessary metric unit (km/h), original data were multiplied by 1.609. To convert space headway, collected in ft, to the necessary metric unit (m), original data were divided by 3.281. Finally, to convert density, collected in veh/mi, to the necessary metric unit (veh/km), original data were divided by 1.609.

The first piece of information required for the calibration method is the standstill distance from the control data. Unfortunately, field data did not produce samples of vehicles at standstill or traveling at near-standstill ranges. Therefore, the team estimated the standstill distance by taking the inverse of the jam density, as shown in equation 41 (Hoogendoorn 2018). It is important to note that the standstill distance and standstill headway are not the same value. The standstill headway is front bumper to front bumper, whereas the standstill distance in the Wiedemann model is from the trailing vehicle's front bumper to leading vehicle's rear bumper (i.e., spatial gap or following distance). Therefore, average vehicle length was subtracted from space headway to generate standstill distance.

$$Standstill\ Distance = \frac{1000}{Jam\ Density} - Vehicle\ Length \quad (41)$$

Where:

Standstill Distance = standstill distance.
Jam Density = jam density.

For equation 41, *Standstill Distance* is in meters, *Jam Density* is in veh/km, and *Vehicle Length* is in meters.

To estimate *Jam Density*, a curve of best fit (i.e., the line in figure 14) was developed for the speed–density diagram (figure 14). This curve is approximated by equation 42 and is shown in figure 14:

$$Speed = \frac{4000}{(Density+12)} - 35 \quad (42)$$

Where:

Speed = speed (km/h).
Density = density (km/h).

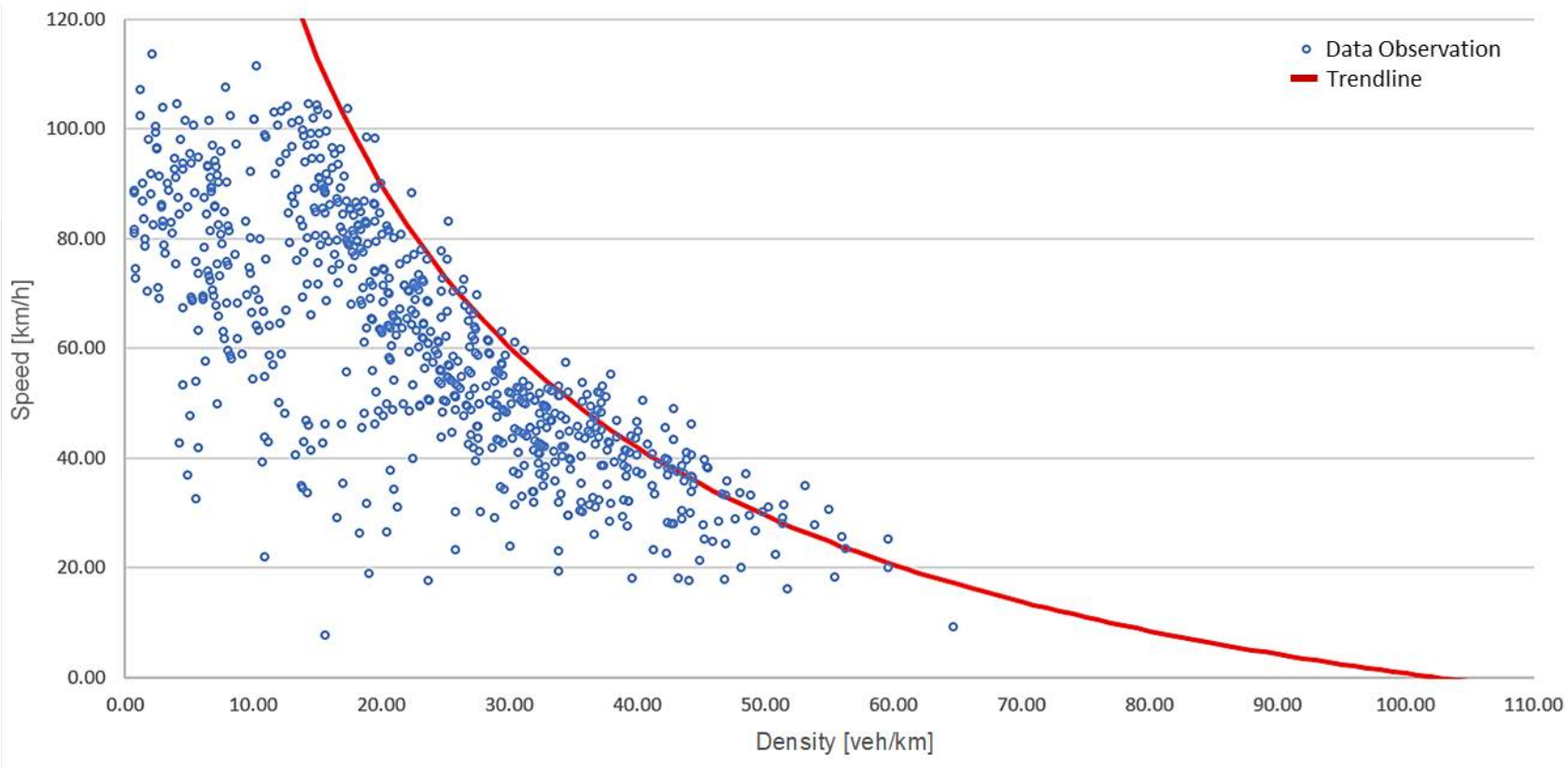

1 km = 0.62 mi.

Figure 14. Chart. Speed–density plot for 12-ft lane width observations.

By definition, jam density occurs when speed is 0 km/h. Thus, to estimate jam density, equation 42 is set equal to 0, and density is calculated algebraically. At a speed of 0 km/h, this approximation equation yielded a jam density of 102 veh/km. As shown in equation 41, standstill distance is computed as the inverse of jam density (i.e., standstill distance = 1/jam density). As such, the final value for *AX* used in the 12-ft calibrated model was 4.804 m (15.76 ft).

The next required input is FFS. As discussed in chapter 4, video clips showing predominantly free flow conditions were excluded from the data processing effort because lane widths are believed to have little effect on driver behavior under such conditions. Nonetheless, many temporary periods of free flow were included among processed data, especially the data points collected from lanes flowing more smoothly than their congested counterparts. Therefore, the decision was made to classify the 95th percentile observed speed as FFS. The final value for FFS used in the model was 98.3 km/h (60.9 mi/h). The next required input was mean saturation flow rate. This value was extracted directly from field data (table 21 and figure 15). The final value for mean saturation flow rate used in the model was 2,100 veh/h/ln.

Using jam density (equation 42), FFS (table 21), and saturation flow rate (table 21) as inputs, the team obtained the following values for *BX* and *EX*: *BX* = 1.707 (equation 36), *EX* = 4.149 (equation 37).

Inputting *BX* and *EX* into equation 34 and equation 35, the results for the 12-ft lane width data bounding equations *ABX* and *SDX* are obtained in equation 43 and equation 44 and shown in figure 16:

$$ABX = 4.804 + 1.707\sqrt{u} \tag{43}$$

$$SDX = 4.804 + 7.081\sqrt{u} \tag{44}$$

The three required Wiedemann 74 calibration parameters, *Ax*, $BX_{additive}$, and $BX_{multiplicative}$, are derived from the s_j, *BX*, and *EX* calculated for the 12-ft lane width data:

- *AX* = 15.76 ft.
- $BX_{additive}$ = 1.71.
- $BX_{multiplicative}$ = 5.374.

The final car-following model calibrated to the control site conditions (12-ft lanes) is governed by equation 45:

$$Safety\ Distance = 15.76 + (1.71 + 5.37z)\sqrt{v} \tag{45}$$

Where *v* is velocity (mi/h).

Table 21. Combined data for 12-ft lane width observations.

Statistic	Count (veh/min)	Speed (mi/h)	Speed (ft/s)	Headway (s)	Headway (ft)	Count (veh/h)	Speed (km/h)	Speed (m/s)	Headway (m)	Density (veh/mi)	Density (veh/km)
Average	20	37.9	55.6	3.1	187.0	1,201	60.7	16.9	56.7	37	23
Maximum	35	71.0	104.3	26.7	2,172.2	**2,100	113.7	31.6	659.1	103	64
Minimum	1	4.8	7.0	0.8	30.6	60	7.7	2.1	9.3	1	0
Standard deviation	7	13.8	20.2	2.7	229.1	478	22.1	6.1	69.5	20	12
0.05 percentile	4	17.5	25.7	1.7	54.2	240	28.1	7.8	16.4	5	3
0.10 percentile	8	20.4	29.9	1.8	63.3	480	32.6	9.1	19.2	9	6
0.15 percentile	9	23.2	34.0	1.8	69.1	588	37.2	10.3	21.0	12	7
0.20 percentile	11	25.4	37.2	1.9	75.8	660	40.6	11.3	23.0	17	10
0.25 percentile	14	26.9	39.5	2.0	82.8	840	43.1	12.0	25.1	22	13
0.30 percentile	18	28.7	42.1	2.0	87.2	1,080	46.0	12.8	26.4	25	15
0.35 percentile	19	30.5	44.8	2.1	91.7	1,140	48.9	13.6	27.8	28	17
0.40 percentile	20	31.8	46.6	2.1	100.2	1,200	50.9	14.1	30.4	30	19
0.45 percentile	21	33.7	49.4	2.2	107.8	1,284	54.0	15.0	32.7	33	20
0.50 percentile	22	36.2	53.1	2.3	117.5	1,320	58.0	16.1	35.6	36	22
0.55 percentile	23	39.1	57.4	2.4	128.6	1,380	62.7	17.4	39.0	39	24
0.60 percentile	24	41.6	61.1	2.4	138.8	1,440	66.7	18.5	42.1	42	26
0.65 percentile	24	44.0	64.5	2.5	151.8	1,440	70.5	19.6	46.1	46	28
0.70 percentile	25	46.5	68.2	2.6	167.1	1,500	74.5	20.7	50.7	49	30
0.75 percentile	26	49.5	72.7	2.7	185.1	1,560	79.4	22.0	56.2	52	32
0.80 percentile	27	51.6	75.7	2.9	209.6	1,620	82.7	23.0	63.6	55	34
0.85 percentile	27	54.2	79.5	3.5	239.7	1,620	86.9	24.1	72.7	59	37
0.90 percentile	28	57.0	83.7	5.4	371.7	1,680	91.4	25.4	112.8	64	40
0.95 percentile	30	*61.4	90.0	8.0	596.3	1,800	*98.3	27.3	180.9	71	44

*FFS: 95th percentile speed.
**Saturation flow rate: maximum observed hourly vehicle count.

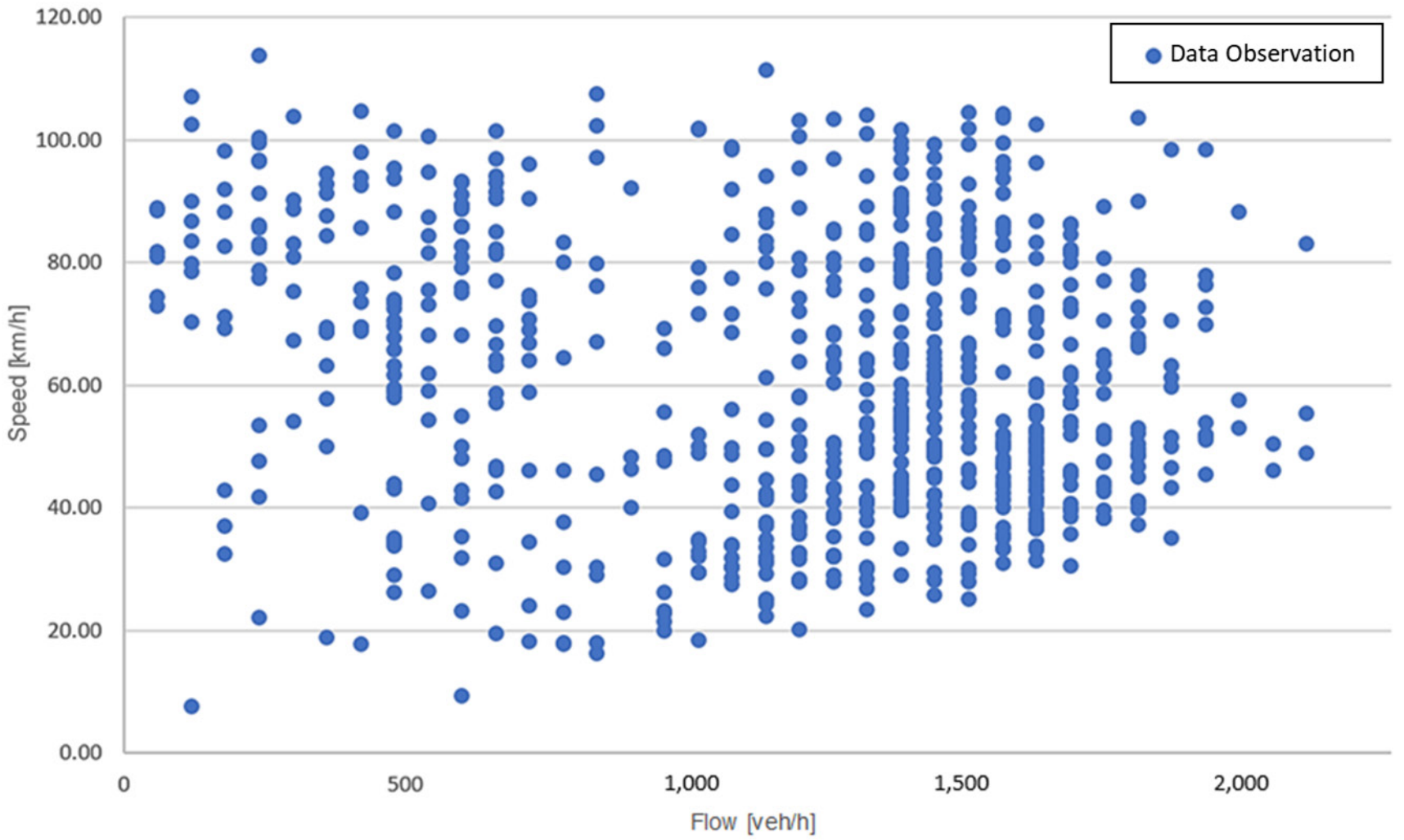

1 km = 0.62 mi.

Figure 15. Chart. Speed–flow plot for 12-ft lane width observations.

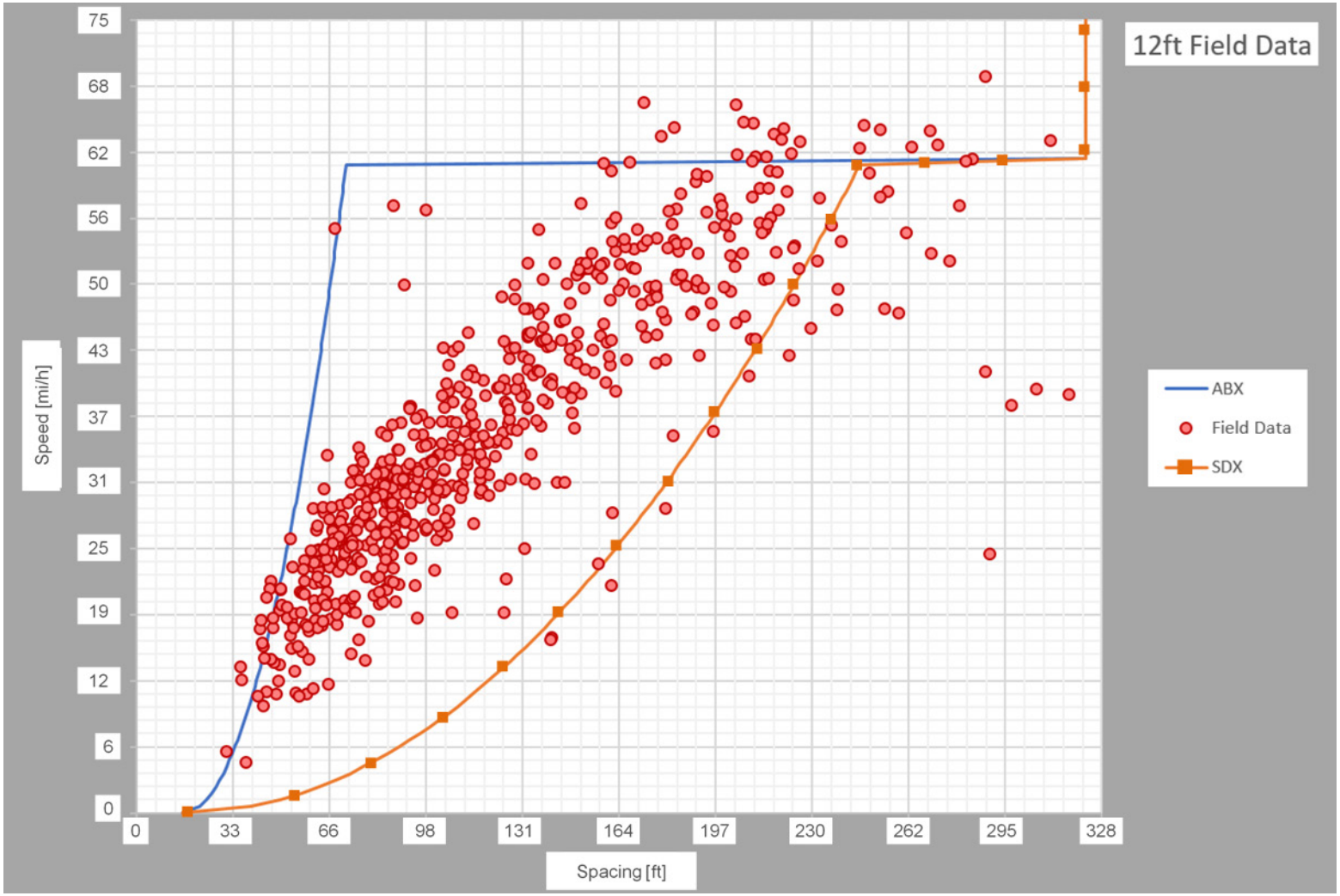

Figure 16. Chart. Calibration bounds plot for 12-ft lane width observations.

11-ft Treatment Car-Following Model Development

For the 11-ft test site data, the procedure for obtaining standstill distance was the same as for 12-ft lanes. A curve of best fit was developed for the speed–density diagram (figure 17). This curve is approximated by equation 46. By definition, jam density occurs when speed is 0 km/h. Thus, to estimate jam density, equation 46 is set equal to 0, and density calculated algebraically. At a speed of 0 km/h, this approximation equation yielded a jam density of 95 veh/km.

$$Speed = \frac{4000}{(Density+5)} - 40 \quad (46)$$

Where *Speed* and *Density* are in units of km/h.

Standstill distance was computed as the inverse of jam density. Thus, the final value for standstill distance used in the 11-ft calibrated model was 5.526 m (18.13 ft). The next required input was FFS. As with the 12-ft model, the 95th percentile observed speed was assumed to be FFS. In this case, the final value for FFS used in the 11-ft model was 103.395 km/h. The final required input was mean saturation flow rate. This value was again extracted directly from field data (table 22 and figure 18). The final value for mean saturation flow rate used in the 11-ft model was 2,640 veh/h/ln.

Using jam density (figure 17 and equation 46), FFS (table 22), and saturation flow rate (table 22) as inputs, the team obtained the following values for *BX* and *EX*: *BX* = 2.212 (equation 36), *EX* = 0.416 (equation 37).

Inputting *BX* and *EX* into equation 34 and equation 35, the results for the 11-ft lane width data bounding equations *ABX* and *SDX* are obtained in equation 47 and equation 48 and illustrated in figure 19:

$$ABX = 5.526 + 2.212\sqrt{u} \quad (47)$$

$$SDX = 5.526 + 5.344\sqrt{u} \quad (48)$$

The three required Wiedemann 74 calibration parameters, *Ax*, $BX_{additive}$, and $BX_{multiplicative}$, are derived from the s_j, *BX*, and *EX* calculated for the 11-ft data:

- *AX* = 18.13 ft.
- $BX_{additive}$ = 2.21.
- $BX_{multiplicative}$ = 3.13.

The final car-following model calibrated to the treatment site (11-ft lane width) conditions is shown in equation 48:

$$Safety\ Distance = 18.13 + (2.21 + 3.13z)\sqrt{z} \quad (49)$$

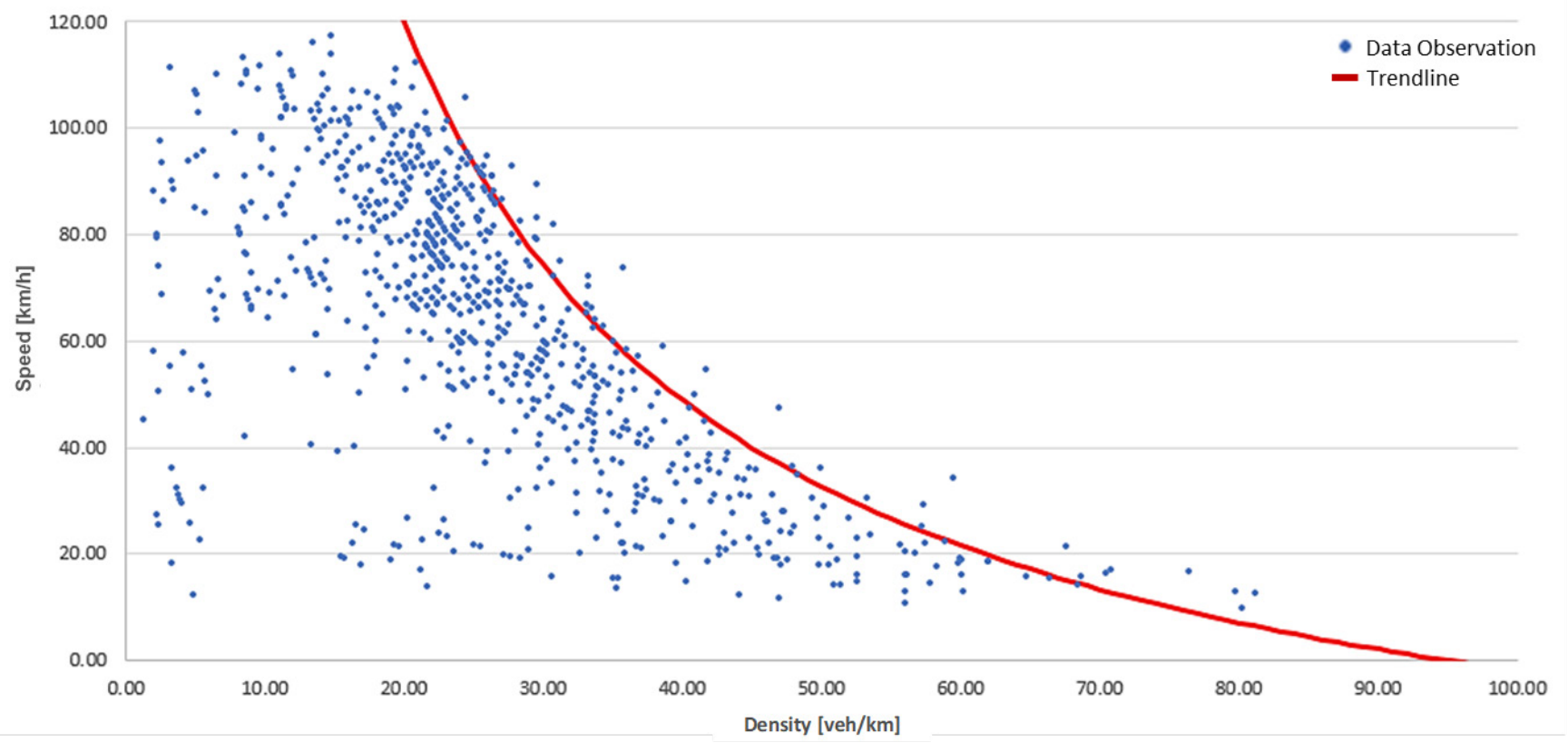

1 km = 0.62 mi.

Figure 17. Chart. Speed–density plot for 11-ft lane width observations.

Table 22. Combined data for 11-ft lane width observations.

Statistic	Count (veh/min)	Speed (mi/h)	Speed (ft/s)	Headway (s)	Headway (ft)	Count (veh/h)	Speed (km/h)	Speed (m/s)	Headway (m)	Density (veh/mi)	Density (veh/km)
Average	24	39.6	93.1	2.3	197.2	1,429	63.5	17.6	37.4	42	26
Maximum	44	73.3	172.3	12.2	1,040.5	**2,640	117.5	32.6	197.1	130	81
Minimum	1	6.1	14.3	1.1	23.1	60	9.7	2.7	4.4	2	1
Standard deviation	9	16.7	39.2	1.1	92.0	543	26.7	7.4	17.4	21	13
0.05 percentile	7	11.5	27.0	1.4	66.6	405	18.4	5.1	12.6	10	6
0.10 percentile	10	13.9	32.6	1.6	90.6	600	22.2	6.2	17.2	18	11
0.15 percentile	14	18.3	43.0	1.6	105.4	840	29.3	8.1	20.0	23	14
0.20 percentile	16	22.3	52.3	1.7	122.6	960	35.7	9.9	23.2	27	17
0.25 percentile	18	26.3	61.9	1.8	136.3	1,080	42.2	11.7	25.8	30	19
0.30 percentile	20	30.6	71.8	1.8	149.2	1,200	49.0	13.6	28.3	32	20
0.35 percentile	22	33.5	78.8	1.9	162.3	1,320	53.7	14.9	30.7	34	21
0.40 percentile	23	36.4	85.5	1.9	171.7	1,380	58.3	16.2	32.5	36	22
0.45 percentile	24	39.4	92.5	2.0	184.3	1,440	63.1	17.5	34.9	37	23
0.50 percentile	25	41.8	98.3	2.0	193.5	1,500	67.0	18.6	36.7	39	24
0.55 percentile	26	43.8	102.9	2.1	202.3	1,560	70.1	19.5	38.3	41	25
0.60 percentile	27	46.1	108.3	2.2	210.1	1,620	73.8	20.5	39.8	42	27
0.65 percentile	28	48.7	114.5	2.2	217.6	1,680	78.1	21.7	41.2	45	28
0.70 percentile	29	50.7	119.2	2.3	229.5	1,740	81.3	22.6	43.5	48	30
0.75 percentile	30	53.2	125.1	2.4	239.3	1,800	85.3	23.7	45.3	52	32
0.80 percentile	32	55.2	129.8	2.6	252.0	1,920	88.5	24.6	47.7	56	35
0.85 percentile	33	57.8	135.8	2.7	271.0	1,980	92.6	25.7	51.3	61	38
0.90 percentile	35	60.4	142.0	3.1	299.3	2,100	96.8	26.9	56.7	69	43
0.95 percentile	37	*64.5	151.6	3.7	355.1	2,220	*103.4	28.7	67.3	82	51

1 m = 3.28 ft.
1 km = 0.62 mi.
*FFS: 95th percentile speed.
**Saturation flow rate: maximum observed hourly vehicle count.

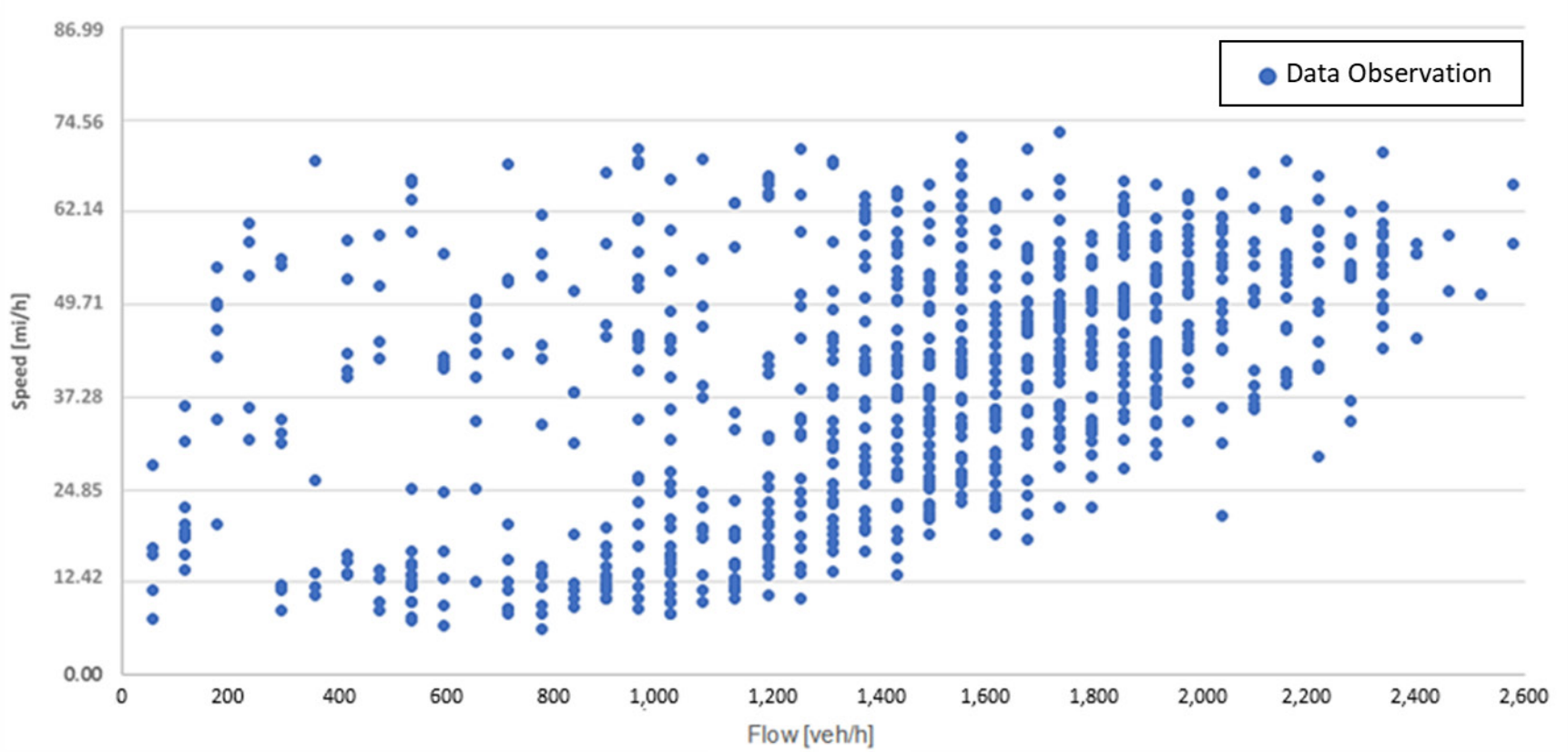

Figure 18. Chart. Speed–flow plot for 11-ft lane width observations.

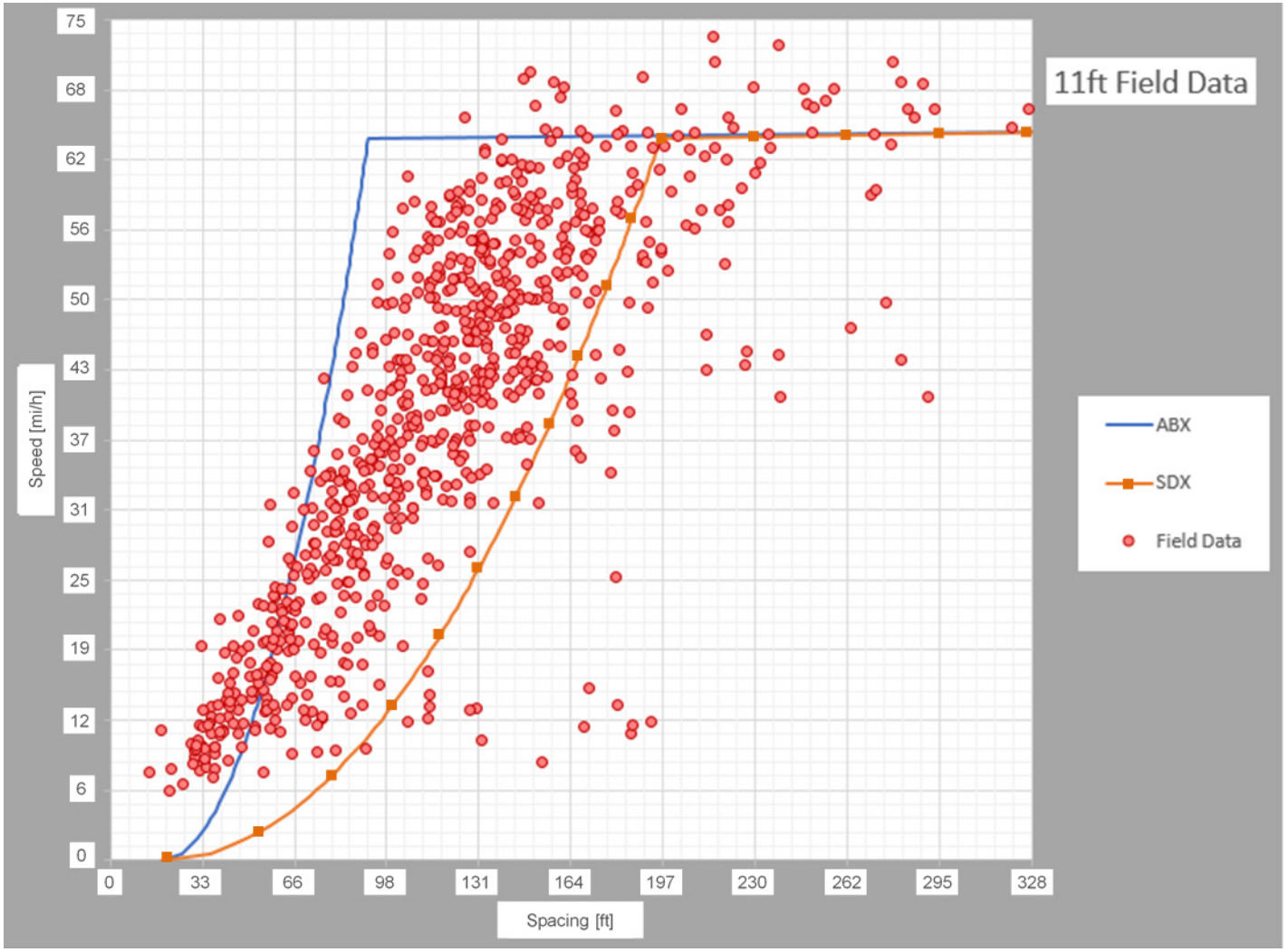

Figure 19. Chart. Calibration bounds plot and 11-ft lane width observations.

10-ft Treatment Car-Following Model Development

Similar to the 12- and 11-ft processes, a curve of best fit was developed for the speed–density diagram (figure 20). This curve is approximated by equation 50. By definition, jam density occurs when speed is 0 km/h. Thus, to estimate jam density, equation 50 is set equal to 0, and density calculated algebraically. At a speed of 0 km/h, this approximation equation yielded a jam density of 140 veh/km.

$$Speed = \frac{2500}{(Density+5)} - 17.25 \quad (50)$$

Standstill distance was again computed as the inverse of jam density. Thus, the final value for standstill distance used in the 10-ft calibrated model was 2.143 m (7.03 ft). The next required input was FFS. As with the 12- and 11-ft models, the 95th percentile observed speed was assumed to be FFS. In this case, the final value for FFS used in the 10-ft model was 81.76 km/h. The next required input was mean saturation flow rate. This value was again extracted directly from field data (table 23 and figure 21). The final value for mean saturation flow rate used in the 10-ft model was 2,040 veh/h/ln.

Using jam density (figure 20 and equation 50), FFS (table 23), and saturation flow rate (table 23) as inputs, the team obtained the following values for *BX* and *EX*: *BX* = 1.865 (equation 36), *EX* = 0.705 (equation 37).

Inputting *BX* and *EX* into equation 34 and equation 35, the results for the 10-ft lane width data bounding equations *ABX* and *SDX* are obtained in equation 51 and equation 52 and illustrated in figure 22:

$$ABX = 2.143 + 1.865\sqrt{u} \quad (51)$$

$$SDX = 2.143 + 6.911\sqrt{u} \quad (52)$$

The three required Wiedemann 74 calibration parameters, *Ax*, $BX_{additive}$, and $BX_{multiplicative}$, are derived from s_j, *BX*, and *EX* calculated for the 10-ft data:

- *AX* = 7.03 ft.
- $BX_{additive}$ = 1.87.
- $BX_{multiplicative}$ = 5.05.

The final car-following model calibrated to the treatment site conditions (10-ft lane width) is governed by equation 53:

$$Safety\ Distance = 7.03 + (1.87 + 5.05z)\sqrt{v} \quad (53)$$

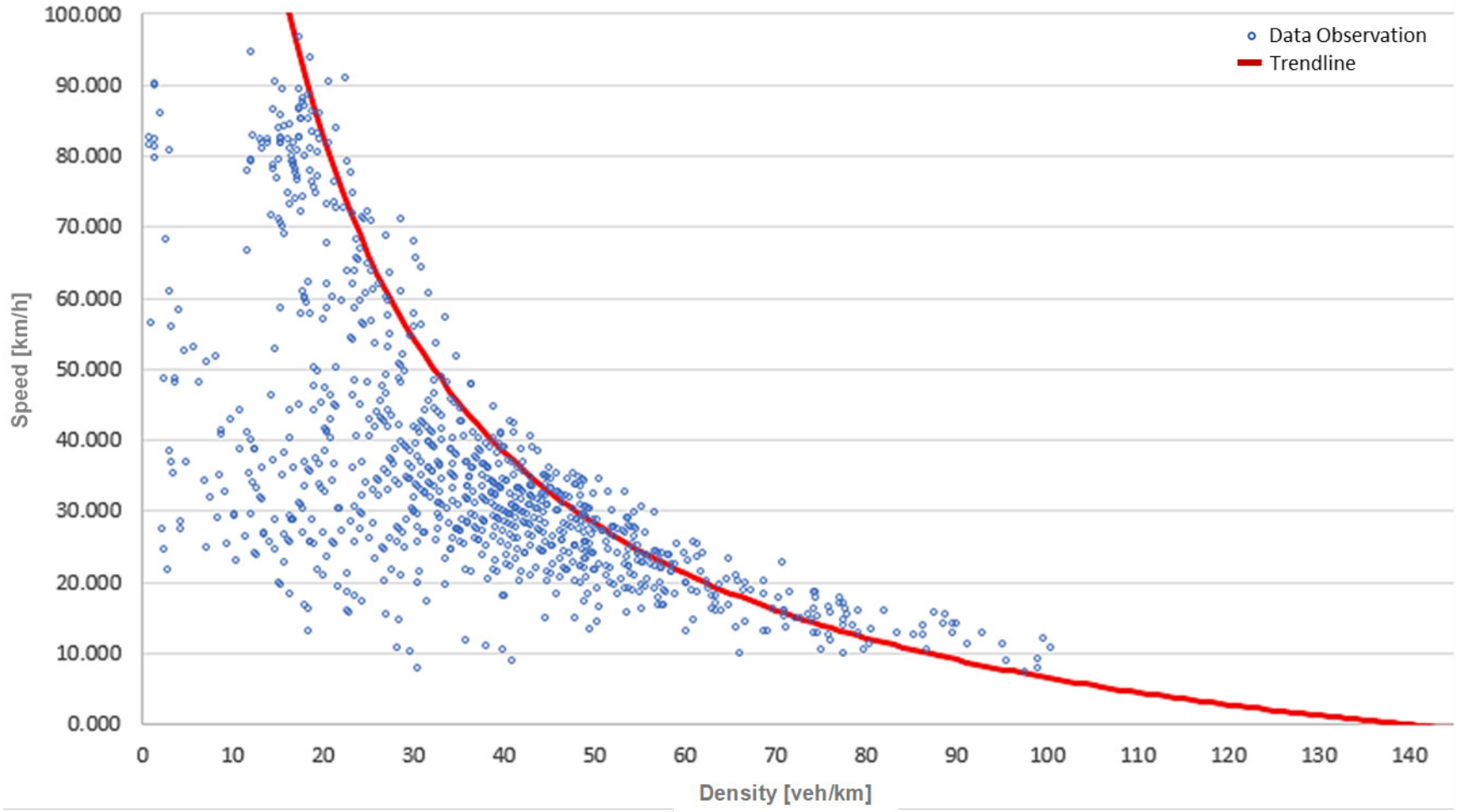

1 km = 0.62 mi.

Figure 20. Chart. Speed–density plot for 10-ft lane width observations.

Table 23. Combined data for 10-ft lane width observations.

Statistic	Count (veh/min)	Speed (mi/h)	Speed (ft/s)	Headway (s)	Headway (ft)	Count (veh/h)	Speed (km/h)	Speed (m/s)	Headway (m)	Density (veh/mi)	Density (veh/km)
Average	19	22.8	53.6	2.9	151.9	1,115	36.5	10.1	28.8	59.1	36.9
Maximum	34	60.3	141.7	37.7	1,917.1	**2,040	96.6	26.8	363.1	160.9	100.4
Minimum	1	4.6	10.8	1.0	19.5	60	7.4	2.1	3.7	1.2	0.7
Standard deviation	6.5	12.0	28.2	2.6	148.7	391	19.2	5.4	28.2	29.9	18.7
0.05 percentile	5	9.0	21.1	1.7	41.3	300	14.4	4.0	7.8	18.1	11.3
0.10 percentile	8	11.2	26.2	1.8	55.2	480	17.9	5.0	10.5	24.6	15.4
0.15 percentile	11	12.5	29.4	1.9	66.7	660	20.1	5.6	12.6	28.0	17.5
0.20 percentile	14	13.9	32.7	1.9	72.0	840	22.3	6.2	13.6	31.2	19.5
0.25 percentile	15	15.1	35.4	2.0	79.5	900	24.1	6.7	15.1	36.3	22.7
0.30 percentile	17	16.0	37.5	2.0	85.4	1,020	25.6	7.1	16.2	40.8	25.5
0.35 percentile	17	16.9	39.7	2.1	90.5	1,020	27.1	7.5	17.1	45.4	28.3
0.40 percentile	18	17.9	41.6	2.2	95.3	1,080	28.3	7.9	18.0	49.4	30.8
0.45 percentile	19	18.5	43.5	2.2	101.5	1,140	29.7	8.2	19.2	53.0	33.1
0.50 percentile	20	19.3	45.5	2.3	108.8	1,200	31.0	8.6	20.6	57.5	35.9
0.55 percentile	20	20.4	48.0	2.4	118.3	1,200	32.7	9.1	22.4	61.3	38.3
0.60 percentile	21	21.4	50.2	2.5	130.4	1,260	34.2	9.5	24.7	64.6	40.4
0.65 percentile	22	22.5	52.8	2.5	141.2	1,320	36.0	10.0	26.7	67.9	42.4
0.70 percentile	22	24.1	56.6	2.7	154.5	1,320	38.6	10.7	29.3	71.8	44.8
0.75 percentile	23	26.0	61.0	2.8	174.2	1,380	41.6	11.5	33.0	76.8	48.0
0.80 percentile	24	29.8	69.9	3.0	205.9	1,440	47.7	13.2	39.0	80.5	50.2
0.85 percentile	25	36.2	85.1	3.2	247.8	1,500	58.0	16.1	47.0	87.2	54.5
0.90 percentile	26	44.8	105.2	3.8	286.9	1,560	71.7	19.9	54.3	96.3	60.1
0.95 percentile	28	*51.0	119.9	5.5	350.1	1,680	*81.8	22.7	66.3	119.0	74.2

1 m = 3.28 ft.
1 km = 0.62 mi.
*FFS: 95th percentile speed.
**Saturation flow rate: maximum observed hourly vehicle count.

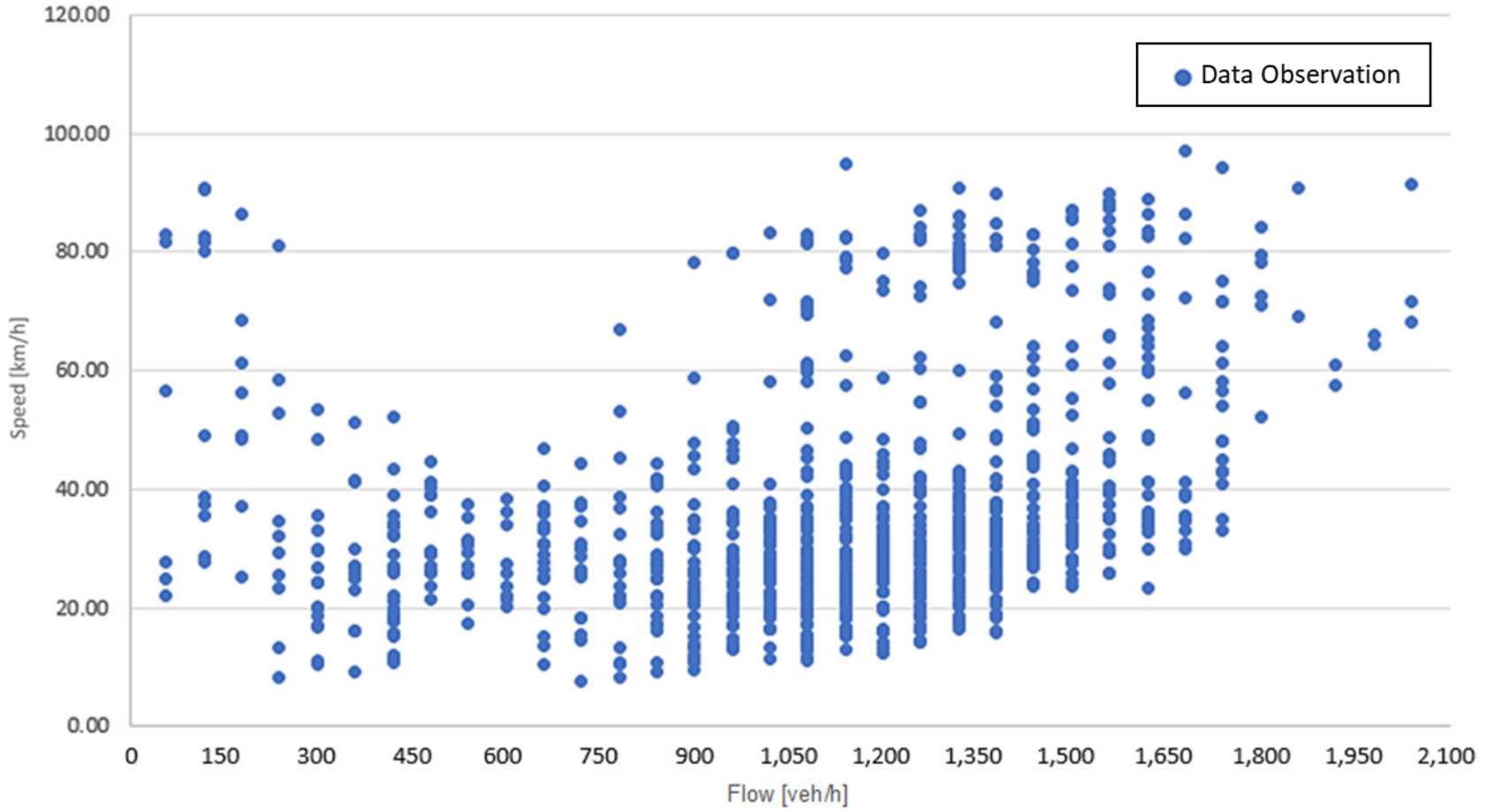

1 km = 0.62 mi.

Figure 21. Chart. Speed–flow plot for 10-ft lane width observations.

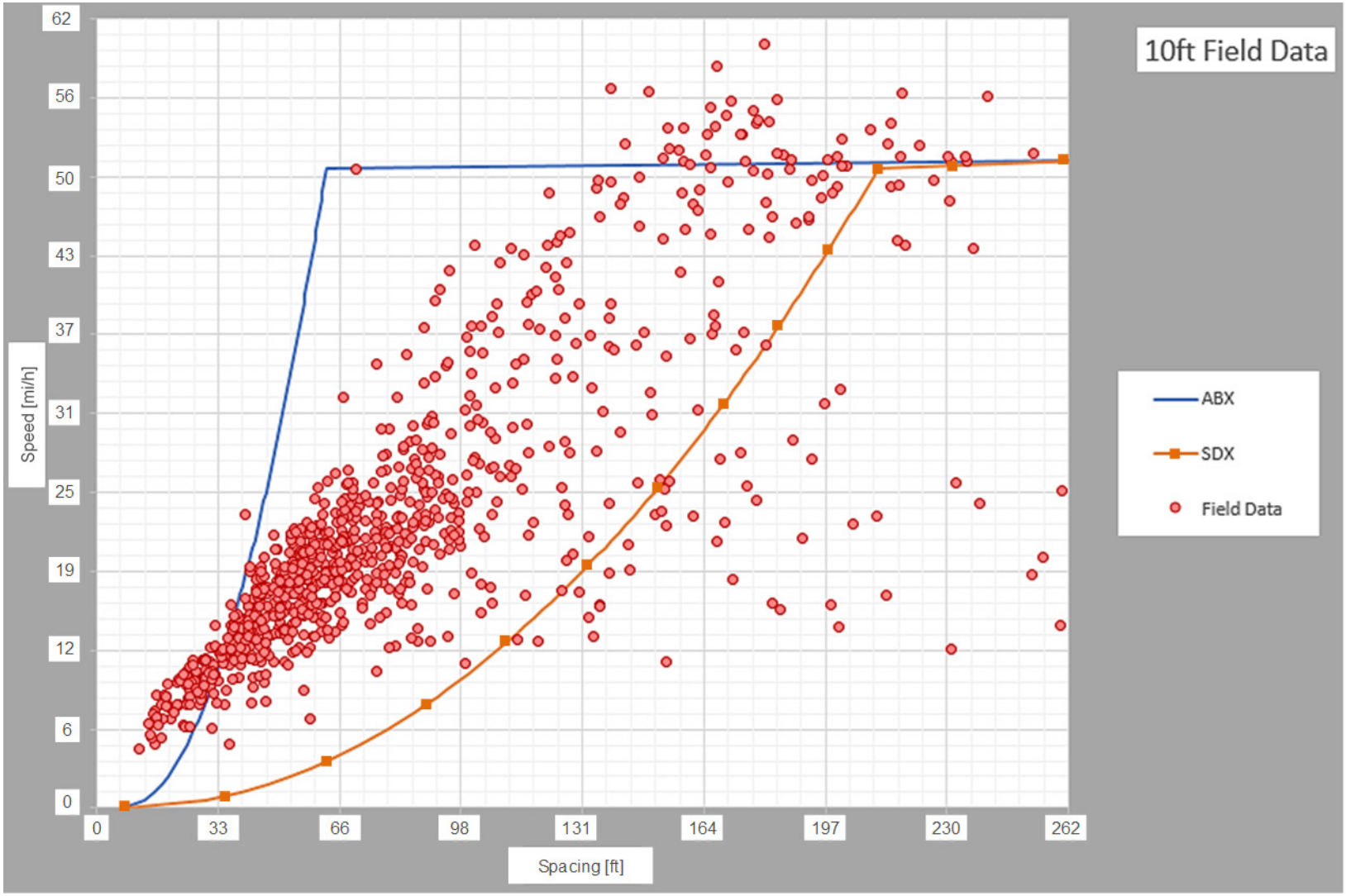

Figure 22. Chart. Calibration bounds plot for 10-ft lane width observations.

Final Analysis and Summary

Interpretation of the Wiedemann 74 calibration parameters (i.e., *AX*, $BX_{additive}$, and $BX_{multiplicative}$) are as follows. If smaller values are inserted into *AX*, vehicles will be closer together when stopped, thus affecting simulated jam density. $BX_{additive}$ controls how simulated drivers will follow at speed, with lower values yielding smaller following distances. $BX_{multiplicative}$ controls the following distance variation among the simulated population.

Using these interpretations, trends observed in the calibrated model show that the 10-ft combined dataset seems to yield more aggressive (shorter) headways than the 11-ft combined dataset, which seemed counterintuitive. Thus, car-following models were calibrated independently for each site using methods described in the previous sections. The resulting models are shown in table 24.

From table 24, it can be observed that the car-following model became more conservative (i.e., larger following distances) for each site containing multiple lane widths as lanes narrowed. The combined 10-ft dataset appeared to be more aggressive than the combined 11-ft dataset because both Honolulu, HI, datasets yielded more aggressive following parameters than their counterparts at other locations. Furthermore, the combined 10-ft dataset only contains data from Honolulu, HI.

Table 24. Site-specific Wiedemann results.

Location	*AX* (m)	*AX* (ft)	$BX_{additive}$	$BX_{multiplicative}$
Dallas, TX (12 ft)	5.000	16.404	1.772	3.104
Dallas, TX (11 ft)	2.143	7.031	2.060	3.466
San Antonio, TX (12 ft)	5.526	18.130	1.476	3.831
San Antonio, TX (11 ft)	8.333	27.339	1.542	4.445
Honolulu, HI (11 ft)	2.143	7.031	1.434	4.565
Honolulu, HI (10 ft)	2.143	7.031	1.865	5.046
Fort Lauderdale, FL (12 ft)	3.333	10.935	2.645	3.353
Fort Lauderdale, FL (11 ft)	2.143	7.031	3.093	3.077
Seattle, WA (11 ft)	6.765	22.195	1.435	2.033
Combined (12 ft)	4.804	15.761	1.707	5.374
Combined (11 ft)	5.526	18.130	2.212	3.132
Combined (10 ft)	2.143	7.031	1.865	5.046

1 m = 3.28 ft.

Due to these findings, the team decided to use default car-following parameters for the 12-ft lane width scenarios and increase the parameters by average percent change for sites with multiple treatments. Specifically, the $BX_{additive}$ parameter was increased by 10 percent per foot of lane narrowing. This produced the hypothesis that drivers will follow at greater distances as lanes narrow.

SAFETY MODEL DEVELOPMENT

The team conducted a literature search and review of relevant research to plan the development of a crash prediction model. At the end of this process, Chapter 18 of the HSM was selected as the basis for developing this model. Moreover, the narrow lanes safety model was100 percent derived from the HSM procedures, albeit with a number of simplifying assumptions described in this section. Before starting the safety model development, the team developed three distinct geometric lane-narrowing scenarios. All scenarios involved existing 12-ft lanes—scenario one narrowed lanes to 11 ft, scenario two narrowed lanes to 10.5 ft, and scenario three narrowed lanes to 10 ft, while the total pavement width remained the same, as shown in table 25.

Table 25. Summary of geometric scenarios for the lane-narrowing safety model.

Geometric Scenario	Lane Width Type	Number of Lanes (Both Directions)	Lane Width (ft)	Inside Shoulder Width (ft) (One Direction)	Outside Shoulder Width (ft) (One Direction)	Total Pavement Width (ft)
One	Standard	4	12	8	8	80
One	Narrow	6	11	4	3	80
Two	Standard	6	12	12	8	112
Two	Narrow	8	10.5	8	6	112
Three	Standard	8	12	12	8	136
Three	Narrow	10	10	10	8	136

For the *Narrowing Freeway Lanes and Shoulders to Create Additional Travel Lanes* project, the team considered the following two models most applicable to the research goals of the task:

- Model calibration for FI crashes.
- Model calibration for PDO crashes.

As mentioned on page 18-25 of the HSM, the base conditions for the safety performance functions (SPFs) for multiple-vehicle crashes on freeway segments are as follows:

- Length of horizontal curve = 0.0 mi (i.e., not present).
- Lane width = 12 ft.
- Inside shoulder width (paved) = 6 ft.
- Length of median barrier = 0.0 mi (i.e., not present).
- Number of hours where volume exceeds 1,000 veh/h/ln = 0.
- Distance to nearest upstream ramp entrances = more than 0.5 mi from segment.
- Distance to nearest downstream ramp entrances = more than 0.5 mi from segment.

Both models are supported by equation 54 and 55, which is customized for not only FI and PDO crashes, but also by the number of pre and postimplementation lanes:

$$N_{spf,fs,n,mv,z} = L^* \times \exp(a + b \times \ln[c \times AADT_{fs}]) \quad (54)$$

Where:

$N_{spf,fs,n,mv,z}$ = predicted average multiple-vehicle crash frequency of a freeway segment with base conditions, n lanes, and severity z (crashes/year).
L^* = effective length of freeway segment (mile).
a, b = regression coefficients.
$AADT$ = annual average daily traffic.
c = $AADT$ scale coefficient.
$AADT_{fs}$ = $AADT$ volume of freeway segment (veh/day).

$$L^* = L_{fs} - \left(0.5 \times \sum_{i=1}^{2} L_{en,seg,i}\right) - \left(0.5 \times \sum_{i=1}^{2} L_{ex,seg,i}\right) \quad (55)$$

Where:

L_{fs} = length of freeway segment (mile).
$L_{en,seg,i}$ = length of ramp entrance i adjacent to subject freeway segment (mile).
$L_{ex,seg,i}$ = length of ramp exit i adjacent to subject freeway segment (mile).

Refer to table 18-5 on page 18-26 of the HSM for the definition and corresponding values of the SPF coefficients of a, b, and c.

Within these two models, the team looked at the pre and postimplementation multiple-vehicle, nonentrance/exit ramp crash frequencies for freeway segments ($N_{spf,mv,n}$) and various crash modification factors (CMFs). Therefore, to calculate crash frequency per assumed site conditions for the lane-narrowing research (both pre- and postimplementation conditions), equation 56 and equation 57 were used:

$$Site\text{-}Specific\ Crash\ Frequency\ for\ FI\ Crashes = N_{spf,mb,n} \times CMF_{lw} \times CMF_{mv,hv} \times CMF_{isw} \times CMF_{mv,mw|agg} \times CMF_{mb|agg} \quad (56)$$

Where:

Site-Specific Crash Frequency for FI crashes = site-specific crash frequency for FI crashes.
CMF_{lw} = CMF for lane width in the test segment.
$CMF_{mv,hv}$ = CMF for high volume conditions in the test segment.
CMF_{isw} = CMF for inside shoulder width in the test segment.
$CMF_{mv,mw|agg}$ = aggregated CMF representing the variability of median widths present within the test segment.
$CMF_{mb|agg}$ = aggregated CMF for variable presence of median barrier within test segment.

$$Site\text{-}Specific\ Crash\ Frequency\ for\ PDO\ Crashes = N_{spf,mv,n} \times CMF_{mv,hv} \times CMF_{isw} \times CMF_{mv,mw|agg} \times CMF_{mb|agg} \quad (57)$$

Where *Site-specific Crash Frequency for PDO Crashes* is the site-specific crash frequency for PDO crashes.

The CMFs in equation 56 and equation 57 were computed as shown in equation 58 through 66:

FI Crashes

- Lane width:

$$CMF_{2,sc,\,ac,at,\,fi} = \begin{cases} \exp\left(-0.0376 \times [W_l - 12]\right) & : \text{If } W_l < 13\,\text{ft} \\ 0.963 & : \text{If } W_l \geq 13\,\text{ft} \end{cases} \quad (58)$$

Where:

$CMF_{2,sc,ac,at,fi}$ = CMF for lane width at a speed-change lane with any cross section *ac*, all crash types *at*, and fatal-and-injury crashes *fi*.

W_l = lane width (foot).

- High-volume conditions:

$$CMF_{6,sc,\,ac,at,\,z} = \exp\left(a \times P_{hv}\right) \quad (59)$$

Where:

$CMF_{2,sc,ac,at,fi}$ = CMF for high-volume at a speed-change lane with any cross-section *ac*, all crash types *at*, and severity *z*.

P_{hv} = proportion of AADT during hours where volume exceeds 1,000 veh/h/ln.

- Inside shoulder width:

$$CMF_{3,sc,ac,at,z} = \exp\left(a \times [W_{is} - 6]\right) \quad (60)$$

Where:

$CMF_{3,sc,ac,at,z}$ = CMF for inside shoulder width at a speed-change lane with any cross-section *ac*, all crash types *at*, and severity *z*.

W_{is} = paved inside shoulder width (foot).

- Median width:

$$CMF_{4,\,sc,ac,at,z} = \left(1.0 - P_{ib}\right) \times \exp\left(a \times [W_m - 2 \times W_{is} - 48]\right) + P_{ib} \times \exp\left(a \times\ [2 \times W_{icb} - 48]\right) \quad (61)$$

Where:

$CMF_{4,sc,ac,at,z}$ = CMF for median width at a speed-change lane with any cross-section *ac*, all crash types *at*, and severity *z*.

P_{ib} = proportion of speed-change lane length with a barrier present in the median (i.e., inside).

W_m = median width (measured from near edges of traveled way in both directions) (foot).

W_{icb} = distance from edge of inside shoulder to barrier face (foot).

- Median barrier:

$$CMF_{5,sc,ac,at,z} = (1.0 - P_{ib}) \times 1.0 + P_{ib} \times \exp\left(\frac{a}{W_{icb}}\right) \quad (62)$$

Where:

$CMF_{5,sc,ac,at,z}$ = CMF for median barrier at a speed-change lane with any cross-section *ac*, all crash types *at*, and severity *z*.

P_{ib} = proportion of segment length with a barrier present in the median (i.e., inside).

PDO Crashes

- High-volume conditions:

$$CMF_{6,sc,ac,at,z} = \exp(a \times P_{hv}) \quad (63)$$

Where $CMF_{6,sc,ac,at,z}$ = CMF for high-volume at a speed-change lane with any cross-section *ac*, all crash types *at*, and severity *z*.

- Median width:

$$CMF_{4,sc,ac,at,z} = (1.0 - P_{ib}) \times \exp(a \times [W_m - 2 \times W_{is} - 48]) + P_{ib} \times \exp(a \times [2 \times W_{icb} - 48]) \quad (64)$$

- Inside shoulder width:

$$CMF_{3,sc,ac,at,z} = \exp(a \times [W_{is} - 6]) \quad (65)$$

- Median barrier:

$$CMF_{5,sc,ac,at,z} = (1.0 - P_{ib}) \times 1.0 + P_{ib} \times \exp\left(\frac{a}{W_{icb}}\right) \quad (66)$$

For a complete list of the nomenclature used in the CMF equations, refer to pages 18-45 through 18-50 of the HSM.

To keep the model as simple as possible, the following assumptions were made with respect to each model's inputs:

- Number of lanes = $N_{spf,mv,n}$ → where n = 4, 6, 8, and 10.
  - $N_{spt,mv,n}$ = multiple-vehicle, non-entrance/exit ramp crash frequencies for freeway segments (crashes/year)
- Area type = urban → hence, I_{rural} = 0.
  - I_{rural} = area type indicator (= 1.0 if area is rural; 0.0 if area is urban).
- Length of each test segment, L_{fs} = 1.0 mi.
- No ramps within test segment:
  - Hence, $L_{en,seg,i}$ = $L_{ex,seg,i}$ = 0.
    - $L_{en,seg,i}$ = length of ramp entrance i adjacent to subject freeway segment (mile).
    - $L_{ex,seg,i}$ = length of ramp exit i adjacent to subject freeway segment (mile).
  - Hence, CMF for lane change, $CMF_{mv,lc|agg}$ = 1.00.
    - $CMF_{mv,lc|agg}$ is the aggregated CMF representing the presence or lack of presence of lane-change conditions within the test segment.
- No horizontal curves within test segment:
  - Hence, CMF for horizontal curves, $CMF_{mv,hc|agg}$ = 1.00.
    - $CMF_{mv,hc|agg}$ is the aggregated CMF representing the individual effect for each horizontal curve within the test segment.
- Maximum lane capacity:
  - Preimplementation = 2,200 veh/h/ln.
  - Postimplementation = 1,800 veh/h/ln.
  - These are generic values that were used to keep them consistent with the capacity model.

With regard to model inputs, after discussing various options, the team decided on the following:

- Hourly volume.
- Total pavement width.
- Preimplementation:
  - Number of lanes.
  - Lane width.
  - Total shoulder width.
    - Inside shoulder width.

- Postimplementation:
  - Number of lanes.
  - Lane width.
  - Total shoulder width.
    - Inside shoulder width.

As such, the model outputs were:

- Preimplementation:
  - FI crash frequency for two-plus vehicles.
  - PDO crash frequency for two-plus vehicles.
- Postimplementation:
  - FI crash frequency for two-plus vehicles.
  - PDO crash frequency for two-plus vehicles.

For each of the three geometric scenarios described in table 25, hourly volume was plotted from 1,000 veh/h/ln to a maximum lane capacity of 2,200 veh/h/ln for the preimplementation (or base) condition. For the postimplementation condition, the hourly volume ranged from 1,000 veh/h/ln to a maximum lane capacity of 1,800 veh/h/ln.

The expected daily volume (vehicles per day per lane) was computed assuming a ratio between peak hour and ADT (*K* factor) value of 10 percent using the formula in equation 67. This can be many different factors. The most common is referred to as *K*-30, which is the ratio between the 30th highest hour and annual ADT (Crownover 2006). According to research studies, *K* factors range from 8–12 percent for urban facilities (Texas Department of Transportation 2014). As such, the team used the mean value of 10 percent:

$$Expected\ Daily\ Volume\ (\text{veh/day/ln}) = \frac{Hourly\ Volume}{K} \quad (67)$$

Where:

Expected Daily Volume = expected daily volume.
Hourly Volume = hourly volume.

ADT was then calculated using equation 68:

$$ADT = Expected\ Daily\ Volume \times Total\ Number\ of\ Lanes \quad (68)$$

Where *Total Number of Lanes* is the total number of lanes.

ADT values were used to compute $N_{spf,mv,n}$ for each scenario. The FI and PDO crash frequencies were calculated with formulas developed in NCHRP 17-45 for *n* number of through lanes, where *n* = 4, 6, 8, and 10 (Bonneson et al. 2012).

As a last step, both types of crash frequencies (crashes/year) were plotted against hourly volume (veh/h/ln). For each scenario, the pre and postimplementation conditions were plotted on the same graph to compare the two lines and observe the trend. As shown in figure 23 through figure 28, the three graphs for both FI and PDO crashes show a similar trend across all geometric scenarios. Once lanes are narrowed, crash frequency increases for all corresponding hourly volumes. It is noticeable, however, that the difference between the two lines is less significant for scenario three (representing 10-ft lanes) in both FI and PDO crashes.

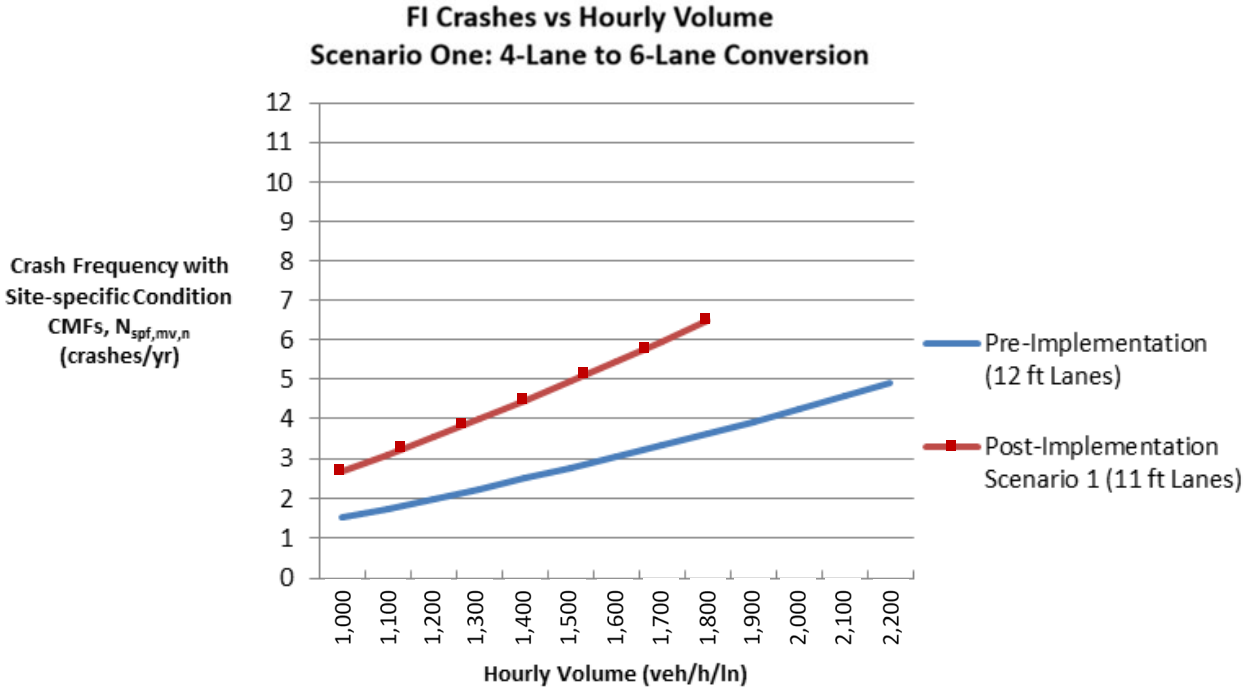

Source: FHWA.

Figure 23. Graph. FI crashes versus hourly volume (four-lane to six-lane conversion).

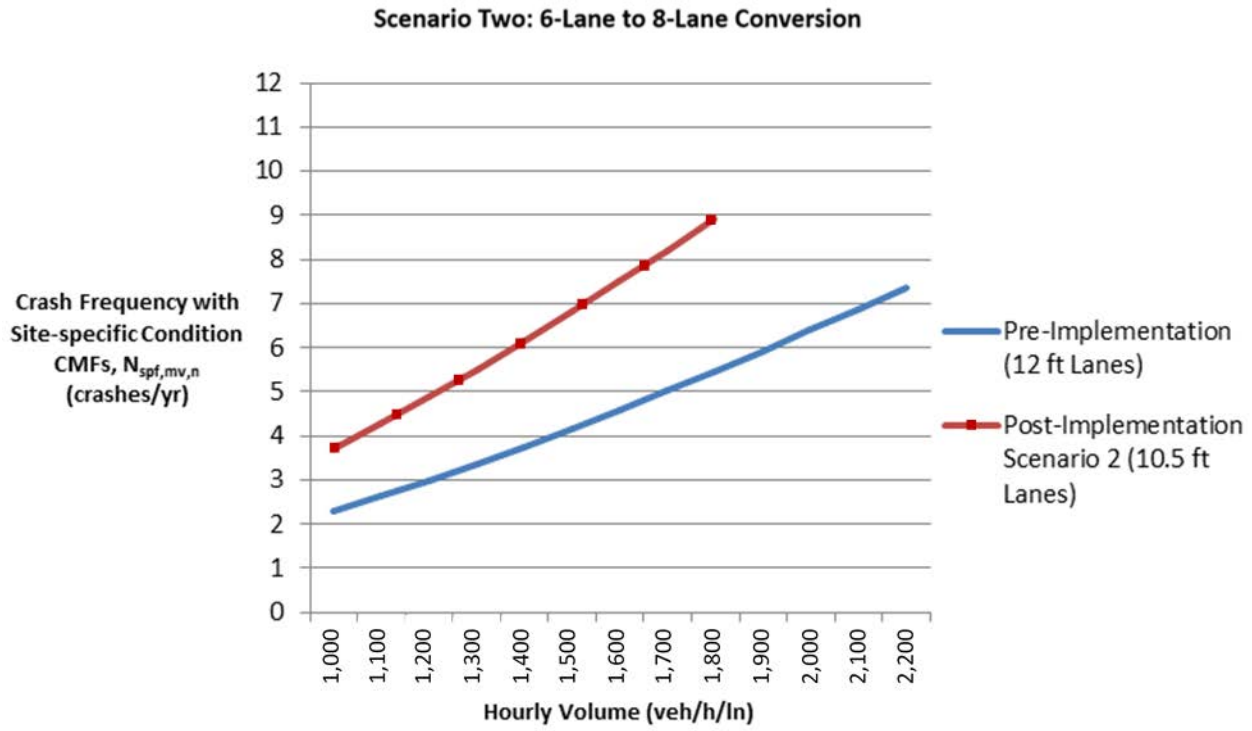

Source: FHWA.

Figure 24. Graph. FI crashes versus hourly volume (six-lane to eight-lane conversion).

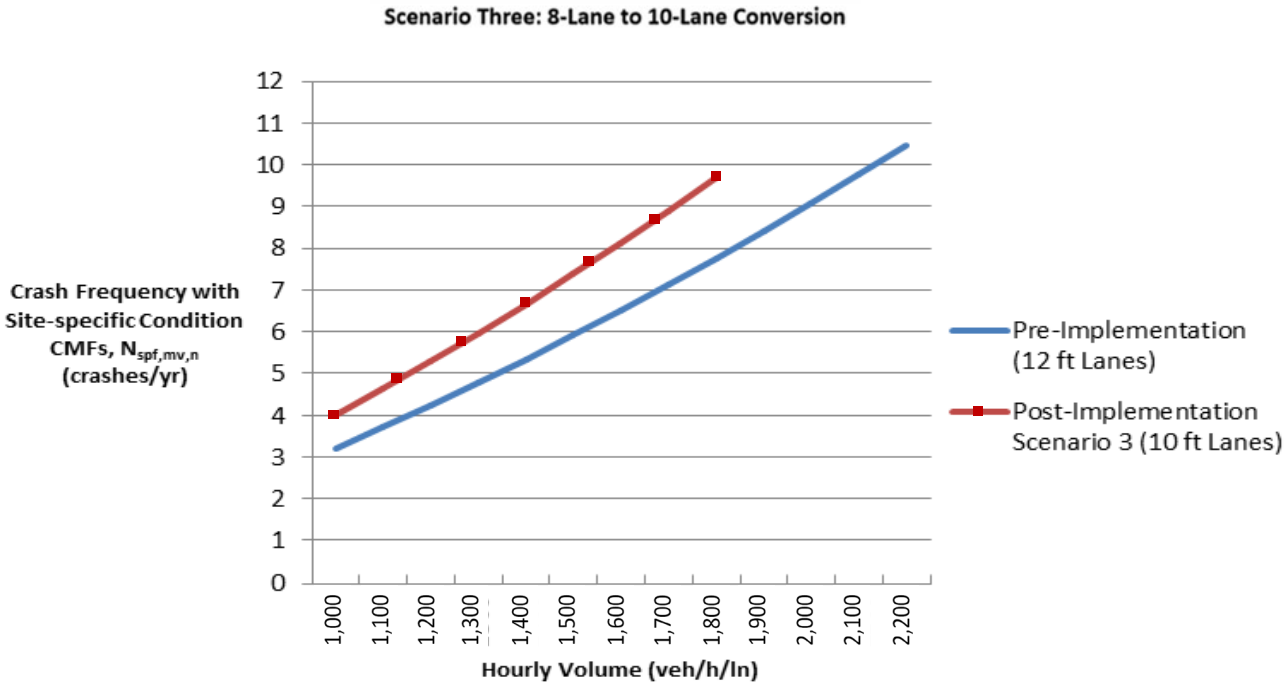

Source: FHWA.

Figure 25. Graph. FI crashes versus hourly volume (8-lane to 10-lane conversion).

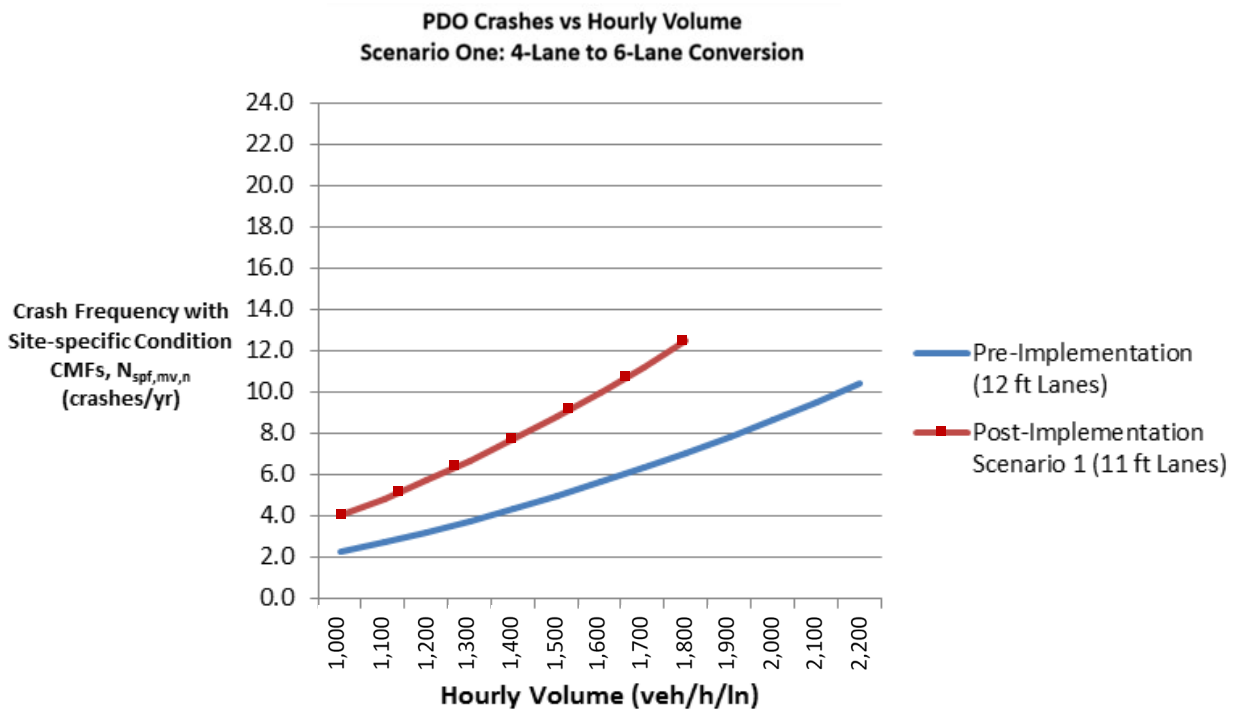

Source: FHWA.

Figure 26. Graph. PDO crashes versus hourly volume (four-lane to six-lane conversion).

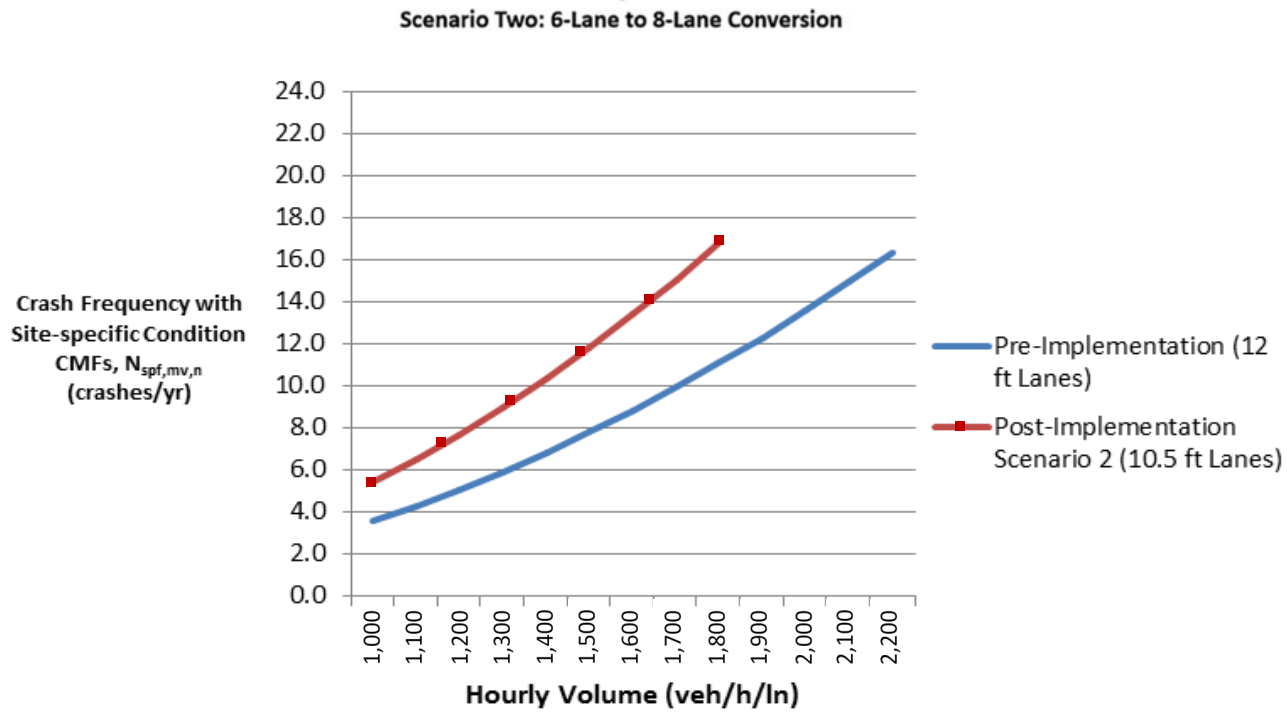

Source: FHWA.

Figure 27. Graph. PDO crashes versus hourly volume (six-lane to eight-lane conversion).

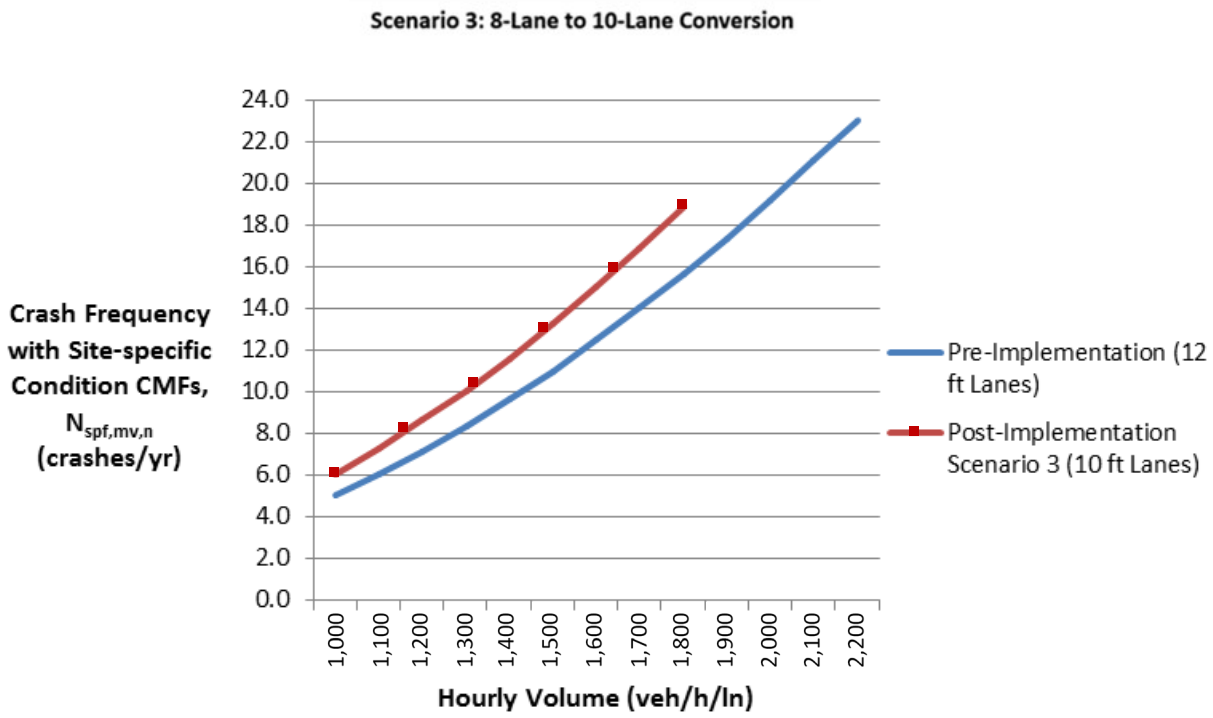

Source: FHWA.

Figure 28. Graph. PDO crashes versus hourly volume (8-lane to 10-lane conversion).

CHAPTER 5. CASE STUDIES

To gain insights from the newly developed mobility and safety models, the team conducted case studies on I-270 in Maryland and I-580 in California. Both of these sites experience significant recurring congestion in the peak hour, but offer different fundamental characteristics (e.g., posted speed limits, number of mainline lanes). Both sites have 12-ft lane widths, but new models were used to forecast narrow lane impacts. The I-270 fundamental characteristics and map are listed as follows and shown in figure 29:

- Hourly volume: 8,200 veh/h (10 percent trucks).
- Speed limit: 55 mi/h.
- Mainline lanes: four.
- Shoulder width: approximately 12 ft on both sides.
- Number of ramps: 1.1 per mile.

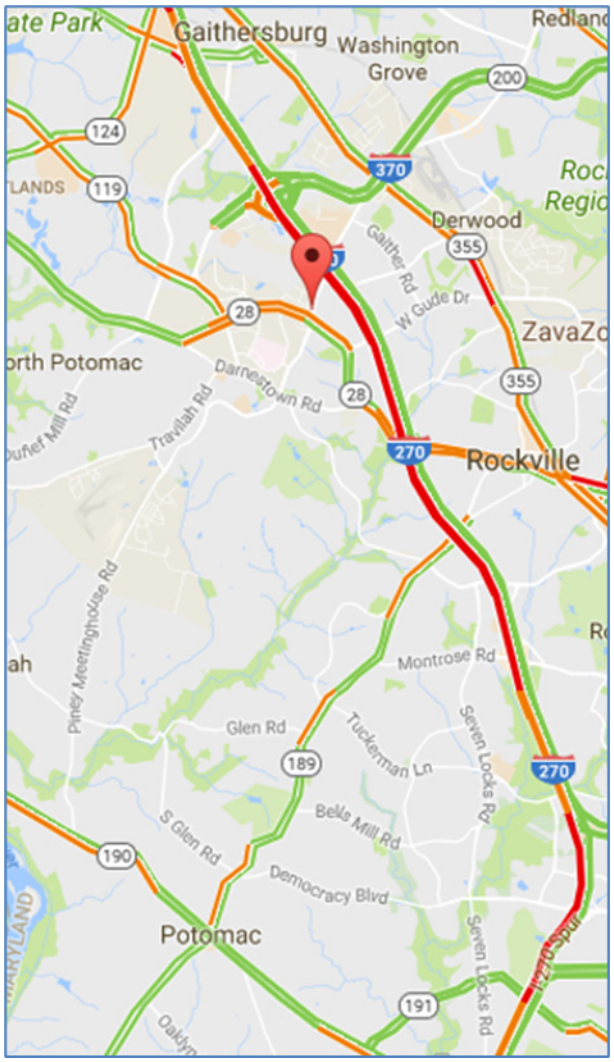

© 2018 Google.

Figure 29. Map. I-270 southbound case study conditions.

The I-580 fundamental characteristics and map are listed below and shown in figure 30:

- Hourly volume: 8,401 veh/h (6 percent trucks).
- Speed limit: 65 mi/h.
- Mainline lanes: five.
- Shoulder width: approximately 10 ft on median, 12 ft on curb.
- Number of ramps: 1.6 per mile.

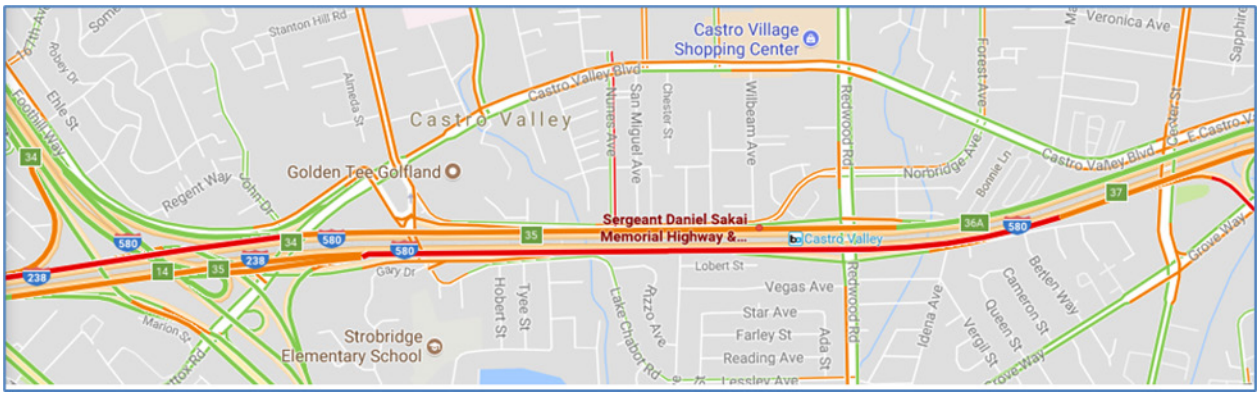

© 2018 Google.

Figure 30. Map. I-580 eastbound case study conditions.

SAFETY ANALYSIS

The analysis of safety benefits focuses on the reduction in crashes associated with two treatments versus no-build scenarios (i.e., no additional lanes). The two treatments are implementation of narrowed lanes (adding one lane in each direction) and construction of new lanes (also one lane in each direction). Two case studies were considered in the analysis, one segment each on I-270 and I-580. The estimation of crashes under three scenarios (no-build, narrow lane, and new lane scenarios) were conducted using traffic volume data available from the respective State DOTs, review of roadway configurations at and surrounding study segments, and crash estimation tools from the HSM. Using these resources, the number of FI and PDO crashes per year was estimated for the study roadway segments for a range of traffic volumes using this project's newly developed safety models.

Monetizing the impacts of the treatments on crashes was done by using United States Department of Transportation (USDOT)-recommended value of statistical life for fatalities ($9,936,727 per fatality) and published costs of PDO crashes ($2,539 per crash). Although the national average for number of fatalities per fatal crash is 1.088, this analysis was conservative and assumed one fatality per fatal crash (National Traffic Highway Safety Administration 2016). The number of crashes and reductions in crashes estimated for one direction for the three scenarios for the two case studies are presented in table 26 through table 37.

Table 26. Estimated FI crash reductions on I-270.

ADT	No-Build	Narrow Lane	New Lane
50,000	2.54	2.00	1.54
55,000	2.93	2.31	1.77
60,000	3.33	2.63	2.02
65,000	3.76	2.96	2.27
70,000	4.20	3.31	2.54
75,000	4.65	3.67	2.82
80,000	5.12	4.04	3.10
85,000	5.61	4.42	3.39
90,000	5.81	4.82	3.70

Table 27. Estimated FI crash reductions versus no-build on I-270.

ADT	Narrow Lane	New Lane
50,000	0.54	1.00
55,000	0.62	1.16
60,000	0.70	1.32
65,000	0.79	1.48
70,000	0.89	1.66
75,000	0.98	1.84
80,000	1.08	2.02
85,000	1.18	2.21
90,000	0.99	2.11

Table 28. Estimated crash benefit versus no-build on I-270.

ADT	Narrow Lane (U.S. Dollars)	New Lane (U.S. Dollars)
50,000	5,342,812	9,978,725
55,000	6,152,817	11,497,147
60,000	6,993,612	13,078,797
65,000	7,890,414	14,747,487
70,000	8,814,592	16,473,351
75,000	9,765,528	18,254,664
80,000	10,742,618	20,089,836
85,000	11,768,068	22,000,176
90,000	9,841,222	20,984,216

Table 29. Estimated PDO crash reductions on I-270.

ADT	No-Build	Narrow Lane	New Lane
50,000	4.25	3.10	3.01
55,000	5.11	3.73	3.62
60,000	6.05	4.41	4.28
65,000	7.06	5.15	5.00
70,000	8.15	5.95	5.77
75,000	9.32	6.80	6.59
80,000	10.55	7.70	7.47
85,000	11.87	8.66	8.40
90,000	12.14	9.67	9.38

Table 30. Estimated PDO crash reductions versus no-build on I-270.

ADT	Narrow Lane	New Lane
50,000	1.15	1.25
55,000	1.38	1.50
60,000	1.63	1.77
65,000	1.91	2.07
70,000	2.21	2.39
75,000	2.52	2.73
80,000	2.85	3.08
85,000	3.21	3.47
90,000	2.47	2.76

Table 31. Estimated PDO crash benefit versus no-build on I-270.

ADT	Narrow Lane (U.S. Dollars)	New Lane (U.S. Dollars)
50,000	2,929	3,166
55,000	3,516	3,801
60,000	4,147	4,484
65,000	4,853	5,248
70,000	5,604	6,059
75,000	6,399	6,919
80,000	7,238	7,827
85,000	8,150	8,813
90,000	6,270	7,010

Table 32. Estimated FI crash reductions on I-580.

ADT	No-Build	Narrow Lane	New Lane
60,000	2.61	2.26	1.73
65,000	2.94	2.55	1.95
70,000	3.28	2.85	2.18
75,000	3.64	3.16	2.42
80,000	4.01	3.48	2.66
85,000	4.39	3.80	2.91
90,000	4.78	4.14	3.17

Table 33. Estimated FI crash reductions versus no-build on I-580.

ADT	Narrow Lane	New Lane
60,000	0.35	0.88
65,000	0.39	0.99
70,000	0.43	1.10
75,000	0.48	1.22
80,000	0.53	1.34
85,000	0.58	1.47
90,000	0.64	1.60

Table 34. Estimated FI crash benefit on I-580.

ADT	Narrow Lane (U.S. Dollars)	New Lane (U.S. Dollars)
60,000	3,447,777	8,706,801
65,000	3,874,001	9,802,719
70,000	4,322,308	10,945,254
75,000	4,791,409	12,132,318
80,000	5,280,226	13,362,100
85,000	5,787,841	14,633,005
90,000	6,313,459	15,943,614

Table 35. Estimated PDO crash reductions on I-580.

ADT	No-Build	Narrow Lane	New Lane
60,000	2.61	3.58	3.53
65,000	2.94	4.24	4.18
70,000	3.28	5.02	4.94
75,000	3.64	5.86	5.78
80,000	4.01	7.20	7.09
85,000	4.39	7.74	7.63
90,000	4.78	8.78	8.64

Table 36. Estimated PDO crash reductions versus no-build on I-580.

ADT	Narrow Lane	New Lane
60,000	−0.97	−0.92
65,000	−1.30	−1.24
70,000	−1.74	−1.66
75,000	−2.23	−2.14
80,000	−3.19	−3.08
85,000	−3.36	−3.24
90,000	−4.00	−3.87

Table 37. Estimated PDO crash benefit on I-580.

ADT	Narrow Lane (U.S. Dollars)	New Lane (U.S. Dollars)
60,000	2,473	2,335
65,000	3,305	3,142
70,000	4,412	4,218
75,000	5,650	5,424
80,000	8,106	7,829
85,000	8,524	8,225
90,000	10,159	9,820

The analyses show reductions in FI crashes under both narrow lane and new lane scenarios. Given the high costs of fatalities, the FI crash reductions equate to high levels of safety benefits, even at the lower levels of traffic. In terms of PDO crashes, the results are mixed, showing reductions on I-270 and increases on I-580. This could be due to several factors specific to the segments themselves, but from a financial standpoint, their impacts are minimal given the low cost per PDO crash.

What stand out are the multimillion dollar benefits of both the narrow lane and new lane scenarios relative to their implementation costs. For the narrow lane scenario, the cost of implementation is approximately $5,000 per lane mi, or $25,000 to $30,000 for the I-270 and I-580 1-mi study segments, respectively. The cost of constructing a new lane is estimated at $2.2 to $3 million per mile and approximately $6,000 per lane mile per year for maintenance (Murshed and McCorkhill 2012). Considering FI and PDO crash impacts versus the cost of narrow lane or new lane treatments, financial breakeven is estimated to be reached within the first year of operation for both new treatments.

The aforementioned analyses assumed that, with the addition of capacity through implementation of narrow lanes or construction of a new lane, total volume would remain constant with volume in individual lanes decreasing. The team examined impacts on crashes, assuming the addition of new capacity via narrow lanes or a new lane. The assumption was that volume in individual lanes would remain constant, and due to the addition of another lane, total volume would increase. Table 38 shows total volume increased 20 to 25 percent for I-580 and I-270 segments, respectively. FI crash frequency decreased by 11 to 16 percent with the construction of a new lane. FI crashes increased under the narrow lanes scenario by 14 and 10 percent for I-580 and

I-270 segments, respectively. Under both the new lane and narrow lanes scenarios, PDO crashes were expected to increase by 9 to 13 percent. Where crashes were expected to increase, the percent increase in crashes was far lower than the percent increase in total volume, indicating that the treatments had a beneficial effect on crashes relative to traffic volumes.

Table 38. Crash impacts holding traffic volumes constant per lane.

Case Study	Total Volume Increase	Narrow Lanes Crash Frequency	New Lane Crash Frequency
I-270 FI	25 percent (four to five lanes)	10 percent	−16 percent
I-270 PDO	25 percent (four to five lanes)	12 percent	9 percent
I-580 FI	20 percent (five to six lanes)	14 percent	−13 percent
I-580 PDO	20 percent (five to six lanes)	13 percent	11 percent

Crash frequency estimates provide insight into the conditions under which adding capacity improves safety in terms of crash avoidance. As traffic volumes increase, safety benefits increase relative to the no-build scenarios.

MACROSCOPIC MOBILITY ANALYSIS

The analysis of mobility benefits focuses on reduction in travel time associated with the lane treatment versus the no-build scenarios. The treatment scenarios include both narrowed lanes (adding one lane in each direction but holding the pavement footprint consistent with the no-build scenario) and construction of new lanes (also one lane in each direction).

Two case studies were considered in the analysis. One segment each on I-270 and I-580. The estimation of travel times under two scenarios (the no-build and narrow lane scenarios) were conducted using traffic volume data available from the respective State DOTs, review of roadway configurations at and surrounding study segments, processed through FREEVAL, a macroscopic simulation tool based on the HCM that performs various freeway analyses, including capacity, managed lanes, reliability, work zone, ramp metering optimization, and so forth. (North Carolina State University 2018). Use of FREEVAL was necessary to obtain travel time and delay data for the BCA. However, FFS and CAF were obtained from the newly developed narrow lane models described in the Macroscopic Model Development section in chapter 4.

To monetize impacts of the treatments on crashes, the team used the USDOT-recommended value of travel time for all purposes of $14.10 per traveler per hour (White 2016). For these analyses, a conservative estimate of one traveler per vehicle was assumed. For the I-270 facility, which is 5.7 mi in length, the base case travel time for a peak volume of 8,200 veh/h was 11.81 min versus 10.23 min under the narrow lane scenario. This is a travel time savings of 1.58 min per vehicle through the facility. For the I-580 facility, which is 5.2 mi in length, the base case travel time for a peak volume of 8,401 vehicles was 8.01 min versus 6.67 min under the narrow lane scenario. This is a travel time saving of 1.34 min per vehicle through the facility.

Calculation of Benefits

Based on a series of email interviews conducted in 2017, University of Nebraska Lincoln, Nevada DOT, and Maryland DOT indicated that restriping treatments (without resurfacing) would cost approximately $5,000 per lane mile. The team's resulting analysis showed that significant value in terms of travel time savings could be realized under the narrow lane scenarios for the two roadway facilities. For this analysis, 11-ft narrow lane scenarios were assumed instead of 10- or 10.5-ft scenarios. The benefits versus costs were calculated as follows.

- I-270 facility:
  - 1.58 min saved per vehicle × 8,200 vehicles = 12,956 min saved/60 min = 216 h saved.
  - 216 h saved × $14.10 value per hour × 260 d per year = $791,599 per year travel time savings.
  - Given five restriped narrow lanes at $5,000 per lane mile for striping × 5.2 mi = $130,000 cost of treatment.

- I-580 facility:
  - 1.34 min saved per vehicle × 8,401 vehicles = 11,257 min saved/60 min = 188 h saved.
  - 188 h saved × $14.10 value per hour × 260 d per year = $687,700 per year travel time savings.
  - Given six restriped narrow lanes at $5,000 per lane mile for striping × 5.2 mi = $156,000 cost of treatment.

Results

The analyses showed minimal travel time benefits on a per-vehicle basis, but given peak volumes, savings from the narrow lane treatments were considerable. What stands out is the level of total benefits versus the costs of implementation of narrow lanes. For both roadway segments (I-270 and I-580), travel time benefits exceeded the cost of implementing narrow lanes within the first year. The benefits exceed costs by 6.1:1 and 4.4:1 in the first year of operation for the I-270 and I-580 segments, respectively.

Worst-Case Scenario

As the above results show, when a new lane is added with no increase in demand volume, delays (and their associated costs) decrease dramatically, producing exceptional benefit–cost ratios. This is despite the reduction in speeds expected due to lower speed limits and the difficulty drivers experience in staying within their lanes. However, as discussed within the safety analysis, the fundamental question is: what would happen if new traffic demand would ultimately "fill in" the new capacity created by the new freeway lane? To answer this, the team reran the two case studies with added mainline demand so that the per-lane demand remained equal to the base case demand. Ramp demands remained the same, however.

For I-270, when the speed limit is 55 mi/h, travel time (originally 11.81 min) becomes 10.74 min. When the speed limit drops to 50 mi/h, travel time becomes 11.05 min. For I-580,

travel time becomes 8.28 min, which is more than the base case travel time. This was apparently due to a bottleneck formation toward the beginning of the facility, which prevented vehicles from entering the network. The team added segments to the beginning of the facility so the analysis could begin with uncongested conditions at the boundary. The result of this exercise was that travel times became essentially identical under the base and narrow lane scenarios. This was an intuitive outcome because densities and operations occurring across five lanes were essentially copied over to a sixth lane. In the limited BCAs possible within this study, this result implied zero benefits and zero costs in terms of mobility impacts. However, there would presumably be benefits and costs associated with increasing the number of trips possible on a freeway, generating more pollution, and removing traffic from alternate routes within the city.

MICROSCOPIC MOBILITY ANALYSIS

Gipps Model Case Studies

The previous model modifications to account for different lane-narrowing scenarios were tested in two case studies involving different sites: a stretch of I-270 near Rockville, MD, and a stretch of I-580 near Castro Valley, CA. For both sites, a baseline scenario was calibrated based on real-world conditions gathered from detector counts. In their original geometric configuration, both sites had standard 12-ft-wide lanes.

The baseline scenario serves as grounds for comparison with five other treatments involving additional lanes, with and without lane narrowing:

- Baseline.
- A scenario with an additional lane where lanes are narrowed to 11 ft.
- A scenario with an additional lane where lanes are narrowed to 10 ft.
- A scenario with an additional 12-ft lane.
- A scenario with an additional 12-ft lane and a homogeneous 15-percent demand increase.
- A scenario with an additional lane where lanes are narrowed to 11 ft and the posted speed limit is reduced by 10 mi/h.

Table 39 summarizes all the scenarios, including their most relevant characteristics.

The following subsections describe in more detail each one of the case study sites and provide the simulation results, which were obtained after simulating each scenario 10 times, keeping the random seed constant across them for the sake of comparison.

Table 39. Gipps model case study scenarios.

Scenario	Number of Lanes	Lane width (ft)	Demand	Speed Limit
One (baseline)	I-270: four I-580: five	12	Baseline	I-270: 55 mi/h I-580: 65 mi/h
Two	Baseline plus one	11	Baseline	Baseline
Three	Baseline plus one	10	Baseline	Baseline
Four	Baseline plus one	12	Baseline	Baseline
Five	Baseline plus one	11	15-percent increase	Baseline
Six	Baseline plus one	11	Baseline	10-mi/h reduction

I-270 Results

The simulated I-270 stretch of highway is the southbound approach aerially photographed in figure 31. The results obtained focus on the mainline, which currently has four 12-ft lanes and a posted speed limit of 55 mi/h. The demand used to recreate baseline conditions extends for a period of 4 h between 6:00 and 10:00 a.m., including both cars and trucks. Demand is further discretized into 1-h periods with a total peak demand of 12,298 veh/h and 9,816 veh/h as the lowest demand during the last simulation h. Total demand has approximately a 1/10 split between heavy vehicles and regular cars.

Figure 31. Map. I-270 case study site.

The I-270 average mainline results obtained for each of the six simulated scenarios are summarized in table 40, which presents the most relevant network statistics for the network sections in which the lane-narrowing treatment was applied aggregated across links and lanes: density, flow, speed, and vehicles waiting to enter. Note that the results across scenarios two through four are similar.

Table 40. Network statistics for the I-270 simulated case study scenarios.

Network Statistic	Scenario One	Scenario Two	Scenario Three	Scenario Four	Scenario Five	Scenario Six
Density (veh/mi)	2.93	2.71	2.70	2.72	3.63	2.90
Flow (veh/h)	11,378	11,400	11,400	11,401	13,069	11,392
Speed (mi/h)	53.9	56.2	56.3	56.1	51.8	52.8
Vehicles waiting to enter	15.80	1.20	1.20	1.20	18.70	1.20

These results illustrate that the effects captured by the model modification on the vehicles' reaction times do not produce significantly distinctive outputs. In all cases, average density was reduced and flow and average speed increased, a consequence of capacity gains achieved by expanding the corridor with an additional lane. The upcoming discussion section includes a series of possible explanations behind the lack of substantial effects observed across the different treatments. On the other hand, scenarios five and six presented expected outcomes. Scenario five had a substantial increase in average density and number of vehicles waiting to enter the network, which is directly tied to congestion effects induced by a 15-percent demand increase. Scenario six had a small decrease in average speed and flow even though the effects are less noticeable since even the scenarios with an additional lane are congested.

I-580 Results

The I-580 stretch of highway simulated is the eastbound approach that can be observed in figure 32. The results obtained focus on the approach mainline, which currently has five 12-ft lanes and a posted speed limit of 65 mi/h. The demand used to recreate the baseline conditions covers a period of 4 h between 4:55 and 8:55 a.m., including both cars and trucks. In this case, demand was discretized into 15-min periods with a total peak demand of 9,624 veh/h (between 7:25 and 7:40 a.m.) and 1,614 veh/h in the lowest demand bin, coinciding with the simulation onset. Total demand has approximately a 1/15 split between heavy vehicles and regular cars.

Figure 32. Map. I-580 case study site.

The I-580 average mainline results obtained for each of the six simulated scenarios are summarized in table 41. The outcomes are in consonance with those obtained for I-270. Scenarios two–four, which consider a lane addition with various lane-narrowing treatments yielded average metrics that are very similar, while scenarios five and six have significant differences, in line with what was expected.

Table 41. Network statistics for the I-580 simulated case study scenarios.

Network Statistic	Scenario One	Scenario Two	Scenario Three	Scenario Four	Scenario Five	Scenario Six
Density (veh/mi)	1.03	1.05	1.05	1.07	1.28	1.08
Flow (veh/h)	5,960	5,949	5,951	5,950	6,828	5,945
Speed (mi/h)	53.3	52.9	53.0	52.5	51.3	51.9
Vehicles waiting to enter	0.10	0.10	0.10	0	0.20	0.10

Discussion

Even though the model calibration uncovered distinctive differences in the steady-state car-following trends across treatment and control sections of the different sites in which headway data were collected, the case study outputs did not reveal dramatic variations for the three scenarios in which a lane was added with different lane-narrowing treatments, ceteris paribus. While reaction times considered in these three scenarios were different, the resulting effects did not yield significant variations on average mainline traffic key performance indicators. This lack of differences could have multiple causes.

First, model modifications considered by lane-narrowing treatments were only imposed on the deceleration component of the car-following regime. However, other possible behavioral effects, such as differences in the lane-changing patterns, were not incorporated. In both case studies, which present a number of merging and diverging areas along the mainline section of study, this could result in an understatement of actual differences that one could observe, since throughput is highly dependent on the lane-change dynamic in these instances.

Second, only sites where statistically significant trends were uncovered presented a slight decrease in inferred driver reaction times with the lane-narrowing treatment. This could be the result of drivers becoming more attentive as they perceive the small lane width difference. However, one could think that, in cases in which the lane-narrowing treatment is more substantial (e.g., transitioning from 12 to 10 ft or even narrower widths), the underlying assumption of a linear relationship between gap and headway may break down. It is possible to conceptualize that, for more drastic treatments, the linear relationship may not hold; instead, one could face sharp nonlinearities, or something of a boundary effect, in the case of treatments that narrowed freeway lanes in excess. Unfortunately, none of the sites where data was collected are geared toward providing answers on effects of more extreme lane-narrowing treatments.

Third, simulated lane occupancy should be considered. Simulation outputs, due to underlying demand patterns and off-ramp configuration, lead to a tendency for queues to appear in the rightmost lanes of the freeway mainline in both sites. This, in turn, could lead to an underestimation of the beneficial effects of adding an extra lane.

In any case, the results show promise for lane-narrowing treatments since they constitute an economic alternative to increasing capacity and may serve to alleviate congestion in saturated freeways. However, one should take the lack of substantial differences observed in case studies with a grain of salt since they include certain model extrapolations that may not hold true due to boundary effects. In conclusion, these results show promise, but call for further investigation, perhaps using a more controlled test site in which a wider array of lane widths could be explored methodically to uncover more complex dynamics that could arise when large lane-narrowing treatments are undertaken.

Wiedemann Model Case Studies

The base model was developed by Maryland DOT for their own purposes and then adapted for the I-270 narrow lanes study. All existing geometry and demand was left unchanged from the original Maryland DOT model. Driver behaviors developed and calibrated for the model's original urban, freeway, and weaving segments were left unchanged with the exception of car-following models, which were changed to match narrow lanes control and treatment site data. The Vissim model was set up in two files (a.m. and p.m.) with each file containing the scenarios shown in table 42. However, due to time constraints, analysis was limited to the p.m. model only. Each scenario was evaluated over 10 simulation runs using random seeds 8, 35, 62, 89, 116, 143, 170, 197, 224, and 251. Each simulation ran for 5,400 s (90 min).

Table 42. Base model scenarios based on Maryland model.

Scenario	Number of Lanes	Lane Width (ft)	Demand	Speed Limit
1 (baseline)	Four	12	Baseline	55 mi/h
2	Baseline plus one	12	Baseline	Baseline
3	Baseline plus one	12	Increase	Baseline
4	Baseline plus one	11	Baseline	Baseline
5	Baseline plus one	11	Increase	Baseline
6	Baseline plus one	10	Baseline	Baseline
7	Baseline plus one	10	Increase	Baseline
8	Baseline plus one	11	Baseline	5-mi/h reduction
9	Baseline plus one	11	Increase	5-mi/h reduction
10	Baseline plus one	10	Baseline	5-mi/h reduction
11	Baseline plus one	10	Increase	5-mi/h reduction

The differences between the different scenarios are described as follows:

1. 12 ft control: existing geometry and demand; 12-ft-wide lanes and 12-ft observation site calibrated car-following behaviors.

2. 12 ft control + one lane: existing demand with 12-ft-wide lanes and 12-ft site calibrated car-following behaviors and one additional 12-ft lane added to the I-270 corridor (northbound and southbound).

3. 12 ft control + one lane (increased demand): standard 12-ft-wide lanes and 12-ft site calibrated car-following behaviors and one additional 12-ft lane added to the I-270 corridor (northbound and southbound) as well as extra demand to maintain a similar average link density to scenario one.

4. 11 ft treatment + one lane: existing demand with 11-ft-wide lanes and 11-ft observation site calibrated car-following behaviors and one additional 11-ft lane added to the I-270 corridor (northbound and southbound).

5. 11 ft treatment + one lane (increased demand): narrow 11-ft-wide lanes and 11-ft observation site calibrated car-following behaviors and one additional 11-ft lane added to the I-270 corridor (northbound and southbound) as well as extra demand to test the facilities under future demand.

6. 10 ft treatment + one lane: existing demand with 10-ft-wide lanes and 10-ft observation site calibrated car-following behaviors and one additional 10-ft lane added to the I-270 corridor (northbound and southbound).

7. 10 ft treatment + one lane (increased demand): narrow 10-ft-wide lanes and 10-ft observation site calibrated car-following behaviors and one additional 10-ft lane added to the I-270 corridor (northbound and southbound) as well as extra demand to test the facilities under future demand.

8. 11 ft treatment + one lane + speed reduction: existing demand with 11-ft-wide lanes and 11-ft observation site calibrated car-following behaviors and one additional 11-ft lane added to the I-270 corridor (northbound and southbound). Decreased desired speeds by 5 mi/h.

9. 11 ft treatment + one lane (increased demand) + speed reduction: narrow 11-ft-wide lanes and 11-ft observation site calibrated car-following behaviors and one additional 11-ft lane added to the I-270 corridor (northbound and southbound) as well as extra demand to test the facilities under future demand. Decreased desired speeds by 5 mi/h.

10. 10 ft treatment + one lane + speed reduction: existing demand with 10-ft-wide lanes and 10-ft observation site calibrated car-following behaviors and one additional 10-ft lane added to the I-270 corridor (northbound and southbound). Decreased desired speeds by 5 mi/h.

11. 10 ft treatment + one lane (increased demand) + speed reduction: narrow 10-ft-wide lanes and 10-ft observation site calibrated car-following behaviors and one additional 10-ft lane added to the I-270 corridor (northbound and southbound) as well as extra demand to test the facilities under future demand. Decreased desired speeds by 5 mi/h.

For the purposes of this analysis, scenarios four through seven were not included, as it was decided that any scenario with a lane width reduction should also contain desired speed (i.e., posted speed limit) reductions. Analysis was completed and results compiled on all 11 scenarios. Each simulation run had a 1,800-s (30-min) seeding period, after which evaluations were performed on the model for 3,600 s (60 min). The following evaluations were collected:

- Link segment evaluations: one evaluation segment per lane per link on the I-270 links only. All ramps, surface streets, and other highways were excluded. Links were numbered sequentially from 1 to 159 in the southbound direction and sequentially from 200 to 345 in the northbound direction. Lane segment results were aggregated every 5 min over the course of the 1-h-long simulation period. The following results were found for each lane segment:
  - Relative delay: link delay time share of total travel time.
  - Density: average density across each 300-s interval.
  - Speed: average measured speed across each 300-s interval.
  - Volume: average flow rate across each 300-s interval.

- Travel time and delay evaluations: three key segments were identified within the network shown in figure 33 through figure 35. Travel time and delay results were aggregated once per simulation run. The following results were found for each travel time and delay measurement:
  - Vehicles: a count of all vehicles completing the segment within the evaluation period.
  - Travel time: average time to complete the segment per vehicle within the evaluation period.
  - Vehicle delay: average delay accrued per vehicle along the segment within the evaluation period.

- Stops: average number of stops per vehicle along the segment within the evaluation period.
- Stop delay: average delay per vehicle accrued while vehicle was stopped along the segment within the evaluation period.

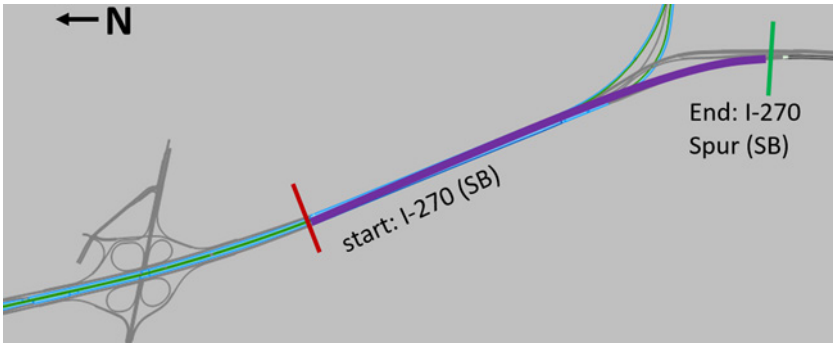

SB = southbound.

Figure 33. Map. Travel time and delay segment one, distance: 1.55 mi.

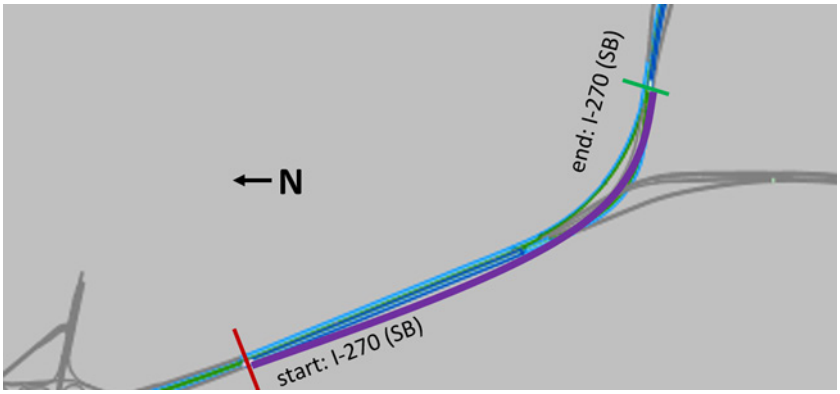

SB = southbound.

Figure 34. Map. Travel time and delay segment two, distance: 1.46 mi.

© 2018 PTV Group.
NB = northbound.

Figure 35. Map. Travel time and delay segment three, distance: 3.2 mi.

- Queue length evaluations: one queue counter placed on the I-270 spur (southbound) exit ramp (figure 36) to measure the spillback from any I-270 spur congestion that affected analysis of the study area. The queue definition was configured as follows:
  - Begin when velocity <3.1 mi/h.
  - End when velocity >6.2 mi/h.
  - Maximum headway = 65.6 ft.

The following results were found for the queue length evaluation:

- Queue length (feet): Average queue length within the evaluation period.
- Queue length maximum (feet): Maximum queue length within the evaluation period.
- Queue stops: A count of all vehicles that entered the queue within the evaluation period.

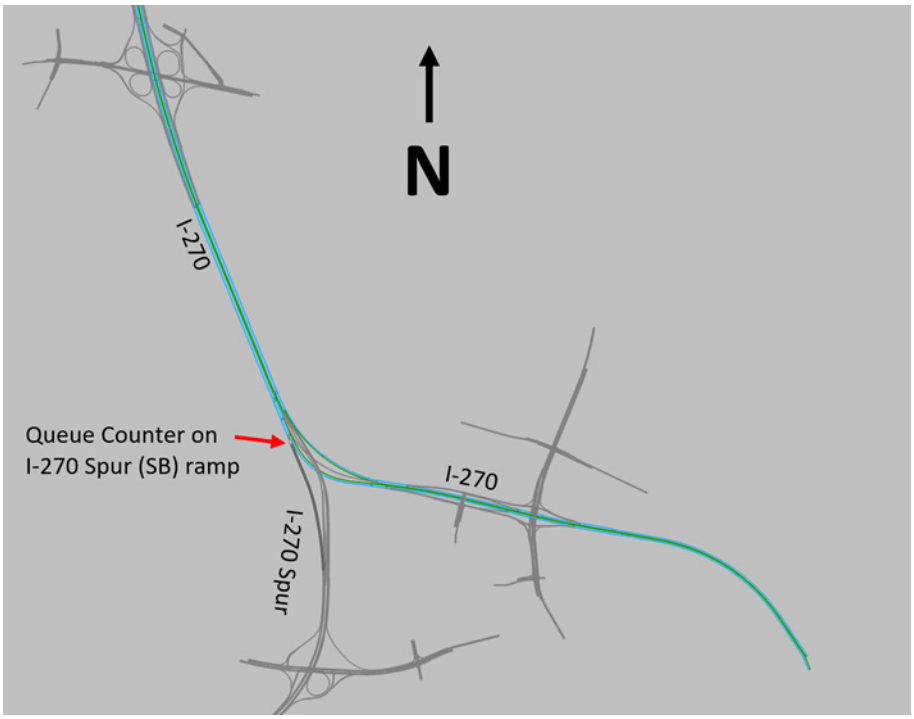

© 2018 PTV Group.
SB = southbound.

Figure 36. Map. Queue counter location.

Scenario Comparisons

For the control scenario, link segment evaluation results revealed three key hotspots, two in the southbound direction and one in the northbound direction:

- I-270 southbound exit 11 MD 124 (links 94 to 99).
- Between I-270 southbound exit 4 and I-270 spur (links 133 to 145).
- Between I-270 northbound exit 1 and exit 4 (links 200 to 220).

At hotspot number one, flow rate and density decreased in the 10- and 11-ft treatment scenarios. However, average speed increased at this location as the lanes narrowed. That result is reflected in the relative delay dropping for the 11-ft scenario, and dropping even more for the 10-ft scenario (figure 41 and figure 42).

Upon closer inspection, the rightmost lanes average speeds less than 30 mi/h, and the leftmost lanes average speeds greater than 40 mi/h. The decrease in density coupled with lower desired speeds of the narrowed lanes scenarios create more opportunities for lane changes and weaving to occur.

This effect can be seen most directly on link number 95. In scenario two, the treatment was to add an additional 12-ft lane to the left-hand side of the freeway. However, this treatment positively impacted the leftmost existing lane (table 43 and table 44), and in fact caused minimal change in delays on most of the right-hand side lanes. When reduced speeds and narrowed lanes

(and following behaviors associated with narrower lanes) were implemented, relative delay improvements were seen across more lanes. Figure 37 through figure 40 illustrate traffic performance throughout the analysis area.

Table 43. Lane-specific delay percentages at hotspot number one.

Lane Number	Scenario 1	Scenario 2	Scenario 8	Scenario 10
One (right)	72.8	72.7	79.1	73.3
Two	68.0	64.8	65.4	58.2
Three	51.3	50.5	49.6	46.7
Four	11.6	12.5	9.0	11.4
Five	7.0	2.0	1.9	2.1
Six (left)	—	1.9	2.2	2.1

—No data.

Table 44. Lane-specific delay change percentages at hotspot number one.

Lane Number	Scenario 1	Scenario 2	Scenario 8	Scenario 10
One (right)	—	−0.06	6.35	0.57
Two	—	−3.21	−2.55	−9.74
Three	—	−0.76	−1.61	−4.52
Four	—	0.91	−2.68	−0.28
Five (left)	—	−4.98	−5.04	−4.88

—No data.

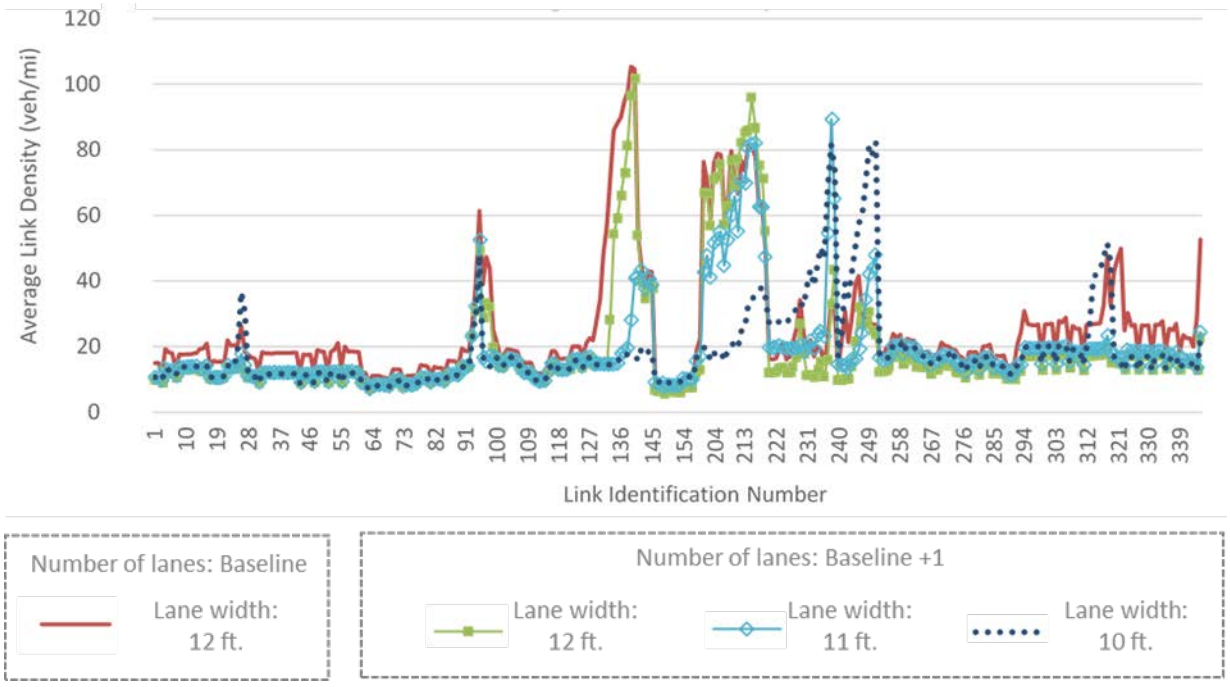

Figure 37. Graph. I-270 link density by link (southbound links are 1–159, northbound links are 200–345).

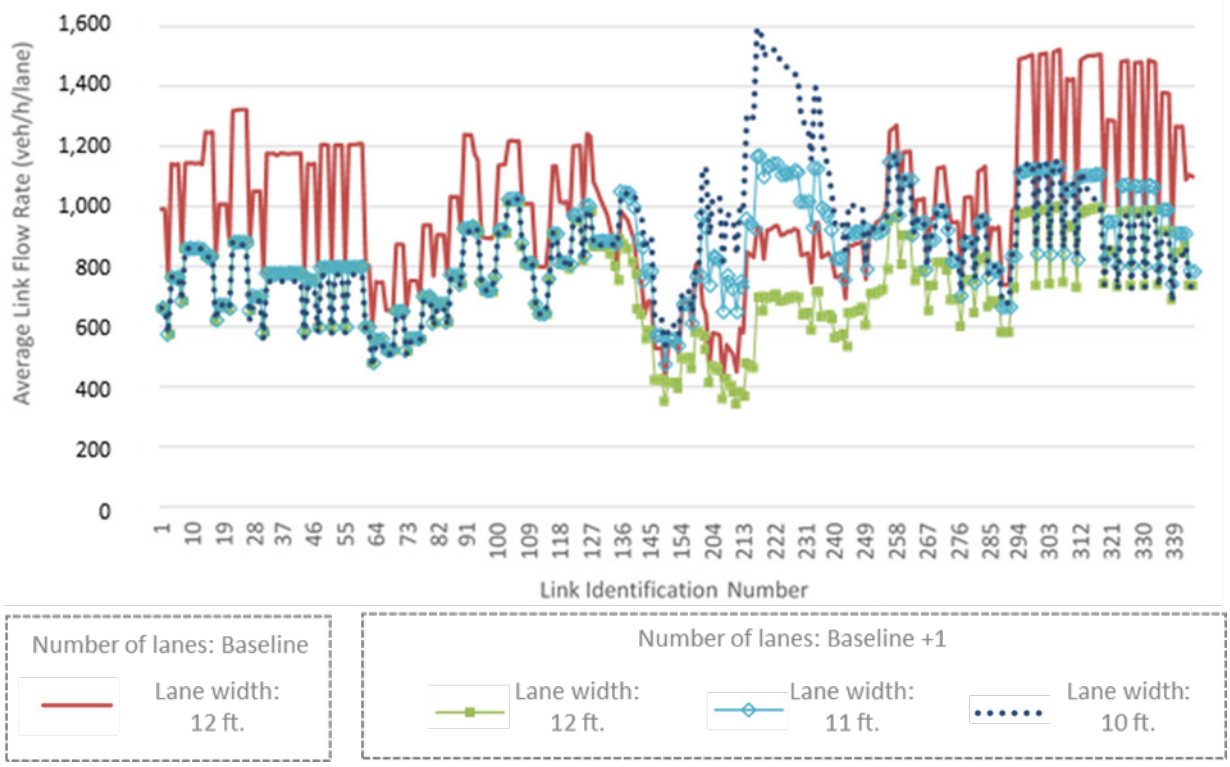

Figure 38. Graph. I-270 flow rate by link (southbound links are 1–159, northbound links are 200–345).

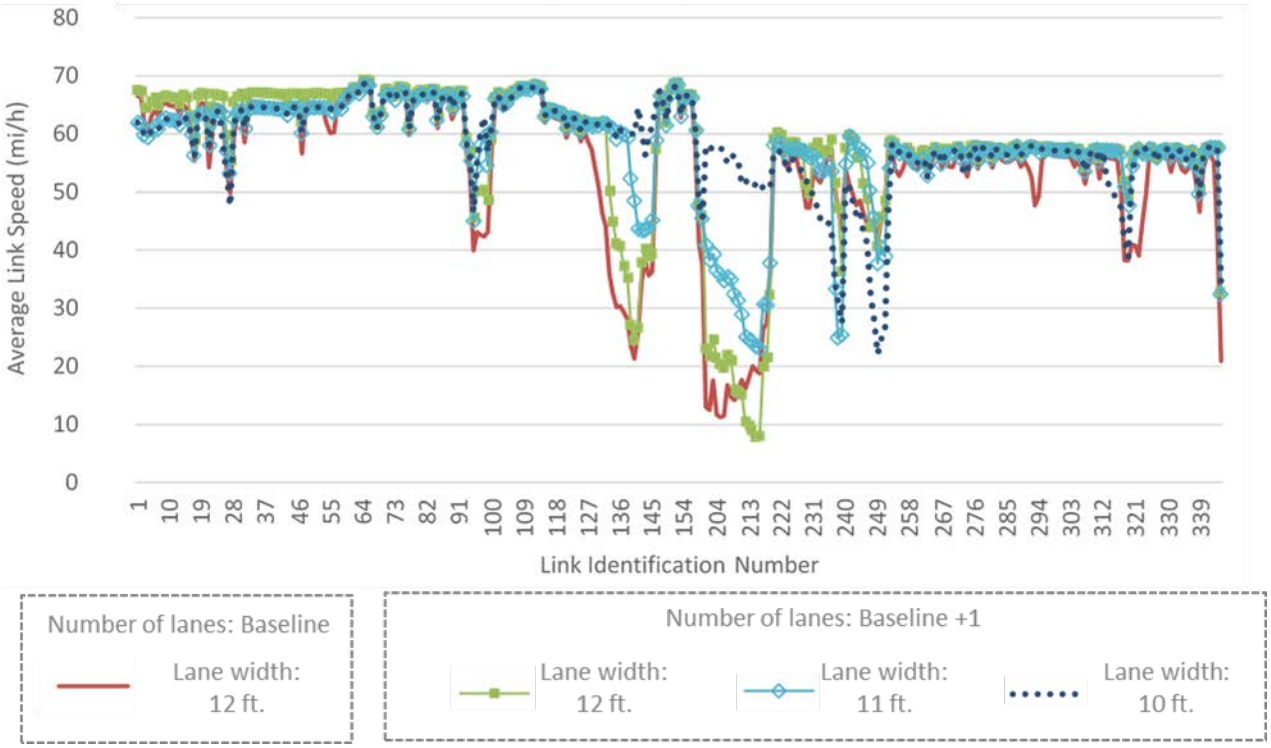

Figure 39. Graph. I-270 speed by link (southbound links are 1–159, northbound links are 200–345).

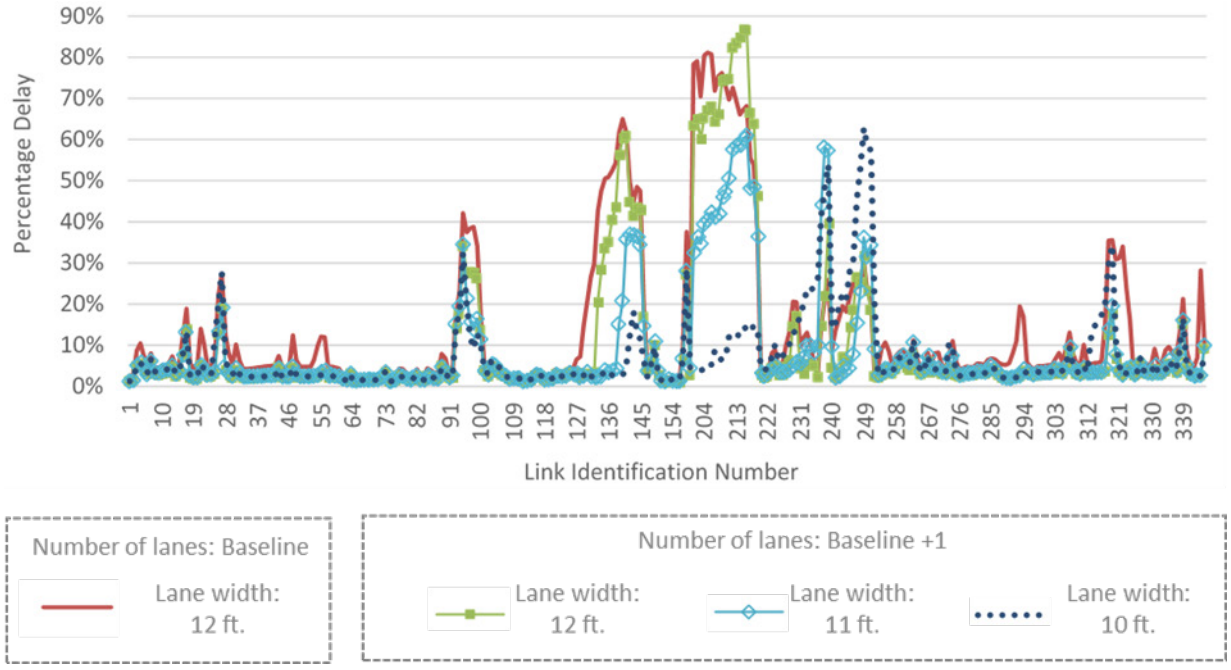

Figure 40. Graph. I-270 relative delay by link (southbound links are 1–159, northbound links are 200–345).

Scenarios 8 and 10 had similar average link flow, speed, and density results and are both improvements over the 12-ft scenarios. However, delay results for scenario 10 (10 ft + one 10-ft lane) showed the highest single-lane delay improvement (lane two) as well as the most delay improvement. Scenario 10 had an average delay improvement of 3.77 percent, whereas the 11-ft alternative showed only a 1.11 percent improvement on average. Therefore, of the scenarios tested, the 10-ft-wide lanes with an additional 10-ft lane and a speed reduction of 5 mi/h was the preferred solution for hotspot number one (I-270 southbound exit 11).

Hotspot number 2 was a known area of heavy congestion and therefore the team not only performed link evaluations, but also evaluated corridor travel time and delay results and collected queuing data. At the link level, drops in density and delay were observed within the hotspot as narrower lane treatments were applied. Average speed and flow rate also increased as narrower treatments were applied (figure 37 through figure 40). Upon closer inspection of the travel time and delay analysis, travel time measurements one and two (representing keeping right at the fork and keeping left, respectively) yielded significant improvements in scenarios with narrowed lanes over the control scenarios in all recorded metrics.

It was observed that scenario two, where a 12-ft lane was added to the network, increased travel time, delay, and number of stops for both movements. Since the additional lane was added to the entire corridor, this change may have been the result of increased demand as upstream bottlenecks improve. The most telling result was the significant drop in number of stops and stopped delay for vehicles moving right at the junction in the scenarios with narrowed lanes, as that was indicative of more continuous flow and improved weaving. Looking more closely at the lane results on link 141 (table 45 and table 46), average lane speeds significantly increased. With the 11-ft improvement, speeds improved by between 14.5 and 17.6 mi/h in all lanes. With the 10-ft improvement, all seven lanes were at free flow.

Table 45. Lane-specific speeds (mi/h) at hotspot number two.

Lane Number	Scenario 1	Scenario 2	Scenario 8	Scenario 10
One (right)	20.4	19.2	37.2	63.3
Two	17.2	16.1	35.0	62.6
Three	18.6	17.4	35.7	61.7
Four	23.7	21.7	40.9	63.5
Five	34.5	29.2	46.7	65.4
Six	42.4	37.9	52.9	66.6
Seven (left)	—	45.0	57.4	68.7

—No data.

Table 46. Lane-specific speed changes (mi/h) at hotspot number two.

Lane Number	Scenario 1	Scenario 2	Scenario 8	Scenario 10
One (right)	—	−1.2	16.8	42.9
Two	—	−1.1	17.8	45.4
Three	—	−1.2	17.1	43.1
Four	—	−1.9	17.3	39.9
Five	—	−5.3	12.2	30.9
Six (left)	—	−4.5	10.6	24.3

—No data.

This result was surprising and counterintuitive, but could be explained by the idea that narrowing lanes to 10 ft wide (causing more conservative following behaviors) could reduce density just enough upstream to keep the facility under its capacity, thus preventing flow from entering the congested regime. This was confirmed in figure 41, where scenarios with increased demand have their link speeds displayed. The 10-ft scenario showed significant improvements over the other treatments. However, with increased demands, even the 10-ft treatment speeds drop below 45 mi/h. Queue data show a similar picture in that, as lanes narrow, queues improve significantly. This can be attributed to more efficient weaving behavior due to lower densities. By these metrics, it should be clear that the 10-ft option with an additional 10-ft lane and a speed reduction of 5 mi/h is the preferred solution for hotspot number two (I-270 southbound/ I-270 spur southbound diverge).

Hotspot number three is the longest hotspot in the control model, spanning 3.2 mi in the northbound direction of I-270 between mile posts 14 and 11. For this hotspot, travel time, as well as link- and lane-level data were collected from the 11 scenarios. When analyzing the link data, it was apparent that the addition of a single lane to the left of the northbound direction influenced downstream weaves. This is seen in figure 39, which shows the base scenario's link speeds improving as vehicles proceed through hotspot number three. Figure 39 also shows that speeds degrade in scenarios that include an additional lane. However, despite this effect, scenarios in which lanes are narrowed (and given their appropriate following behaviors), large improvements are seen in speed, flow, and relative delay (figure 38 through figure 40), while link densities also decrease significantly. In particular, scenarios that include 10-ft lane widths show roughly 50 percent less density while yielding roughly a 50-percent increase in average speeds.

Link number 211 is a five-lane segment that has a ramp merge on the right-hand side and a diverge on the left-hand side. This same link also showed some of the worst results in this section of the northbound I-270 corridor during the base run. Table 47 shows speeds across all lanes improving by as much as 41.64 mi/h in the 10-ft-lane-width scenario. Lane three showed 83 percent of the average vehicles' relative delay in the base network, which improved to 60.2 percent in scenario 8 (11-ft lanes) and to 11.9 percent in scenario 10 (10-ft lanes). Table 48 further illustrates massive delay reductions across all existing lanes in scenario 10.

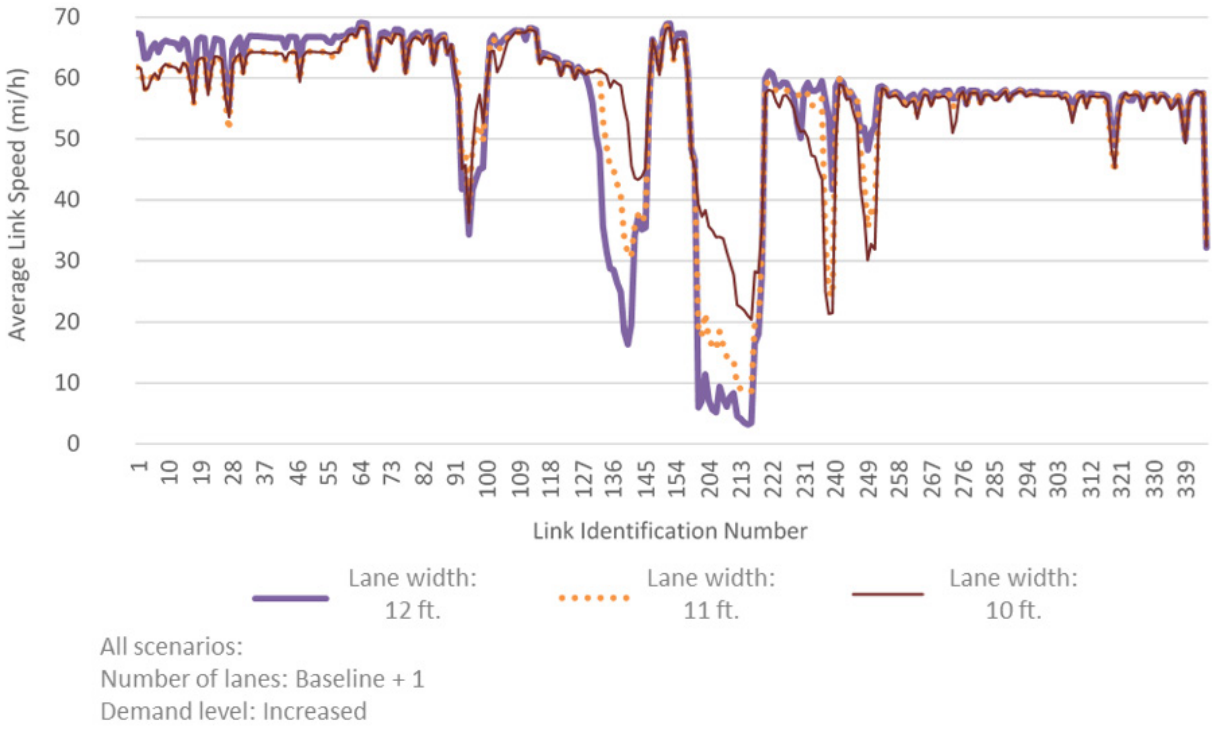

Figure 41. Graph. I-270 speed by link under increased demand.

Table 47. Lane-specific relative delay percentages at hotspot number two.

Lane Number	Scenario 1	Scenario 2	Scenario 8	Scenario 10
One (right)	69.2	77.4	55.4	18.8
Two	76.4	82.3	59.6	18.5
Three	83.0	86.7	60.2	11.9
Four	78.2	84.9	57.9	9.0
Five	41.9	83.1	55.8	8.2
Six (left)	—	34.0	14.8	5.5

—No data.

Table 48. Lane-specific relative delay percentage changes at hotspot number two.

Lane Number	Scenario 1	Scenario 2	Scenario 8	Scenario 10
One (right)	—	8.2	−13.8	−50.4
Two	—	6.0	−16.8	−57.8
Three	—	3.6	−22.8	−71.1
Four	—	6.8	−20.2	−69.1
Five (left)	—	41.2	13.9	−33.7

—No data.

Even after increasing demand to account for more freeway utilization in scenario 11, lane-based speed results are comparable to the 11-ft speed results without an increase in demand. Therefore, it was concluded that the 10-ft lane width with an additional 10-ft lane and a 5 mi/h speed reduction was the preferred solution for hotspot number three.

Throughput Results

When the team initially reported the benefits of the 10-ft lane-narrowing option, project stakeholders pointed out that the 10-ft treatment might not be effective unless it showed throughput greater than or equal to no-build conditions. In other words, the 10-ft option appeared effective on the surface, but in reality, many vehicles were trapped upstream. In response to this feedback, the team obtained throughput results for key scenarios. Table 49 shows that scenario 10 (10-ft option) consistently produced the most favorable throughput results at all three hotspots.

Table 49. Throughput (veh/h) for key case study scenarios.

Hotspot Number	Scenario 1	Scenario 2	Scenario 8	Scenario 10
One start	4,534	4,523	6,118	6,936
One end	1,942	1,919	2,578	3,143
Two start	4,534	4,523	6,118	6,936
Two end	2,120	2,120	2,867	3,147
Three start	1,955	2,151	3,696	4,483
Three end	4,413	3,533	7,731	10,623

Final Recommendation and Caveats

Based on Vissim microsimulation analysis of the I-270 corridor, the 10-ft lane-narrowing option was recommended. This option includes the addition of a 10-ft lane and posted speed limit reductions of 5 mi/h throughout the corridor. This treatment option consistently showed improved speed and flow through merging, diverging, and weaving sections in both directions. Some sections not explored above show that, with the treatment utilized in scenarios 10 and 11, there were significant spikes in delay, and some minor hotspots grew into major points of congestion (e.g., the northbound section between West Montgomery Avenue and Shady Grove Road exits, simulated by links 236–249). Upstream bottlenecks regulated flow into these sections. Improvements to upstream bottlenecks activated previously hidden downstream bottlenecks. Scenario two (i.e., 12-ft treatment with an additional left-side lane) showed the most improvement in speed, flow, and delay. Therefore, it was not recommended to extend the 10-ft treatment into this section of the northbound corridor.

Analysis

The Gipps model analysis concluded that narrow freeway lanes have a tendency to reduce driver reaction times, whereas the Wiedemann analysis found roughly a 7-percent increase in headways for each foot of lane narrowing. The team discussed possible reasons for these fundamental differences in bottom line outcomes.

The Gipps τ parameter and the Wiedemann parameters of Ax, at-speed average safety distance ($BX_{additive}$), and at-speed average variance ($BX_{multiplicative}$) are not directly comparable. The calibration parameters interact with one another to produce similar outputs: relative gap (Gipps) and safety distance (defined as the minimum following distance) (Wiedmann 74). Intuitively, the calibrated value of headway from one model should match the calibrated headway from another model if they are calibrated to the same underlying data because headway has a physical meaning. However, the measured values of physical parameters can only be used to set the boundary values for calibration:

> Optimal values for model parameters must be obtained from calibration: this is evident from Fig. 6(c), where we can observe that the estimated distribution of "maximum acceleration" is clearly different from what we could measure in reality (i.e., if we measured the empirical distribution of vehicles' max accelerations). In other words, this is further empirical evidence that parameters that are measurable in reality (i.e., those that have physical meaning) need to be calibrated in order to cover modeling uncertainties. (Punzo, Montanino, and Ciuffo 2015)

Calibrating the most sensitive parameters substantially reduces the calibration time effort, while not reducing the predictive power of the model. Uncalibrated parameters may be fixed at reasonable values while not being completely eliminated from the model. Thus, when one calibrates to trajectory data, one is calibrating to the trajectory, not each individual attribute. Moreover, it's been shown multiple times that maximum likelihood methods cannot calibrate parameters independently because this would violate the assumption of independent and identically distributed random variables (Treiber and Kesting 2013). Thus, it is only the interaction of variables that can replicate driver behavior.

In summary, the team viewed differences in output car-following parameters as natural outcomes based on fundamentally different structures of the Gipps and Wiedemann models. The question then becomes whether or not the Gipps and Wiedemann models produce similar outcomes when used in practice. In case study results presented earlier in this chapter, both models predicted significant benefits from the lane-narrowing treatment. The question of whether the Gipps and Wiedemann model adjustments (documented in chapter 5) produce similar predictions is addressed further in the next section, which pertains to the impact of lane narrowing on freeway capacities.

CAPACITY IMPACTS OF LANE NARROWING

In the case studies from this chapter, mobility impacts were expressed primarily in terms of speed, delay, density, and throughput. However, one of the most important performance measures for understanding lane-narrowing benefits is capacity. Nominally, if a fifth mainline lane were added to a freeway having four lanes in one direction, one might expect a 25-percent capacity increase because the number of lanes was increased by 25 percent. With narrower lanes, one would not expect a 25-percent capacity increase because of two reasons. The main reason, as discussed in the chapter 2 synthesis of research and findings, is that drivers must reduce their speeds simply to achieve lane keeping (i.e., staying within their lane). Waard et al. (1995) suggested that, when lanes are narrow, it becomes more difficult for a driver to stay in their lane. They must concentrate more and drive slower to achieve this. Posted speed limits are typically

lowered along narrow lane segments to facilitate safe driving conditions. This predictable lowering of speeds implies that capacity increase will almost certainly be lower than 25 percent if lanes are narrowed and a new narrow lane is added.

Another reason one would not expect a 25-percent capacity increase is driver behavior. Lane widths affect driver behavior, as expressed by car-following and lane-changing parameters. The effects on car-following parameters were shown in the chapter 5 discussion of model development. One of these effects was an approximate 10-percent increase in headways for each foot of lane narrowing. A 10-percent headway increase on its own would decrease capacities by 10 percent, but the case studies from this chapter showed that other factors (e.g., smoother merge maneuvers) make the impact of driver behavior on capacity less predictable. Nonetheless, it is possible that driver behavior diminished the capacity increase and amplified the capacity decrease already caused by travel speed reductions.

Although the capacity increase is likely lower than 25 percent, it is important to know, within a reasonable range, what amount of capacity increase can be expected. This is because a 5-percent capacity increase may not warrant significant interest from State agencies, especially given the construction costs of retrofitting a freeway segment. Instead, a 10–20-percent capacity increase would be more desirable. In addition, a reasonable expectation for capacity would help to compare the lane-narrowing treatment to other advanced transportation demand management-style treatments in a BCA. To ascertain the likely capacity increase of the lane-narrowing treatment, this section investigates the issue using macroscopic model analysis, Gipps model analysis, and Wiedemann model analysis from this project. This section answers the question: If four 12-ft lanes with a 65 mi/h speed limit were converted to five narrow lanes with a 55 mi/h speed limit, what would happen to the overall freeway capacity?

Macroscopic Field Data Analysis

According to table 5, capacity is 1,781, 1,695, and 1,547 passenger cars per hour per lane (pc/h/ln) for 12-, 11-, and 10-ft lanes, respectively. For the baseline case with four 12-ft lanes, total capacity is $4 \times 1{,}781 = 7{,}122$ pc/h. If this segment was converted to five 11-ft lanes, capacity would become $5 \times 1{,}695 = 8{,}474$ pc/h (19-percent increase). If converted to five 10-ft lanes, capacity would become $5 \times 1{,}547 = 7{,}734$ pc/h (9-percent increase). In the case of the macroscopic model, the reduced speed limit is implicitly included in the calculation because these capacities were derived from real-world freeways: along these real-world freeways, narrow lane segments already had lower posted speed limits than segments with conventional 12-ft lane widths. Similar examples are shown in chapter 5 where developed models were used. In these examples, a four-lane basic segment with a 70-mi/h speed limit was converted to a five-lane segment with11-ft-wide lanes and a 65-mi/h speed limit and a five-lane segment with 10-ft-wide lanes and a 65-mi/h speed limit. Before restriping, capacity of the four 12-ft lanes was $4 \times 2{,}400 = 9{,}600$ pc/h. Converting to five 11-ft lanes resulted in capacity of $5 \times 2{,}241$ pc/h/ln = 11,204 pc/h (17-percent increase). Converting to five 10-ft lanes resulted in capacity of $5 \times 2{,}043 = 10{,}217$ pc/h (6-percent increase). The difference between these percentages and percentages shown from field data was due to the speed limit; a 70-mi/h speed limit for narrow lane segments would have resulted in the same percentages (i.e., 19- and 9-percent increases).

Macroscopic Model Analysis

A brief sensitivity analysis was conducted with the new model. The previous 19- and 9-percent capacity increases were based on field data only (aggregate results). Table 50 shows that speed limit has a modest impact on capacity, but number of lanes has a bigger impact. Therefore, ranges of capacity could increase depending on the number of lanes.

For the case of four lanes to five lanes while reducing speed limit from 65 to 55 mi/h, capacity increased 4 percent for 10-ft lanes, as shown above. However, for 11-ft lanes, table 50 shows a speed limit reduction from 65 to 60 mi/h. When this calculation was updated to reflect a speed limit of 55 mi/h for the 11-ft lane case, capacity increased 14 percent. Table 51 shows larger capacity increases for the case of transitioning from three to four lanes.

Gipps Model Analysis

Previous case study results shed light on potential gains by implementing a lane-narrowing treatment to increase the number of lanes in a freeway section. However, the results do not directly address the impact that this treatment could have on freeway capacity. To tackle this question in more direct fashion, the team devised three additional simulation scenarios focusing on I-270. First, to obtain baseline capacity with the original site configuration, case study calibrated demands were increased by 50 percent between 8:00 and 10:00 a.m. This demand increase resulted in a queue that eventually spills back into the mainline from an off-ramp located in the south–central area of the corridor.

Table 50. Macroscopic model sensitivity analysis adjusting number of lanes from four to five.

Lane Width (ft)	Shoulder Width (ft)	Speed Limit (mi/h)	FFS (mi/h)	Capacity (veh/h/ln)	Breakpoint	CAF	Percent Capacity Improvement
12	8	75	75.2	2,452	992	1.00	—
11	1	70	70.1	2,281	1,080	0.95	16
10	6	65	65.0	2,044	1,061	0.87	4
12	8	70	70.6	2,406	1,176	1.00	—
11	1	65	65.6	2,238	1,243	0.95	16
10	6	60	60.0	2,006	1,194	0.87	4
12	8	65	66.0	2,360	1,361	1.00	—
11	1	60	61.1	2,195	1,406	0.95	16
10	6	55	56.1	1,968	1,328	0.87	4
12	8	60	61.3	2,313	1,546	1.00	—
11	1	55	56.5	2,152	1,269	0.95	16
10	6	50	57.1	1,975	1,300	0.87	7
12	8	55	56.7	2,267	1,731	1.00	—
11	1	50	56.2	2,149	1,580	0.95	18
10	6	50	57.1	1,975	1,300	0.87	9

—Base scenario, so no percent improvement was calculated.

Table 51. Macroscopic model sensitivity analysis adjusting number of lanes from three to four.

Lane Width (ft)	Shoulder Width (ft)	Speed Limit (mi/h)	FFS (mi/h)	Capacity (veh/h/ln)	Breakpoint	CAF	Percent Capacity Improvement
12	8	75	74.1	2,441	1,037	1.00	—
11	0	70	68.9	2,269	1,124	0.95	24
10	4	65	63.7	2,033	1,100	0.87	11
12	8	70	69.5	2,395	1,222	1.00	—
11	0	65	64.4	2,226	1,286	0.95	24
10	4	60	59.3	1,995	1,233	0.87	11
12	8	65	64.8	2,348	1,406	1.00	—
11	0	60	59.9	2,184	1,449	0.95	24
10	4	55	54.9	1,956	1,366	0.87	11
12	8	60	60.2	2,302	1,591	1.00	—
11	0	55	55.3	2,141	1,612	0.95	24
10	4	50	55.8	1,964	1,339	0.87	14
12	8	55	55.6	2,256	1,776	1.00	—
11	0	50	55.0	2,138	1,623	0.95	26
10	4	50	55.8	1,964	1,339	0.87	16

—Base scenario, so no percent improvement was calculated.

The other two scenarios in consideration are treatment scenarios with an additional lane and lane widths of 11 ft and 10 ft, respectively, where original demand was also increased by 50 percent between 8:00 and 10:00 a.m. to force the onset of congestion. Additionally, to consider a realistic treatment implementation, the two treatment scenarios also included a decrease of 5 mi/h in the posted speed limit, which brought the speed limit in this I-270 corridor down to 50 mi/h.

To capture corridor capacity in each of these three scenarios, speed and flow time series directly upstream from the bottleneck were analyzed. Figure 42 through figure 44 show results obtained in representative replications for each of the three simulated scenarios. In each case, capacity was inferred as the maximum flow value registered at (or near) the moment in which a significant drop in average speed was detected (e.g., 8:35 a.m. for the baseline scenario and 9:10 a.m. for the two treatment scenarios).

The analysis performed on the results of 10 different replications for each scenario revealed average capacity values of 8,060 veh/h for the baseline scenario; 9,806 veh/h for the 11-ft treatment scenario; and 9,749 veh/h for the 10-ft treatment scenario. This corresponded to a 21.7- and 21.0-percent capacity increase for the 11- and 10-ft lane-narrowing treatments, respectively, when narrowing the lane width enables the creation of additional lanes.

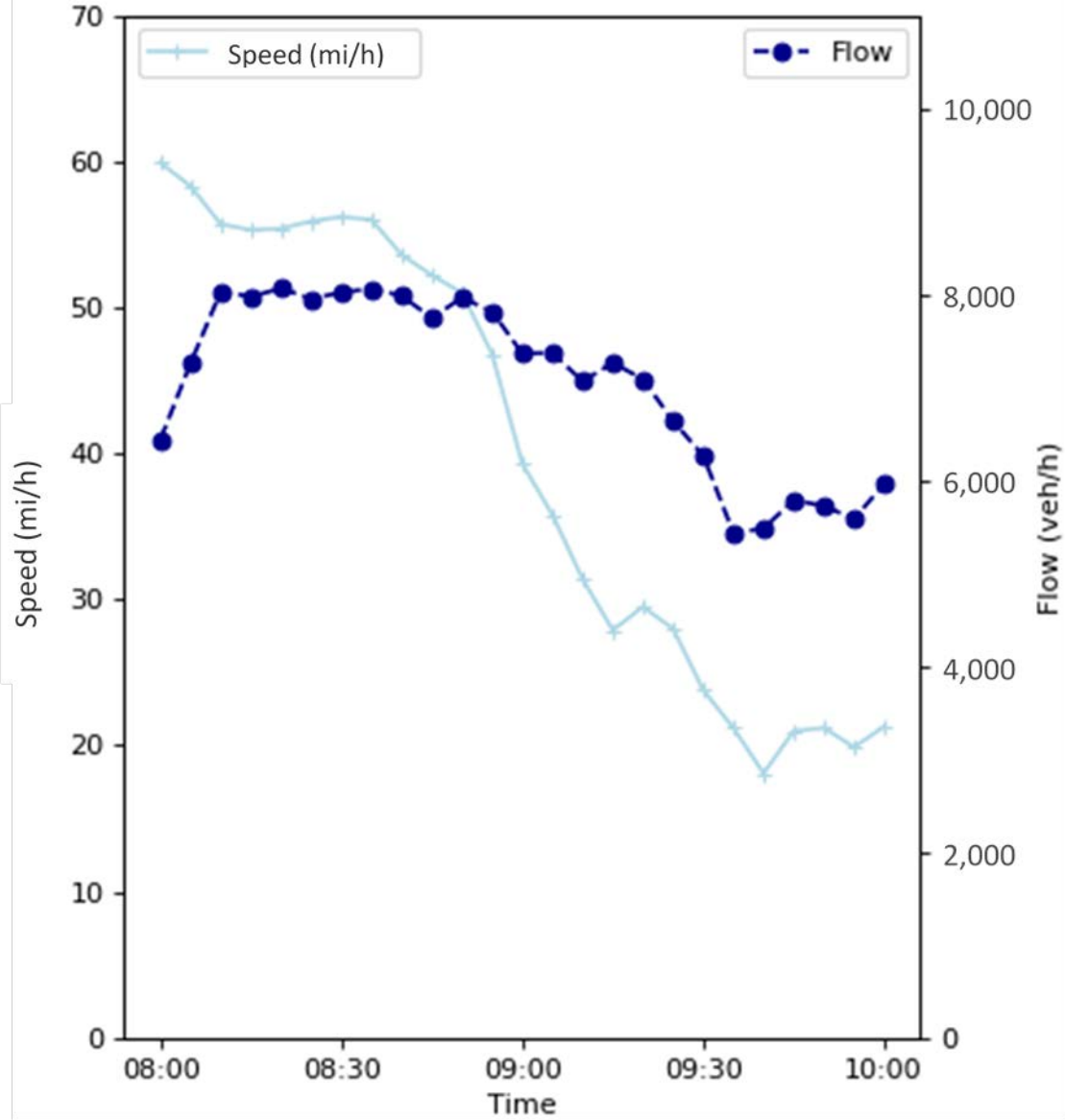

Figure 42. Graph. Baseline throughput time series (Gipps model) for I-270.

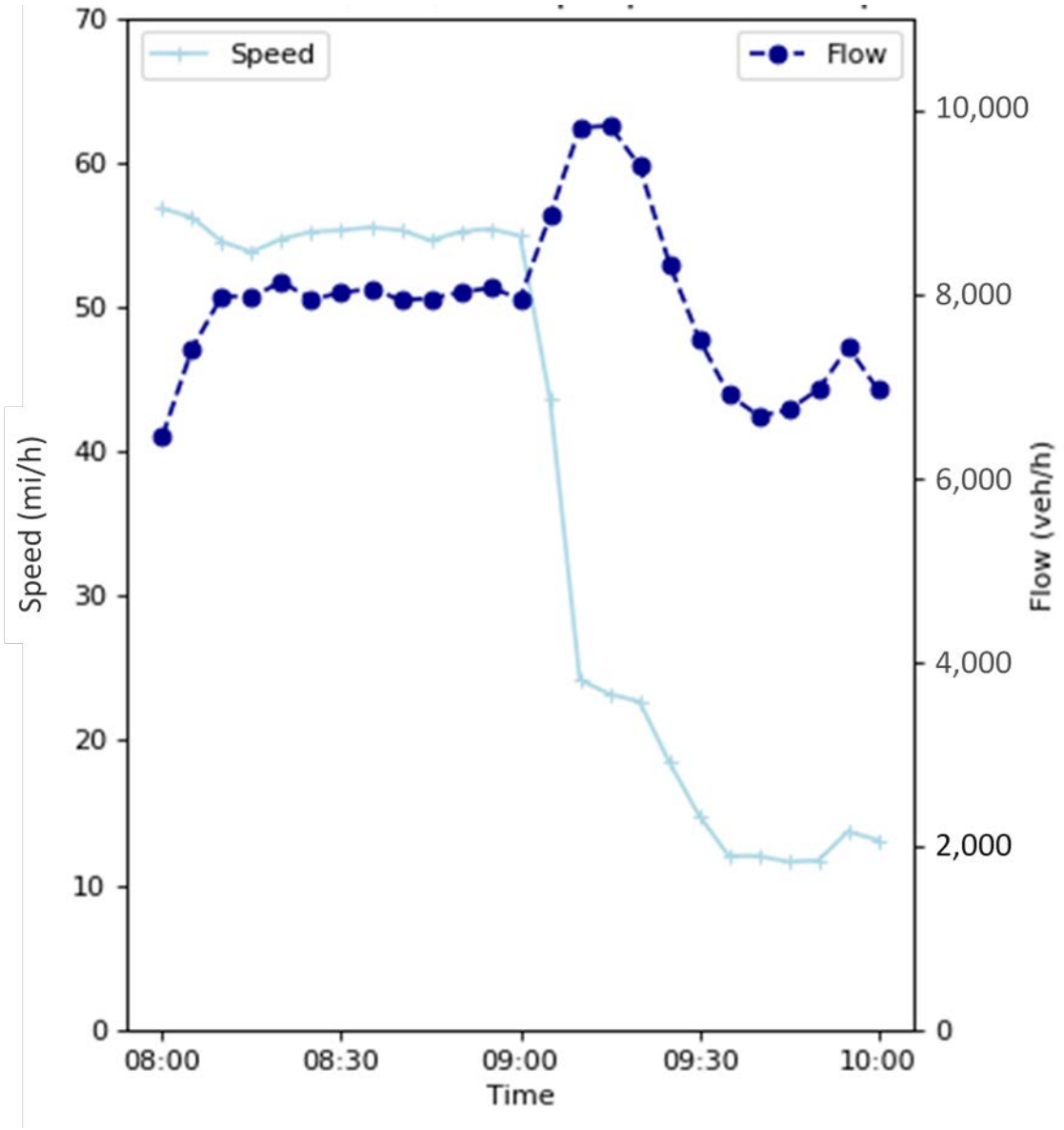

Figure 43. Graph. Throughput time series for 11-ft lane scenario (Gipps model) with 5-mi/h speed limit decrease.

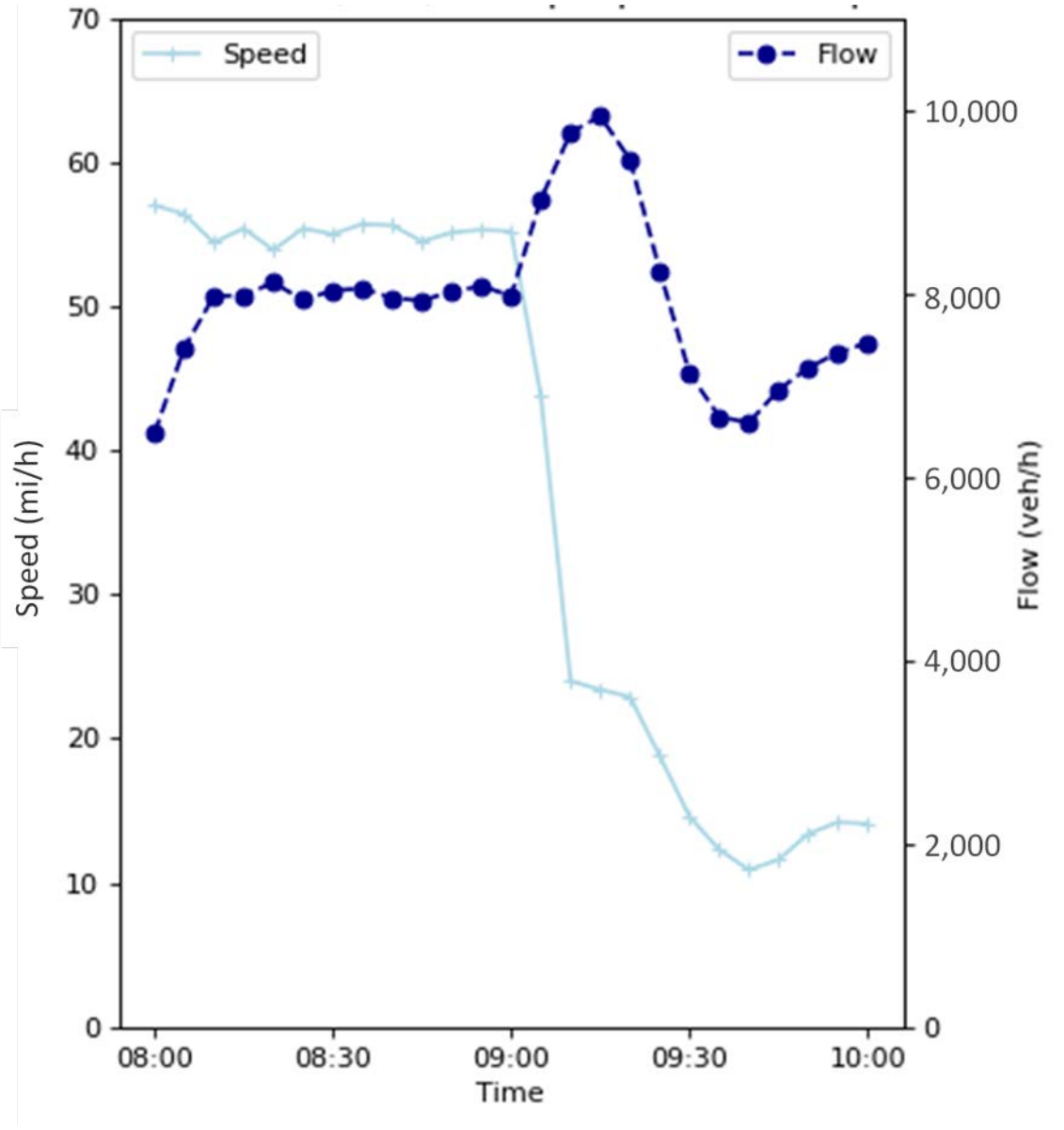

Figure 44. Graph. Throughput time series for 10-ft lane scenario (Gipps model) with 5-mi/h speed limit decrease.

Wiedemann Model Analysis

The Wiedemann model analysis was unique in that 10-ft lane scenarios produced better outcomes than all other scenarios, including the scenario of adding a 12-ft lane. However, this was not solely a capacity issue, as there were other factors at play (e.g., hidden bottlenecks). In any event, the team performed a similar time series analysis to estimate capacity impacts of lane narrowing for the I-270 case study scenarios.

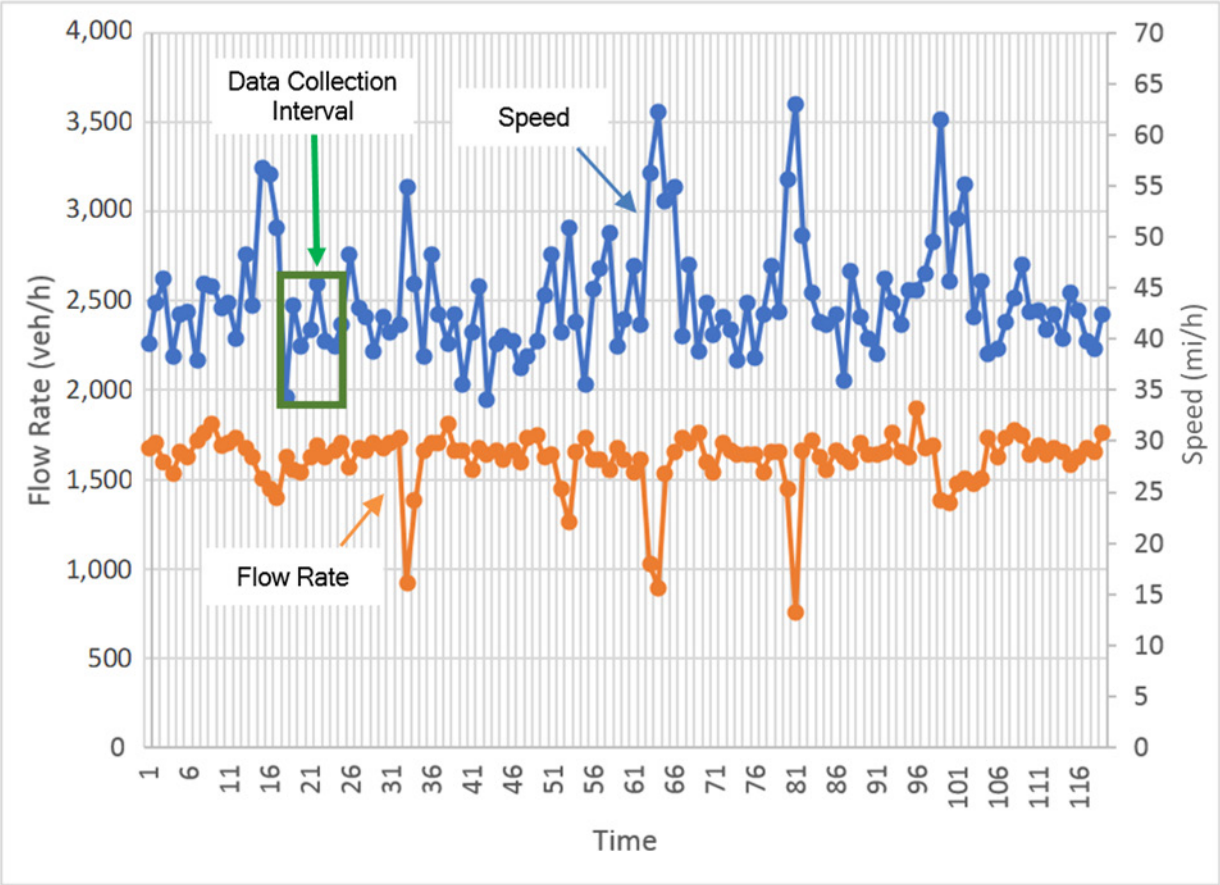

Figure 45. Graph. Throughput time series (Wiedemann model).

Figure 45 is an example of speed and flow rate changes over time, on link 100, for the right-most lane. For each scenario, simulations were conducted 10 times with different random number seeds for 1.5 h per run. The first 30 min during each run was a warm-up time, thus data were not collected. Then, lane-specific data were collected at intervals of 5 min. As a result, there were 12 data points per simulation run for a total of 120 data points. Prebreakdown flow rates were then identified and averaged across all link segments and lanes. The results are summarized in table 52. However, since the overall freeway segment contained five lanes instead of four lanes in narrow lane scenarios, estimated capacity increases depended on whether breakdown could be assumed to affect either one or two of the rightmost lanes (note that items with an asterisk mean that speed limits were reduced by 5 mi/h):

- Capacity for the 12-ft lane scenario: 4 × 1,585 = 6,340 veh/h.
- Capacity for the 11-ft lane scenario: (4 × 1,585) + 1,298 = 7,638 veh/h (20.5-percent increase).
- Capacity for the 10-ft lane scenario: (4 × 1,585) + 1,317 = 7,657 veh/h (20.8-percent increase).

- Capacity for the 11-ft lane scenario: (3 × 1,585) + (2 × 1,298) = 7,351 veh/h (15.9-percent increase).
- Capacity for the 10-ft lane scenario: (3 × 1,585) + (2 × 1,317) = 7,389 veh/h (16.5-percent increase).

Table 52. Prebreakdown capacity (Wiedemann model).

Capacity	Scenario 2 (12-ft Lane)	Scenario 8 (11-ft Lane Plus Reduced Speed Limit)	Scenario 10 (10-ft Lane Plus Reduced Speed Limit)
Prebreakdown capacity (veh/h)	1,585	1,298	1,317

Secondary Macroscopic Model Analysis

The Wiedemann model analysis assumed that only the rightmost lanes would have lower capacities in narrow case scenarios. The macroscopic analysis can be performed in a similar manner:

- Model Analysis:
  - Capacity for 12-ft lane scenario: 2,360 × 4 = 9,438 pc/h.
  - Capacity for 11-ft lane scenario: (4 × 2,360) + 2,152 = 11,591 pc/h (23-percent increase).
  - Capacity for 10-ft lane scenario: (4 × 2,360) + 1,968 = 11,406 pc/h (21-percent increase).
  - Capacity for 11-ft lane scenario: (3 × 2,360) + (2×2,152) = 11,383 pc/h (21-percent increase).
  - Capacity for 10-ft lane scenario: (3 × 2,360) + (2×1,968) = 11,014 pc/h (17-percent increase).

- Field Data Analysis:
  - Capacity for 12-ft lane scenario: 4 × 1,781 = 7,122 pc/h.
  - Capacity for 11-ft lane scenario: (4 × 1,781) + 1,695 = 8,817 pc/h (24-percent increase).
  - Capacity for 10-ft lane scenario: (4 × 1,781) + 1,547 = 8,669 pc/h (22-percent increase).
  - Capacity for 11-ft lane scenario: (3 × 1,781) + (2 × 1,695) = 8,732 pc/h (23-percent increase).
  - Capacity for 10-ft lane scenario: (3 × 1,781) + (2 × 1,547) = 8,435 pc/h (18-percent increase).

Summary

This section asked the question: If four 12-ft lanes with a 65-mi/h speed limit were converted to five narrow lanes with a 55-mi/h speed limit, what would happen to overall freeway capacity? Table 53 illustrates estimated capacity impacts.

Table 53. Estimated capacity impact (four- to five-lane and 65- to 55-mi/h speed limit conversion).

Analysis	11-ft Lanes (Percent Increase)	10-ft Lanes (Percent Increase)
Macroscopic data	23–24	18–22
Macroscopic model	21–23	17–21
Gipps model	22	21
Wiedemann model	16–20	17–21

These values are generally in the favorable and expected range. They are lower than the 25-percent increase that could potentially occur when transitioning from four to five 12-ft lanes (with no changes to posted speed limit). In most cases, the values are higher than the 5-percent increase that might be unattractive to State agencies. They are consistent with the significant mobility benefits recently observed across the United States (Neudorff et al. 2016). The general range of these values (i.e., 16–23 percent) is probably more trustworthy than actual values due to the limited number of real-world sites where this project was able to collect data and because lane-changing effects have not yet been integrated into the microscopic modeling. This is mostly a favorable outcome because it further supports the hypothesis that the lane-narrowing treatment is likely to produce significant mobility benefits. Based on earlier observations in macroscopic analysis sections, and based on common sense, capacity increases would be larger than those shown in table 53 when transitioning from three standard lanes to four narrow lanes. However, capacity increases would be smaller when transitioning from five to six lanes.

CHAPTER 6. CONCLUSIONS

Lane narrowing on freeways is an emerging bottleneck mitigation strategy. However, at this time, most popular traffic analysis models either do not recognize the impacts of lane narrowing or were developed based on outdated data. This project developed new macroscopic and microscopic models to analyze freeways having narrow lanes and shoulders based on data collected at U.S. treatment sites (i.e., sites where lanes have been narrowed for the explicit purpose of bottleneck mitigation).

Case study results showed that lane-narrowing strategies net positive mobility benefits so long as overall demands remained constant (i.e., without induced travel demand because of mobility improvements). The safety analysis revealed a significant decrease (approximately 20 percent) in overall crashes in narrowed freeway lane segments, primarily due to decreased congestion. Economic analyses applying the newly developed analysis and simulation models concluded the lane-narrowing treatment would pay for itself within the first year of implementation. Its feasibility and attractiveness could be further enhanced by future deployment of CAVs, which—in theory—will allow higher vehicle speeds in narrower lanes because of their precise longitudinal and lateral vehicle control.

The cost-effectiveness of lane narrowing is less clear when accounting for other extenuating factors:

- Number of months or years until new traffic demands fill in the new capacity.
- Costs of diverting traffic (and resultant congestion) while freeway lanes are restriped.
- Hidden bottlenecks.
- Percentage of heavy vehicles.
- Horizontal curvature.
- Costs of pollution and noise.
- Benefits of increased throughput.
- Benefits of possibly taking congestion away from alternate routes.

Some of these factors suggest the need for additional engineering analysis before pursuing the lane-narrowing approach to bottleneck mitigation. For example, what is the likelihood of side-by-side heavy vehicles? To avoid this unsafe occurrence on a narrow lane facility, the percentage of heavy vehicles should perhaps not exceed 10 percent. Alternatively, an agency may consider narrowing all lanes except the rightmost mainline lane, which is typically used by heavy vehicles. Significant horizontal curvature may also make it more difficult for drivers to keep their vehicles within an 11- or 10-ft lane.

Next, there is marginal benefit in relieving one bottleneck if it causes a new hidden bottleneck to form downstream. At a minimum, agencies should conduct an analysis of surrounding areas to rule out this possibility. In one notable anecdote, a diverging diamond interchange was constructed at great expense, only to increase congestion in the surrounding area due to bottleneck migration. Although the diverging diamond interchange is known to produce great safety and mobility benefits in isolation, surrounding areas must be analyzed prior to implementation. Lane narrowing would certainly fall into this category.

Finally, what would happen if new demands quickly filled in the newly created capacity? Would an agency feel positive about the significant increase in vehicle trips and possibly reducing congestion on alternate routes, or would added pollution, increased overall crashes (not crash rate), and lack of tangible benefits make it better to take no action? It is possible, if not likely, that different agencies would make different decisions when faced with these variables.

After viewing and considering the full set of project results, lane narrowing can be a viable and effective bottleneck mitigation strategy. Its feasibility and attractiveness could be further enhanced by future deployment of CAVs, which—in theory—will facilitate narrowing lane keeping at high speeds.

MODELING RESULTS: GENERAL

New macroscopic and microscopic modeling tools were created to evaluate mobility and safety benefits of narrowing freeway lanes. Case studies were conducted to assess the treatment in real-world scenarios. The general range of benefits predictions (e.g., 16–22-percent capacity increase when transitioning from four standard lanes to five narrow lanes) is probably more trustworthy than actual values due to the limited number of real-world sites where this project was able to collect data and because lane-changing effects have not yet been integrated into microscopic modeling. If the lane-narrowing treatment becomes more prevalent in the United States and elsewhere, these models could be recalibrated for improved accuracy.

The macroscopic and microscopic modeling approaches developed during this study both have specific shortcomings. For both modeling types, the number of real-world implementation sites was limited; only Honolulu, HI, provided 10-ft-lane-width sites. The macroscopic model does not provide a robust treatment of speed harmonization effects, upstream metering effects, or unequal lane utilization effects. The microscopic model is primarily based on basic freeway segment data, as opposed to merge or diverge segment data, and did not include an updated lane-changing model.

MODELING RESULTS: MACROSCOPIC

The developed models provide adjustments to FFS and capacity of freeway segments attributable to lane and shoulder width narrowing. Field observations of capacity and FFS at 25 sites across the United States were collected to develop the proposed models. Data-collection sites included 6 control segments (12-ft lanes), 18 segments with 11-ft lanes, and 2 segments with 10-ft lanes. Field observed FFSs ranged from 51–71 mi/h, whereas capacities ranged from 1,400–2,400 pc/h/ln.

The FFS model predicts FFS as a function of the lane width, shoulder width, number of lanes, speed limit, and segment type (basic, merge, and diverge) according to the HCM definitions. The model does not predict FFSs at weaving segments, as these were not included in the original dataset. However, given that merge and diverge segments had 1–2 mi/h lower FFSs compared to basic freeway segments, it can be assumed that speed reduction at weaving segments will be in the same range.

The developed regression model shows that, when controlling for the remaining statistically significant variables, FFS decreases by 1 mi/h for each foot of lane narrowing. This reduction is

less than that suggested in the HCM (table 2), where 11- and 10-ft lanes reduce FFS by 1.9 and 6.6 mi/h, respectively. The team also found that total ramp density (number of ramps per mi, measured within 3 mi upstream and 3 mi downstream of the segment's midpoint), which is a variable that exists in the current HCM model, does not affect FFS. However, posted speed limit was found to affect FFS significantly. A comparison between the two models (HCM and regression) showed that the regression model predicts FFS more accurately, especially at lower speeds (55–65 mi/h).

Capacities were measured at all narrow lane and control segments that were bottlenecks; CAFs were calculated as the ratio of narrow lane segment capacity over control segment capacity. According to field observations, CAF for 11-ft lanes was 0.95 (5-percent reduction in capacity), while CAF for 10-ft lanes was 0.87 (13-percent reduction in capacity). In the context of this report, capacities were defined as the average prebreakdown flow rates (i.e., the flow rate right before the breakdown event).

Observations from UAV videos showed that, at narrow lane segments, the rightmost lanes usually did not carry a great deal of traffic, and speeds were significantly less compared to inside lanes' speeds. This means that prebreakdown flow rates at the leftmost lanes were higher than in the rightmost lanes; moreover, this suggests that merging, weaving, and diverging maneuvers could potentially be performed more freely due to gap availability. However, since the HCM does not analyze traffic operations on each lane separately, and because per-lane data were not available at all sites, capacities and resulting CAFs were calculated based on the average cross section; thus, variability of operations among lanes is not captured here. In addition, the number of observed capacities at 10-ft lane segments was limited due to the low number of sites across the United States that have 10-ft narrow lanes (i.e., only one 10-ft-wide segment was found to be an active bottleneck). Therefore, CAF for 10-ft lanes (0.87) should be treated with caution and should be used only when field observations are unavailable.

When analyzing a narrow lane segment, the following procedure is used:

1. Calculate FFS based on equation 11.
2. Calculate unadjusted capacity of the basic segment using equation 10.
3. Adjust capacity according to table 8 CAFs.

The adjustments proposed here are sufficient to capture the impact of lane narrowing because the HCM assumes that capacity of the merge/diverge segment is constrained by capacity at the immediately downstream/upstream basic segment. However, capacities at bottleneck locations, such as those studied in this report, are significantly lower than capacities estimated in the HCM based on equation 4. This is due to driver behavior and increased vehicle interactions and lane changes. If field data suggest that unadjusted capacities are less than those produced by equation 4, then additional CAFs need to be introduced to capture the bottleneck impact. Although data did suggest that field-measured capacities at control sites were less than the HCM-estimated capacities, a CAF that captures this difference is not proposed here due to the limited number of sites studied (six control sites with varying geometric and operational conditions).

To evaluate mobility impacts across an entire freeway facility with multiple segments, a procedure similar to analyzing a narrow lane segment is used:

1. Calculate FFSs of each segment along the facility based on equation 11, given each segment's speed limit and geometric characteristics.
2. Calculate unadjusted capacities (equation 10) for all segments.
3. Apply appropriate CAF to the bottleneck(s) along the facility.

The analyst should take into consideration that the speed limit at narrow lane facilities is typically reduced by 5–10 mi/h compared to the 12-ft lane facilities.

MODELING RESULTS: MICROSCOPIC

The team recommends modifying the reaction time component of the car-following model by up to 8 percent. The details of modifying the Gipps car-following model are described in the appendix. For the Wiedemann 74 car-following behavior calibration, the team recommends increasing the $BX_{additive}$ parameter by 10 percent per foot of lane narrowing. This adjustment reflects the hypothesis that drivers will follow at greater distances as lanes narrow.

The team recommends a field analysis of existing conditions to calibrate the car-following behaviors and to avoid accepting default values that likely do not accurately represent local conditions. If field data are not available to calibrate existing conditions, default parameters may be used. If the existing condition is a narrowed lane, the team recommends collecting field data on that section rather than using this project's proposed adjustments. This project did not examine lane widths larger than 12 ft or smaller than 10 ft, so no specific recommendations are given for those conditions.

APPENDIX. GIPPS MODEL IMPLEMENTATION

Based on the results observed in the Model Development section in chapter 4 and the Case Studies section in chapter 5, the team recommended modifying the reaction time component of the car-following model based on the lane width of the section in which the agents are circulating. The reaction time parameter of Aimsun's microsimulator is the main parameter limiting road capacity. Its use, apart from setting the frequency at which decisions of lane changing, giveway, and so forth, are made for each vehicle, defines the relation between the spacing and the speed via the Gipps (1981) car-following equation of speed in shown in equation 69:

$$V_n(t+\tau_n) = b_n\tau_n + \sqrt{(b_n\tau_n)^2 - b_n\left[2(x_l(t) - x_n(t) - l_l - s_n) - V_n(t)\tau_n - \frac{V_{l(t)}^2}{b_l}\right]} \quad (69)$$

From equation 69, the spacing between two consecutive vehicles can be derived as shown in equation 70:

$$Spacing(t) = \left(x_l(t) - x_n(t)\right) = \frac{V_l^2(t)}{2b_l} - \frac{V_n^2(t+\tau_n)}{2b_n} + (0.5V_n(t) + V_n(t+\tau_n))\tau_n + (l_l + s_n) \quad (70)$$

Considering a homogeneous flow where all vehicles have the same speed, this reduces to equation 71:

$$Capacity = \frac{3600 \times V}{Spacing} = \frac{3600}{1.5\tau + \frac{(l+s)}{V}} \quad (71)$$

Solving for τ in equation 71 then yields equation 72:

$$\tau \approx \frac{2400}{Capacity} - \frac{(l_l+s_n)}{1.5\,V} \quad (72)$$

The HCM indicates capacities of 2,300 pc/h/ln appropriate for a 60-mi/h motorway. This would yield a reaction time of 0.9 s (considering an average car length of 5 m (15 ft) and minimum intervehicular distance of 1 m [3 ft]). Since lane changing decreases the capacity of multiple-lane highways, the reaction time derived from observed capacity from equation 69 through equation 72 should be considered as an upper limit. Equation 72 is illustrated in figure 46 for per-lane capacities ranging from 1,800 to 2,500 pc/h at 60 mi/h.

Reaction times between 0.8 and 1.0 are reasonable for freeways. Regarding the simulation time used in Aimsun's microsimulator, it should always be kept equal to the reaction time unless it is necessary to use different reaction times for different vehicles. In that case, all reaction times must be a multiple of the simulation step which can be set as low as 0.1 s. Note that the use of a simulation step distinct from the reaction time slows the calculation down and does not provide more accurate results. The Gipps car-following model was developed for a simulation step equal to the reaction time and the implementation allowing the use of different reaction times is an interpolation of the model using some approximations. In this project, lane narrowing only had a statistically significant impact on reaction times at a minority of sites. For this reason, the reaction time may be decreased by up to 7 percent for narrow lane sites. This effect seems marginal and location-dependent. The range of reaction times used for narrower lanes is therefore of the same order as stated before (i.e., reaction times between 0.8 and 1.0 are reasonable for freeways).

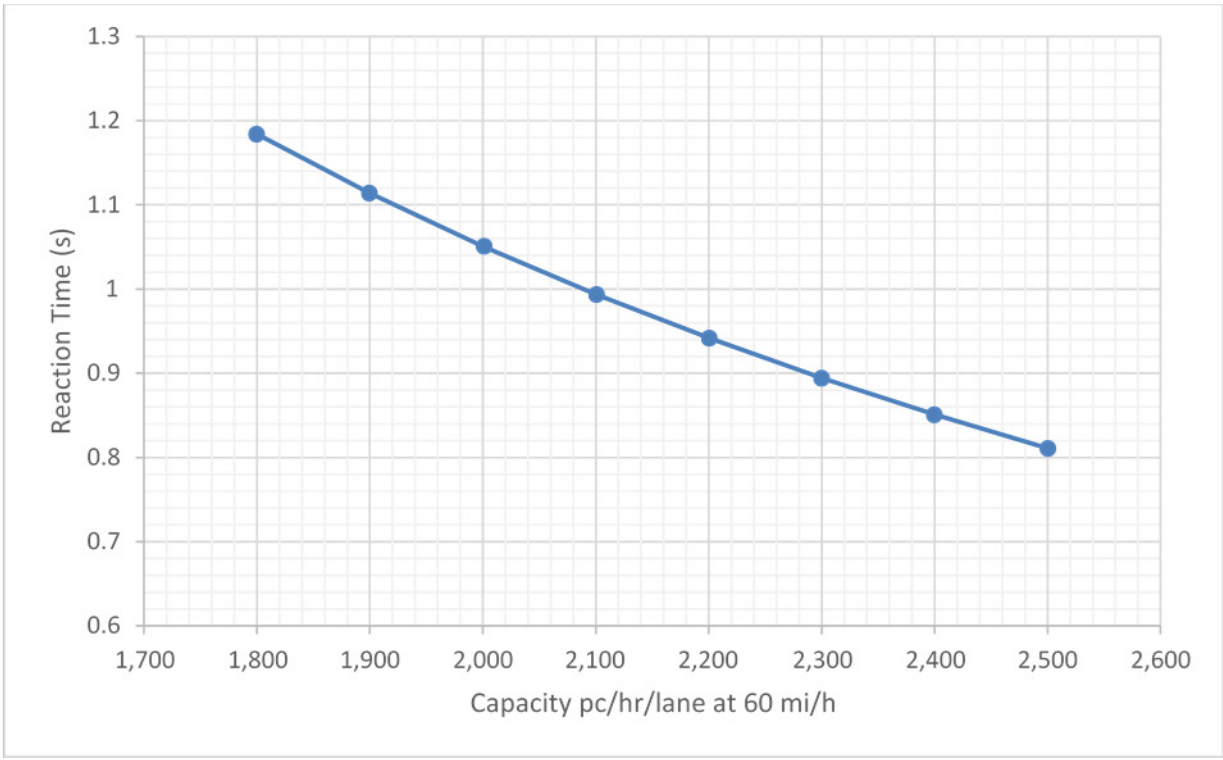

Figure 46. Graph. Reaction time versus freeway capacity.

REFERENCES

AASHTO. 2014. *Highway Safety Manual*. Washington, DC: American Association of State Highway and Transportation Officials.

Aimsun, Inc. 2017. "Aimsun Next User Manual version 8.2." Barcelona, Spain.

Babinec, A., and Jiří Apeltauer. 2016. "On Accuracy of Position Estimation from Aerial Imagery Captured by Low-Flying UAVs." *International Journal of Transportation Science and Technology* 5, no. 3 (October): 152–166. https://doi.org/10.1016/j.ijtst.2017.02.002.

Barceló, J., J. Casas, and G. Funes. 2006. *Report on Testing the NGSIM Lane Selection Model with Aimsun*. Barcelona, Spain: TSS-Transport Simulation Systems S.L.

Bauer, K., Douglas Harwood, Warren Hughes, and Karen Richard. 2004. "Safety Effects of Narrow Lanes and Shoulder-Use Lanes to Increase Capacity of Urban Freeways." *Transportation Research Record* 1897, no. 1 (January): 71–80. https://doi.org/10.3141/1897-10.

Ben-Bassat, T. and David Shinar. 2011. "Effect of Shoulder Width, Guardrail and Roadway Geometry on Driver Perception and Behavior." *Accident Analysis & Prevention* 43, no. 6 (November): 2142–2152. https://doi.org/10.1016/j.aap.2011.06.004.

Berthaume, A. 2015. "Microscopic Modeling of Driver Behavior Based on Modifying Field Theory for Work Zone Application." Amherst, MA: University of Massachusetts at Amherst. https://scholarworks.umass.edu/cgi/viewcontent.cgi?article=1328&context=dissertations_2.

Bonneson, J, Srinivas Geedipally, Michael Pratt, and Dominique Lord. 2012. *Safety Prediction Methodology and Analysis Tool for Freeways and Interchanges*. Washington, DC: National Academy of Sciences. http://onlinepubs.trb.org/onlinepubs/nchrp/docs/nchrp17-45_fr.pdf.

Brackstone, M. and Mike McDonald. 1999. "Car-following: A Historical Review." *Transportation Research Part F: Traffic Psychology and Behavior* 2(4): 181–196. https://doi.org/10.1016/S1369-8478(00)00005-X.

Brockfeld, E., Reinhart Kühne, and Alexander Skabardonis. 2003. "Toward Benchmarking of Microscopic Traffic Flow Models." *Transportation Research Record: Journal of the Transportation Research Board* 03: 124–129. https://doi.org/10.3141/1852-16.

Brockfeld, E., Reinhart Kühne, and Peter Wagner. 2005. "Calibration and Validation of Microscopic Models of Traffic Flow." *Transportation Research Record* 1934, no. 1 (January): 179–187. https://doi.org/10.3141/1934-19.

Cambridge Systematics, Inc. and Texas Transportation Institute. 2004. *Traffic Congestion and Reliability: Linking Solutions to Problems*. Washington, DC: Federal Highway Administration. https://ops.fhwa.dot.gov/congestion_report_04/congestion_report.pdf.

Casas, J. and A. Lenorzer. 2009. *Report on the Validation of the Oversaturated Freeway Flow Algorithm and the Cooperative Lane Changing and Forced Merging Model with Acceleration and Lane Selection Model with Aimsun*. Barcelona, Spain: TSS-Transport Simulation Systems S.L.

Chandler, R., Robert Herman, and Elliott Montroll. 1958. "Traffic Dynamics: Studies in Car Following." *Operations Research* 6, no. 2 (March–April): 165–184. https://www.mathstat.dal.ca/~iron/math4190/Papers/traffic.pdf.

Chase, P. and Erel Avineri. 2008. "Maximizing Motorway Capacity Through Hard Shoulder Running: UK Perspective." *Open Transportation Journal* 2, no. 1 (June) 7–18. https://doi.org/10.2174/1874447800802010007.

Chen, C., Li Li, Jianming Hu, and Chenyao Geng. 2010. "Calibration of MITSIM and IDM Car-Following Model Based on NGSIM Trajectory Datasets." In *Proceedings of 2010 IEEE International Conference on Vehicular Electronics and Safety, QingDao, China, July 15–17, 2010*, 48–53. Piscataway, NJ: Institute of Electrical and Electronics Engineers. https://doi.org/10.1109/ICVES.2010.5550943.

Chitturi, M. and Rahim Benekohal. 2005. "Effect of Lane Width on Speeds of Cars and Heavy Vehicles in Work Zones." *Transportation Research Record* 1920, no. 1 (January): 41–48. https://doi.org/10.3141/1920-05.

Curren, J.E. 1995. *Use of Shoulders and Narrow Lanes to Increase Freeway Capacity*. Washington, DC: Transportation Research Board. http://onlinepubs.trb.org/Onlinepubs/nchrp/nchrp_rpt_369.pdf.

Dixon, K., Kay Fitzpatrick, Raul Avelar, Marcie Perez, Stephen Ranft, Roma Stevens, Steven Venglar, and Tony Voigt. 2015. *Reducing Lane and Shoulder Width to Permit an Additional Lane on a Freeway*. Washington, DC: Federal Highway Administration. https://static.tti.tamu.edu/tti.tamu.edu/documents/0-6811-1.pdf.

Dowling, R., Paul Ryus, Bastian Schroeder, Michael Kyte, F. Thomas Creasey, Nagui Rouphail, Ali Hajbabaie, and Danica Rhoades. 2016. *Planning and Preliminary Engineering Applications Guide to the Highway Capacity Manual*. Washington, DC: National Academies Press. https://doi.org/10.17226/23632.

Federal Highway Administration. 2014. Mitigation Strategies for Design Exceptions (website). Accessed November 13, 2019. https://safety.fhwa.dot.gov/geometric/pubs/mitigationstrategies/chapter3/3_lanewidth.cfm.

Fitzpatrick, K., Karen Dixon, and Raul Avelar. 2016. "Evaluating Operational Implications of Reduced Lane and Shoulder Widths on Freeways." *Journal of Transportation Engineering* 142, no. 11 (June). https://doi.org/10.1061/(ASCE)TE.1943-5436.0000884.

FREEVAL. 2018. North Carolina State University (website). Accessed November 13, 2019. http://freeval.org.

Fritzsche, H.T. 1994. "A model for Traffic Simulation." *Traffic Engineering & Control* 35, no 5: 317–321.

Gazis, D.C., Robert Herman, and Richard W. Rothery. 1961. "Nonlinear Follow-the-Leader Models of Traffic Flow." *Operations Research* 9, no 4 (July–August): 545–567. https://doi.org/10.1287/opre.9.4.545.

Gipps, P.G. 1981. "A Behavioural Car-Following Model for Computer Simulation." *Transportation Research Part B: Methodological* 15, no 2 (April): 105–111. https://doi.org/10.1016/0191-2615(81)90037-0.

Gipps, P.G. 1986. "A Model for the Structure of Lane-Changing Decisions." *Transportation Research Part B: Methodological* 20, no. 5 (October): 403–414. https://doi.org/10.1016/0191-2615(86)90012-3.

Hale, D., Ramanujan Jagannathan, Michalis Xyntarakis, Peng Su, Ximiao Jiang, Jiaqi. Ma, Jia Hu, and Cory Krause. 2016. *Traffic Bottlenecks: Identification and Solutions*. Washington, DC: Federal Highway Administration. https://www.fhwa.dot.gov/publications/research/operations/16064/16064.pdf.

Hammit, B.E. 2018. "Methods to Explore Driving Behavior Heterogeneity Using SHRP2 Naturalistic Driving Study Trajectory-Level Driving Data." Laramie, WY: University of Wyoming. PhD dissertation.

James, R.M. 2019. "The Development of a Holistic Approach to Modeling Driver Behavior: Accounting for Driver Heterogeneity in Car-Following Models." Austin, TX: University of Texas at Austin. PhD dissertation. http://dx.doi.org/10.26153/tsw/2642.

Kesting, A., and Martin Treiber. 2008. "Calibrating Car-Following Models by Using Trajectory Data: Methodological Study." *Transportation Research Record* 2088, no. 1 (January): 148–156. https://doi.org/10.3141/2088-16.

Li, L., Xiqun Chen, and Lei Zhang. 2016. "A Global Optimization Algorithm for Trajectory Data Based Car-Following Model Calibration." *Transportation Research Part C: Emerging Technologies* 68, (July): 311–332. https://doi.org/10.1016/j.trc.2016.04.011.

Lochrane, T. 2014. "A New Multidimensional Psycho-Physical Framework for Modeling Car-Following in a Freeway Work Zone." Orlando, FL: University of Central Florida. https://stars.library.ucf.edu/etd/4592.

Margiotta, R., Michalis Xyntarakis, Alex Skabardonis, Weimin Huang, and Mike McGurrin. 2014. *Development of Modeling Capabilities for Shoulders Using Part-Time Travel Lanes*. Washington DC: Federal Highway Administration.

Melo, P., António Lobo, António do Couto, and Carlos Rodrigues. 2012. "Road Cross-Section Width and Free-Flow Speed on Two-Lane Rural Highways." *Transportation Research Record* 2301 (December): 28–35. https://doi.org/10.3141/2301-04.

Montgomery, D.C., Elizabeth A. Peck, and Geoffrey G. Vining. 2012. *Introduction to Linear Regression Analysis*. Fifth Edition. Hoboken, NJ: Wiley.

Murshed, D. and Paul McCorkhill. 2012. *Manual for Planning Level Cost Estimation (PLCE) Tool*. Olympia, WA: Washington State Department of Transportation. https://www.wsdot.wa.gov/mapsdata/travel/pdf/PLCEManual_12-12-2012.pdf.

Neudorff, L., P Jenior, R. Dowling, and B. Nevers. 2016. *Use of Narrow Lanes and Narrow Shoulders on Freeways: A Primer on Experiences, Current Practice, and Implementation Considerations*. Washington DC: Federal Highway Administration. https://ops.fhwa.dot.gov/publications/fhwahop16060/fhwahop16060.pdf.

Newell, G.F. 2002. "A Simplified Car-Following Theory: a Lower Order Model." *Transportation Research Part B: Methodological* 36, no 3 (February): 195–205. https://doi.org/10.1016/S0191-2615(00)00044-8.

Ossen, S., and Serge Hoogendoorn. 2005. "Car-Following Behavior Analysis from Microscopic Trajectory Data." *Transportation Research Record* 1934, no. 1 (January): 13–21. https://doi.org/10.1177/0361198105193400102.

Ossen, S., and Serge Hoogendoorn. 2008. "Validity of Trajectory-Based Calibration Approach of Car-Following Models in Presence of Measurement Errors." *Transportation Research Record* 2088 (December): 117–125. https://doi.org/10.3141/2088-13.

Ossen, S., Serge Hoogendoorn, and Ben G.H. Gorte. 2006. "Interdriver Differences in Car-Following: a Vehicle Trajectory-Based Study." *Transportation Research Record* 1965, no. 1 (January): 121–129. https://doi.org/10.1177/0361198106196500113.

Petzoldt, T., Patrick Roßner, Claudia Mair, Angelika Bullinger-Hoffmann, and Josef Krems. 2016. "How Does Left Lane Width in Motorway Work Zones Affect Driver Behaviour and Perception?" *Advances in Transportation Studies* Special Issue, vol. 1 (January): 51–58.

Potts, I., Douglas W. Harwood, and Karen R. Richard. 2007. "Relationship of Lane Width to Safety on Urban and Suburban Arterials." T*ransportation Research Record* 2023, no. 1 (January): 63–82. https://doi.org/10.3141/2023-08.

PTV Vissim. 2019. PTV Group (website). https://vision-traffic.ptvgroup.com/en-us/products/ptv-vissim, last accessed November 13, 2019.

Punzo, V., and Fulvio Simonelli. 2005. "Analysis and Comparison of Microscopic Traffic Flow Models with Real Traffic Microscopic Data." *Transportation Research Record* 1934, no. 1 (January): 53–63. https://doi.org/10.3141/1934-06.

Punzo, V., Marcello Montanino, and Biagio Ciuffo. 2015. "Do we Really Need to Calibrate All the Parameters? Variance-Based Sensitivity Analysis to Simplify Microscopic Traffic Flow Models." *IEEE Transactions on Intelligent Transportation Systems* 16, no. 1 (February): 184–193. https://doi.org/10.1109/TITS.2014.2331453.

Rakha, H., and Yu Gao. 2010. *Calibration of Steady-State Car-Following Models using Macroscopic Loop Detector Data*. Blacksburg, VA: Virginia Tech Transportation Institute. https://pdfs.semanticscholar.org/e9ce/dca8b19cb57b88742c4212156f2837051f42.pdf.

Ranjitkar, P., Takashi Nakatsuji, and Motoki Asano. 2004. "Performance Evaluation of Microscopic Traffic Flow Models with Test Track Data." *Transportation Research Record* 1876, no. 1 (January): 90–100. https://doi.org/10.3141/1876-10.

Ranney, T.A. 1994. Models of Driving Behavior: A Review of Their Evolution. *Accident Analysis & Prevention* 26(6): 733–750. https://doi.org/10.1016/0001-4575(94)90051-5.

Rice, R., and San Lee. 2016. "Part Time Shoulder Use" (webinar). Washington, DC: National Operations Center of Excellence. https://transops.s3.amazonaws.com/uploaded_files/Part%20Time%20Shoulder%20Use%20%28002%29.pdf.

Roess, R. and Elena Prassas. 2014. *The Highway Capacity Manual: A Conceptual and Research History*. New York: Springer.

Rosey, F., Jean-Michel Auberlet, Oliver Moisan, and Guy Dupré. 2009. "Impact of Narrower Lane Width: Comparison Between Fixed-Base Simulator and Real Data." *Transportation Research Record* 2138 (December): 112–119.

Rothery, R.W. 2001. *Revised Monograph on Traffic Flow Theory, Chapter 4: Car-following*. Washington, DC. https://www.fhwa.dot.gov/publications/research/operations/tft.

Saifuzzaman, M. and Zuduo Zheng. 2014. "Incorporating Human-Factors in Car-Following Models: A Review of Recent Developments and Research Needs." *Transportation Research Part C: Emerging Technologies* 48: 379–403. https://doi.org/10.1016/j.trc.2014.09.008.

Schrank, D., Bill Eisele, and Tim Lomax. 2017. *Urban Mobility Report*. College Station, TX: Texas A&M Transportation Institute.

Shahin, M., Frank Engelmann, and Bernhard Friedrich. 2003. "Using the Motorway Hard Shoulder in Congestion to Allow Drivers to Exit." *Traffic Engineering & Control* 44, no 7: 258–263.

Stamatiadis, N., Jerry Pigman, John Sacksteder, Wendel Ruff, and Dominique Lord. 2009. *Impact of Shoulder Width and Median Width on Safety*. Washington, DC: National Academies Press. https://doi.org/10.17226/14252.

Tampère, C. 2004. *Human-Kinetic Multiclass Traffic Flow Theory and Modelling*. Delft, Netherlands: Delft University of Technology.

Thomas, R. 2003. "Can the Dutch Teach Us How to Manage Motorway Traffic?" *Local Transport Today* (July 24): 10–11.

Toledo, T. 2007. "Driving Behavior: Models and Challenges." *Transport Reviews* 27(1): 65–84. https://doi.org/10.1080/01441640600823940.

Transportation Research Board. 2016. *Highway Capacity Manual, Sixth Edition: A Guide for Multimodal Mobility Analysis*. Washington, DC: National Academies of Sciences, Engineering, and Medicine.

Treiber, M., and Arne Kesting. 2013. "Microscopic Calibration and Validation of Car-Following Models–a Systematic Approach." *Procedia-Social and Behavioral Sciences* 80, no. 7 (June): 922–939. https://doi.org/10.1016/j.sbspro.2013.05.050.

Treiber, M., Ansgar Hennecke, and Dirk Helbing. 2000. "Congested Traffic States in Empirical Observations and Microscopic Simulations." *Physical Review E* 62 (February): 1805–1824. https://doi.org/10.1103/PhysRevE.62.1805.

Tukey, J.W. 1977. *Exploratory Data Analysis*. Volume 2. Boston, MA: Addison-Wesley Publishing Company.

Urbanik, T., and Carlos R. Bonilla. 1987. "California Experience with Inside Shoulder Removals." *Transportation Research Record* 1122: 37–46. http://onlinepubs.trb.org/Onlinepubs/trr/1987/1122/1122-005.pdf.

Van Aerde, M. 1995. "Single Regime Speed-Flow Density Relationship for Congested and Uncongested Highways." Presented at *The 74th Transportation Research Board Annual Conference*, Washington, DC, January 27, 1995.

Waard, D.D., Maaike Jessurun, Franciscus, J. J.M. Steyvers, Peter T.F. Raggatt, and Karel A. Brookhuis. 1995. "Effect of Road Layout and Road Environment on Driving Performance, Drivers' Physiology and Road Appreciation." *Ergonomics* 38, no. 7 (July): 1395–1407. https://doi.org/10.1080/00140139508925197.

Wang, H., Wei Wang, Jun Chen, and Ming Jing. 2010. "Using Trajectory Data to Analyze Intradriver Heterogeneity in Car-Following." *Transportation Research Record* 2188, no. 1: 85–95. https://doi.org/10.3141/2188-10.

White, V. 2016. “Revised Departmental Guidance on Valuation of Travel Time in Economic Analysis.” Washington, DC: U.S. Department of Transportation. https://www.transportation.gov/office-policy/transportation-policy/revised-departmental-guidance-valuation-travel-time-economic.

Wiedemann, R. 1974. “Simulation des Strassenverkehrsflusses.” Karlsruhe, Germany: Universitaet Karlsruhe. PhD dissertation.

Zheng, J., Jian Sun, and Jianhao Yang. 2015. “Relationship of Lane Width to Capacity for Urban Expressways.” *Transportation Research Record* 2483 (October): 10–19. https://doi.org/10.3141/2483-02.

Zheng, J., Koji Suzuki, and Motohiro Fujita. 2012. “Evaluation of Car-Following Models Using Trajectory Data from Real Traffic.” *Procedia-Social and Behavioral Sciences* 43 (December): 356–366. https://doi.org/10.1016/j.sbspro.2012.04.109.

Recycled
Recyclable

HRDO-20/06-21(WEB)E